SYSTEM IDENTIFICATION OF FULL-SCALE PROPULSION SYSTEMS

by

K.L.Hageman

M. M. Nelissen
April '20

TUDelft

SDPO.20.030.m

DAMEN

Fingerprinting II

System Identification of Full-scale Propulsion Systems

by

K.L. Hageman

to obtain the degree of Master of Science in Marine Technology
at the Delft University of Technology,
to be defended publicly on Monday January 25, 2021 at 10:00.

This thesis is confidential and cannot be made public until January 25, 2023.

An electronic version of this thesis is available at
`http://repository.tudelft.nl/`.

TUDelft Delft University of Technology

Preface

Abstract

With the use of simulation models, predicting and optimizing the correct dynamic behaviour and parameters of a propulsion system of a ship can be performed cheap and safe. However, capturing the right dynamic behaviour is very difficult. Besides, building simulation models and determining the correct parameters is a time consuming process. System identification is a new proposed method to create simulation models of the propulsion system of a ship. With system identification, in- and output data of a controlled test are used to identify the parameters of the created grey box model structure, which reflects the underlying physical laws. A so called "fingerprint" is generated that imitates the behaviour of the system. The first attempt of system identification of a full-scale propulsion system by Martinus [1] showed promising results but asked for further research. This thesis further investigates if system identification is a suitable method to obtain the dynamic model- behaviour and parameters of a full-scale propulsion system in a short time, with the use of controlled tests.

The measured data is used from a backward bollard push test with a Stan Tug 1205. A model structure defined by Martinus [1] is used, containing a governor, diesel and shaft loop. Linear system identification is used as the initial method to obtain dynamic model- behaviour and parameters of a full-scale propulsion system. Furthermore, the performed full-scale system identification of Martinus [1] is used as benchmark. The three pillars of system identification, data, model structure and searching criterion are analysed and if possible improved to increase the quality of the linear system identification.

The measured data of a multiple sine waves test is transformed from time domain to frequency domain. With a Gaussian filtering approach, the frequencies of interest are selected. The noise of the measured data is cancelled out at the frequencies where the sines have no power and the system identification speeds up. Open and closed loop sensitivity analysis are performed with the model structure, which showed that in open loop a more clear response and influence of the individual parameters is visible compared to closed loop. Furthermore, the model structure is split up in open loop sub-model structures as this creates more simple model structures with a lower amount of identifiable parameters. Based on the performed sensitivity analysis of the sub-models, a second order system and time delay are added to the model structure to increase the quality of the model response compared to the measured data.

Linear system identifications are performed with closed and open loop model structures, with and without a second order system and time delay and frequency domain measured data. The identified models are compared with the measured data and the benchmark. The results of the linear system identifications showed that the addition of a time delay and second order system increase the quality of the dynamic behaviour and identified parameters. The response of these identified models compare well with the measured data and the parameters show trustworthy results.

Based on the results, it is concluded that linear system identification is a suitable method to obtain dynamic model- behaviour and parameters of a full-scale propulsion system in short time. There are still some deficiencies which influence the quality of the linear system identification of the full-scale propulsion system. First, the identified value of the parameter describing the shaft loop does not match with what is known. Secondly, the amount of measurement points in the critical region of the propulsion system of the Stan Tug 1205 is too low. Furthermore, there is not enough damping in the identified model and the identified time delay is still not sufficient. However, these deficiencies are solvable and most likely further increase the quality of system identification of a full-scale propulsion when solved. Therefore, it is recommended to continue developing linear open loop system identification with a second order system and time delay combined with frequency domain data.

Contents

List of Figures

List of Tables

List of Symbols

B	Width overall	[m]
D_p	Propeller diameter	[m]
e_n	Error between n_{set} and n_e	[rpm]
g	Relation engine speed and engine torque	[-]
I	Current	[A]
i_{gb}	Gearbox ratio	[-]
I_p	Moment of inertia	[kg·m^2]
J	Advanced ratio	[-]
K_d	Derivative gain	[-]
K_i	Integral gain	[-]
K_p	Proportional gain	[-]
K_Q	Torque coefficient	[-]
K_T	Thrust coefficient	[-]
L_{oa}	Length overall	[m]
M_s	Shaft torque	[Nm]
M_b	Engine torque	[Nm]
M_p	Propeller torque	[Nm]
n_{set}	Set point of engine speed	[rpm]
n_e	Engine speed	[rpm]
n_s	Shaft speed	[rps]
Q	Propeller open water torque	[Nm]
P_b	Engine brake power	[kW]
T	Thrust force	[N]
T_p	Pulse period	[s]
t	Time	[s]
U	Voltage	[V]
v	Relation fuel rack and engine torque	[-]
v_a	Advanced velocity	[m/s]
v_d	Design speed	[m/s]
X_{set}	Set point fuel rack	[mm]
X_f	Fuel rack	[mm]
y	Output signal	[Nm,rpm]
ζ	Damping ratio	[-]
η_R	Relative rotative efficiency	[-]
η_{trm}	Transmission losses	[-]
η_{trm}	Transmission losses	[-]
ω	Frequency	[rad/s]
ρ	Water density	[kg/m^3]
τ_n	Integration constant	[s]

1

Introduction

1.1. Motivation

Globally, the maritime industry has a large and important role. Due to the globalisation, shipping of goods is increasing by day. Almost every country is depending on oil, which is transported and mostly extracted at sea. Installation of offshore wind farms is performed with support and installation ships. There are endless applications of ships and people use products and services that are dependent on the maritime industry daily. You want your package to be shipped as fast as possible, still being cheap. Petrol and gas must be low-priced to drive cheap and to enjoy warm water. On the other hand, sustainability is rising as priority by the day. Regulations are ensuring that ship emissions will decrease.

A method to create cleaner, safer and more effective ships is the use of simulation models. Simulation models are cheap and safe in usage to predict and optimize the dynamic behaviour of systems. However, capturing the right dynamic behaviour is extremely difficult. These models vary from simple, small systems to the overall ship dynamics and propulsion systems. Simulation models of propulsion systems are used for system performance, controller design and monitoring. High performance and commendable controllers of the propulsion system cause that ships possibly sail with low operational expenses and low emissions. Monitoring the decay of components prevent damage of components and could create a predictive maintenance model.

For ship builders the necessity of having simulation models of propulsion systems is high. The model has to be build, but also the parameters have to be determined. Suppliers of equipment of the propulsion system are not very willing to share the details of their product. This causes a difficult and time consuming process during the creation of simulation models of the propulsion system. Besides, propulsion systems become more complex by the day, as the amount of components and controlling systems are increasing with a rapid speed. Therefore, the complexity of simulation models of the propulsion system increase as well.

Simulation models of propulsion systems are built using different methods. Simulations models of propulsion systems build with physical laws are applicable for system performance predictions and controller design. Building a simulation model with physical relations and determination of the parameters of a propulsion system is a time consuming process [2][3]. Setting up a propulsion system model with determined parameters requires large amounts of data from the equipment manufacturers [4]. Data driven modelling (DDM) is an approach based on historical data and advanced algorithms. Models can be generated without any prior knowledge creating a black box. DDMs are applicable for continuously monitoring of the propulsion equipment and their decay [5]. Obtaining data sets in real world scenarios that are suitable for data driven models is difficult and time consuming [5]. To fit the measured data, a mean of the obtained data is created. The behaviour of the model only covers a small part of the reality and will become unreliable for slightly more extreme situations.

1

An intermediate method to create simulation models of propulsion systems is grey box system identification. System identification uses a mathematical model structure from which the parameters are estimated with the use of measured in- and output data. The measured data is obtained during short and controlled tests and the model structure is build upon known physical relations. The potential advantage of system identification of propulsion systems with controlled tests is the usage to quantify system performance during sea acceptance trails, after periodic maintenance or after system modifications in a relative short time span[3]. Moreover, the so called fingerprints that are generated after performing system identification are useful to understand the state of decay of components and help create a predictive maintenance model. Furthermore, the pace of creating models and the certainty of the measured data and models might increase.

1.2. Literature Review

For this research a separate literature review is performed. The literature review exists out of three main parts [6]. First, an overview is given of literature concerning simulation models of ship propulsion systems and their application. Secondly, the general working principle of system identification is described. Moreover, an overview of the variety of applications of system identification in the maritime industry is given. The content of this separate performed literature review will be considered as known during this research [6]. However, a short overview of the defined gap concerning system identification of the propulsion system of a ship from the literature review is presented.

System identification of the propulsion system is a field that is scarcely investigated. The identification of a propulsion system is proven on model-scale [3]. The first attempt of Martinus [1] on full-scale grey box linear system identification of the propulsion system based on a controlled test is promising but needs to be improved. Besides, only linear system identification is performed with one type of model structure, one type of searching criterion and one set of experiments. Literature shows that there is a gap concerning system identification of the propulsion system. Recommendations are given by Martinus [1] to improve the system identification of a full-scale marine propulsion system. These recommendations underline the importance of this research and the present gap in system identification of propulsion systems. Grey box system identification of a propulsion system is a method that might fill the gap concerning the drawbacks of the conventional methods.

1.3. Research Goal

This research aims to improve the system identification results obtained by Martinus [1]. The research of Martinus [1] focused mainly on identifying the correct parameters of the propulsion system. This research focuses on identifying the correct parameters but also the correct behaviour of the propulsion system. Damen Shipyards and TU Delft are keen to find a "fingerprinting" method to obtain the dynamic model- behaviour and parameters of a propulsion system of a ship in a short time, with the use of controlled tests.

Main goal
Define a method that obtains the dynamic model- behaviour and parameters of a propulsion system in a short time, with the use of controlled tests.

Sub goal
Implementation on board of a ship concerning input data, output data, sensors needed etc. Define what is needed to create a "fingerprinting" system on board of a ship.

1.4. Research Questions

From the research goal it is possible to define the main research question. The following main research question is defined:

> **"What is a suitable method to obtain dynamic model- behaviour and parameters of a full-scale propulsion system in short time, based on controlled tests?"**

The main question is divided in sub-questions.

- *What are the possible improvements concerning data, model structure and searching criterion for the linear system identification of a full-scale propulsion system?*

- *How does the implementation of a nonlinear model structure affect the full-scale system identification?*

- *What is required to implement the most suitable fingerprinting method on a Damen ship?*

1.5. Scope

A backward bollard push test was executed as controlled test in November 2019 with a Stan Tug 1205 of Damen Shipyards. The measured data that was collected during this test will be used for this research. Therefore, no other test will be executed. The diesel engine and governor of the Stan Tug 1205 will have the main focus in obtaining dynamic model- behaviour and parameters. The governor of the Stan Tug 1205 controls the fuel injection and uses the feedback of the engine speed, this will be imitated in the models. For modelling and programming, Matlab & Simulink, System Identification Toolbox of Matlab and scripts & models from the research of Martinus [1] will be used. Linear grey box system identification is the initial method to obtain dynamic model- behaviour and parameters of a full-scale propulsion system.

1.6. Approach

The research approach is based upon the improvements that can be made for system identification. In figure 1.1 the system identification loop is presented with the possible improvement steps. Improvements can be made concerning the three pillars of system identification: measured data, model structure and the searching criterion. During the iterative process of improvements, the sub-questions and eventually the main research question will be answered. Important to note is that the linear system identification is improved and the findings are used to answer the research questions.
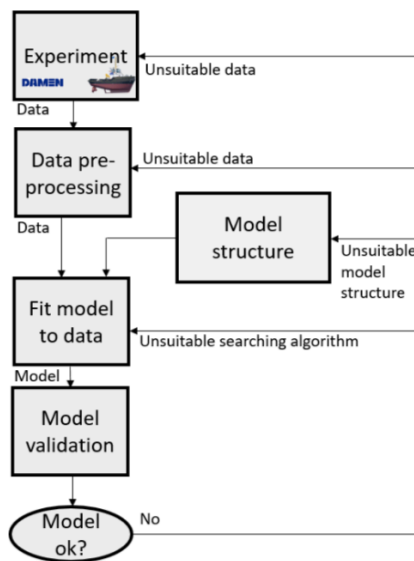
Figure 1.1: System identification loop is presented with the possible improvements [1].

The first step performed is analysing and improving the measured data. Creating better and clean data has an improving effect on the system identification. The raw measured data is pre-processed to create a usable data set. Thereafter, errors concerning a time delay and the measurement of the rpm are analysed and and if necessary improved. Furthermore, the usage of frequency domain data is analysed. During the whole process possible changes are applied to the measured data.

The second step is analysing and improving the linear model structure. With a sensitivity analysis of the initial linear model structure of the propulsion system, the behaviour of each parameter is analysed. Thereafter, the individual sub-models of the model structure and the addition of possible new terms to the model structure are investigated. Examining the possibilities of improving the linear model structure gives insight if linear system identification is the correct method to obtain the dynamic model-behaviour parameters of a propulsion system.

The third pillar of system identification, the searching criterion is reviewed during the third step. Mainly, the searching criterion is improved concerning optimisation to increase the chance to find a global minimum instead of a local minimum. Eventually, the improved measured data, model structures and searching criterion are brought together to perform different linear system identifications. The results of the linear system identifications are compared in frequency domain and validated in time domain. The different linear system identifications are also compared with the benchmark identification that is performed by Martinus [1]. This is performed to see if the method to obtain the dynamic model-behaviour parameters of a propulsion system is improved.

1.7. Outline
The thesis outline gives an overview of the contents of each chapter in this report. The thesis outline is based on the approach steps and the improvement loop presented in figure 1.1. This report exist out of 6 chapters, the outline presents a short explanation of the upcoming chapters.

Chapter 2 *"Background"* contains background information concerning the aspects of the research of Martinus [1] that are used during this thesis.

Chapter 3 *"Data Processing & Improvements"* contains analysis and improvements concerning the measured data. This chapter contains the pre-processing of measured data, analysis of errors in the data, analysis of frequency domain data and presents the data sets that are used.

Chapter 4 *"Linear Model Analysis & Improvements"* contains possible improvements of the linear model structure that are determined. This chapter contains a sensitivity analysis, simplification of the model structure, analysis of the sub-models and the addition of new terms to the model structure.

Chapter 5 *"Linear System Identification"* contains the results of different performed linear system identifications with the improved model structures and measured data sets. This chapter contains an explanation of the used searching criterion, open and closed loop linear system identifications results and the validation of the identified models.

Chapter 6 *"Conclusions & Recommendations"* gives answers to the main and sub-questions that are presented in section 1.4. Thereafter, recommendations concerning future research and use of full-scale system identification are given.

2

Background

The aspects of the research of Martinus [1] used are the nonlinear model, linear model, experimental data, searching criterion and the results of the performed system identification. In this chapter background information is given concerning these aspects. More detailed descriptions can be found in the research of Martinus [1]. This chapter exist out of five main sections. First, the system of interest is discussed. Moreover, the performed experiment and the obtained measured data are presented. Thereafter, the nonlinear model of the system of interest is discussed. Further, the linear model obtained from the nonlinear model is presented. After that, the used searching criterion is reviewed. This chapter ends with system identification as performed by Martinus [1], which is used as benchmark during this research.

2.1. System of Interest

The vessel of interest during this research is the Stan Tug 1205. This ship is selected by Martinus [1] because it has a relatively simple propulsion drive train, containing a governor, fuel actuator, diesel engine, gearbox and propeller. Besides, the Stan Tug 1205 is a small ship, so when damage would have occurred during experiments, the cost and consequence would be minimal. Important to note is that the Stan Tug 1205 is equipped with a fixed pitch propeller (FPP). Therefore, the simulation model will only have one input signal, the engine speed set point. The engine control system of the Stan Tug 1205, controls the fuel injection and uses the feedback of the engine speed[1]. The governor is fed with an error between the actual engine speed and the engine speed set point and actuates the fuel injection for a diesel engine. The full-scale experiment that is performed is a backward bollard push, which is a bollard pull performed in a somewhat different way. This backward bollard push is executed for safety and simplification reasons. The backward bollard push condition simplifies the model because the speed loop can be neglected. A detailed product sheet of the Stan Tug 1205 can be found in appendix A. In table 2.1 an overview of the main particulars of the Stan Tug 1205 is presented.

Table 2.1: Overview of the main particulars of the Stan Tug 1205 [1].

Symbol	Physical quantity	Value
L_{oa}	Length overall	13.08 [m]
B	Width overall	5.28 [m]
DWT	Deadweight	54 [t]
v_d	Design speed	1 [Kn]
i_{gb}	Gearbox ratio	3.82 [-]
$P_{b,max}$	Maximum engine brake power	221 [kW]
$n_{e,max}$	Maximum engine speed	1800 [rpm]
D_p	Propeller diameter	1.05 [m]
P/D	Pitch ratio	1.110 [-]

2.2. Experimental Data

A controlled test is performed to obtain measured data that can be used for system identification. The experiment is executed in calm water during a day with average weather conditions. A backward bollard push set up is used because the Stan Tug 1205 was already moored in a backward position. Therefore, no captain was needed to change the mooring position, which eased the preparations of the experiment[1].

Two different parties have measured the input and outputs of the system. JVS and Damen Shipyards with DEWEsoft equipment have performed measurements. Three types of experiments were carried out, multiple sine waves experiments, chirp waves experiments and step response experiments. Input of the experiments was the engine speed set point, in voltage. The output of each experiment was the engine speed, the shaft speed measured with one pulse and four pulses and the shaft torque. Important to note is that only one shaft line was instrumented during the experiment, namely the port side shaft line. In figure 2.1 an overview is given of the measurement set up, with both DEWEsoft and JVS measurements. Table 2.2 clarifies the symbols of the overview.
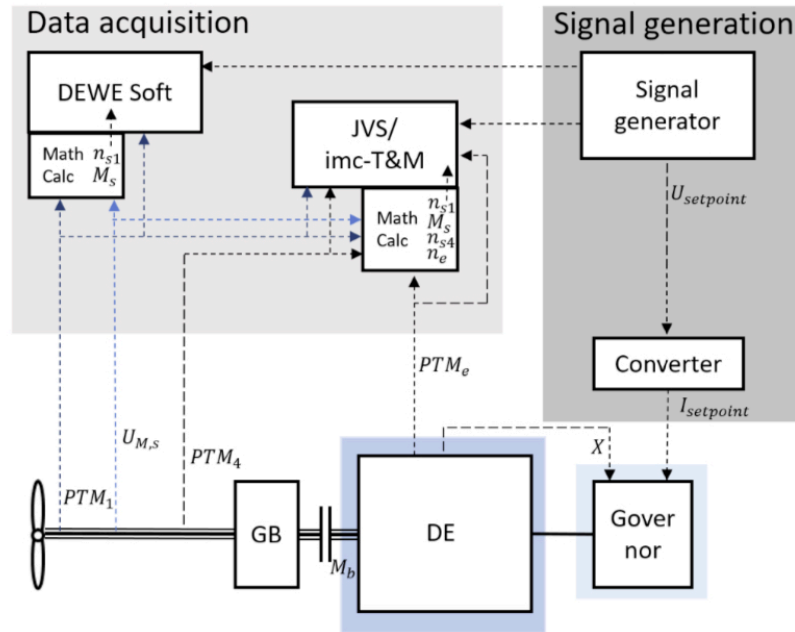
Figure 2.1: Overview of measurement set up during experiments [1].

Table 2.2: Clarification of symbols in figure 2.1 [1].

Symbol	Physical quantity	Unit
$I_{setpoint}$	Set point current	[mA]
X	Feedback signal	[-]
M_b	Engine torque	[Nm]
M_s	Shaft torque	[Nm]
PTM_1	Pulse time modulation [1 pulse]	[s]
PTM_4	Pulse time modulation [4 pulse]	[s]
PTM_e	Pulse time modulation [Engine]	[s]
n_{s1}	Shaft speed 1 pulse	[rpm]
n_{s4}	Shaft speed 4 pulse	[rpm]
n_e	Engine speed	[rpm]
$U_{setpoint}$	Set point voltage	[V]
$U_{M,s}$	Shaft torque voltage	[V]

Martinus [1] concluded that the JVS data was most suitable for system identification. The raw data is used and therefore needed to be processed to usable data sets. Besides, the data is normalised because the identification is performed with a linear model structure. The pre-processing and normalisation are revised and performed again to get better insight of measured data sets, which is shown in section 3.1. The raw JVS measurements used are the shaft torque M_s, the three pulse time modulation measurements and the set point voltage $U_{setpoint}$. The following enumeration shortly explains how the raw data sets are measured and processed.

- Shaft torque - M_s: The measurement is performed with strain gauges on the shaft between the gearbox and propeller. The shaft torque data set in [Nm] is used and normalised.

- Pulse time modulation [1 pulse] - PTM_1: The measurement is performed with one reflection strip attached to the shaft, creating a measurement of one pulse per rotation. The pulse measurement of the shaft speed is transformed into engine speed measurement $n_{e,1}$ in [rpm] and is normalised.

- Pulse time modulation [4 pulse] - PTM_4: The measurement is performed with four reflection strips attached to the shaft, creating a measurement of four pulses per rotation. The pulse measurement of the shaft speed is transformed into engine speed measurement $n_{e,4}$ in [rpm] and is normalised.

- Pulse time modulation [Engine] - PTM_e: The measurement is performed with one reflection strip attached to the shaft, creating a measurement of one pulse per rotation. The pulse measurement of the engine speed is transformed into an engine speed measurement n_e in [rpm] and is normalised.

- Set point voltage - $U_{setpoint}$: The input of the system is done in voltage. The input is transformed into the engine speed set point n_{set} in [rpm] and is normalised.

The raw JVS data is measured during the different performed experiments. In table 2.3 the input of each experiment is shown, concerning the start and stop time, frequency and amplitude. There are 16 different sine wave experiments performed, each with another operating frequency. Four different chirps are carried out, which can be divided in a short chirp (C11) and a long chirp (C21 - C23). The test is ended with two different step response experiments.

The three types of experiments can be used for system identification, validation and comparisons. Due to the large amount of different experiments with different frequencies, the data gives information about the system dynamics over the entire frequency range of interest. The data sets are measured in time domain but could be transformed to frequency domain. To visualise the different performed experiments, a time domain plot of the unprocessed set point voltage is shown in figure 2.2. Each experiment type will be discussed in the following parts.
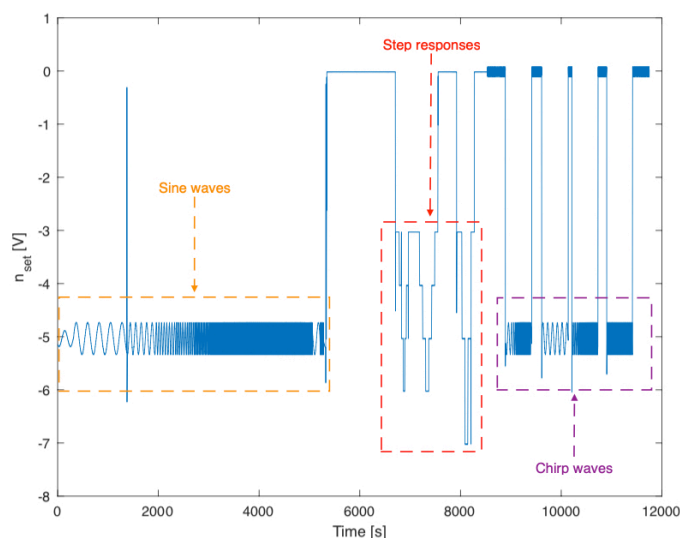
Figure 2.2: Overview of measurement of unprocessed set point voltage in time domain with indication of different experiments.

Table 2.3: Overview of the executed experiments with the Stan Tug 1205.

Sine	Freq [Hz]	-	Ampl. [V]	Start [s]	Stop [s]
S1	0.0044	-	0.6	480	1270
S2	0.0092	-	0.6	1450	1900
S3	0.0193	-	0.6	1970	2300
S4	0.0275	-	0.6	2400	2700
S5	0.0405	-	0.6	2750	2950
S6	0.06	-	0.6	3100	3200
S7	0.084	-	0.6	3300	3500
S8	0.11	-	0.6	3600	3700
S9	0.1778	-	0.6	3800	3950
S10	0.3728	-	0.6	4050	4150
S11	0.7814	-	0.6	4250	4350
S12	1.637	-	0.6	4440	4580
S13	3.433	-	0.6	4640	4690
S14	7.19	-	0.6	4840	4900
S15	15.01	-	0.6	5020	5050
S16	31.644	-	0.6	5234	5254
Chirp	**Start freq.**	**Stop freq.**	**Ampl. [V]**	**Start [s]**	**Stop [s]**
C11	0.001	3.981	0.6	8850	9450
C21	0.001	0.02	0.6	9600	10150
C22	0.015	0.27	0.6	10200	10750
C23	0.1	3.3981	0.6	10900	11450
Step	**Stepsize [V]**	**Min. [V]**	**Max. [V]**	**Start [s]**	**Stop [s]**
St1	1	-3	6	7150	7600
St2	2	-3	7	7900	8300

Multiple Sine Waves
The 16 different sine wave experiments are induced with different input frequencies. These frequencies vary between 0.0044 and 31.644 [Hz]. The sine waves fluctuate around a working point of -5 [V]. The experiments at low frequencies resulted in the longest experiments, which is also visible in table 2.3. The multiple sine waves can be presented in time domain but also in frequency domain. Due to constant frequencies per experiment it is easy to convert the multiple sine wave experiments in frequency domain. In frequency domain it is possible to selected the desired points and cancel out the noise. Martinus [1] cancelled out the noise by first transferring the data to frequency domain and after that selecting the highest amplitude peak in frequency domain. The frequency domain data of the multiple sine waves obtained by Martinus [1] can be seen in figure 2.4. For most of the sine waves experiments this filtering approach worked, but unfortunately for some experiments it went wrong.

Chirp Waves
Four different chirps are carried out, which can be divided in a short chirp (C11) and a long chirp (C21 - C23). The long chirp is in essence the same as the short chirp because both vary from 0.001 to 3.981 [Hz]. However, the difference is the amount of time that is used to increase the frequency. The chirps C21 to C23 are merged, which creates a long chirp with a duration of approximately 1500 [s]. The chirp waves fluctuate around a working point of -5 [V].Martinus [1] used the chirp waves data sets in time domain for both system identification and time domain validation. In section 3.4 time domain plots of the long and short chirp waves, after the revised pre-processing, are shown.

Step Responses
The step response experiments are performed for different purposes. First, the step responses contain constant input and output measurements. These constant values can be used for pre-processing of the data. Another usage of the step response data sets is for time domain validation. By implementing the identified parameters in the simulation model, the response can be compared with the measured step response. Martinus [1] used the step response for both pre-processing and time domain validation. In section 3.4 time domain plots of the step responses, after the revised pre-processing, are shown.

2.3. Nonlinear Model

In figure 3.1 the lay-out of the nonlinear simulation model in block diagrams is presented. Corresponding with the relatively simple drive train of the Stan Tug 1205, the simulation model exists out of a governor, fuel actuator, diesel engine, gearbox, shaft loop and propeller (FPP). Equation (2.1) to (2.12) show the differential and algebraic equations (DAE) of the Stan Tug 1205 in bollard pull condition. Important to note is that the nonlinear model does not contain any limiters, such as upper and lower limits for engine brake power, engine speed and amount of fuel injection. Besides, ramp rates and other nonlinear software of the governor are also not present in this model structure.
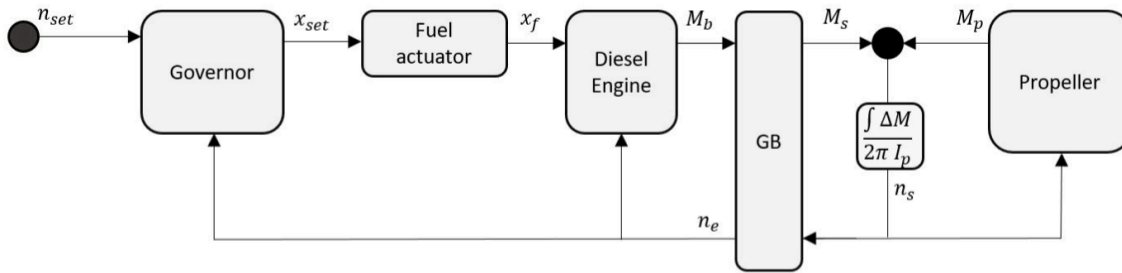
Figure 2.3: Nonlinear simulation model of the Stan Tug 1205 [1].

$$2\pi \cdot I_p \frac{d(n_s)}{dt} = M_s - M_p \tag{2.1}$$

$$e_n = n_{set} - n \tag{2.2}$$

$$E_n = \int_0^t e_n dt \tag{2.3}$$

$$X_{set} = K_p e_n + K_i E_n \tag{2.4}$$

$$X_f = X_{set} \tag{2.5}$$

$$M_b = A_1 X_f + A_2 n_e + A_3 \tag{2.6}$$

$$M_s = M_b i_{gb} \eta_{trm} \tag{2.7}$$

$$n_e = n_s i_{gb} \tag{2.8}$$

$$Q = D_p^5 \rho n_s^2 K_Q(J) \tag{2.9}$$

$$T = D_p^4 \rho n_s^2 K_T(J) \tag{2.10}$$

$$M_p = \frac{Q}{\eta_r} \tag{2.11}$$

$$J = \frac{v_a}{n_s D_p} \quad with \quad v_a = 0 \tag{2.12}$$

The shaft loop is described by a first order differential, presented in equation (2.1). The shaft loop is dependent on the moment of inertia, the shaft speed and the balance between the shaft and the static propeller torque.

The governor is described by equation (2.2) to (2.4). The governor is modelled by a proportional-integral (PI) controller and is dependent on the engine speed error. The error is calculated in equation (2.2) between the engine speed set point and the actual engine speed. In equation (2.4) the error e_n is multiplied with the proportional gain K_p and the time integrated error E_n with the integral gain K_i, calculating a fuel rack set point X_{set}. It is important to note that it is unknown if the Stan Tug 1205 is equipped with a PI or PID controller with or without limiters.

The fuel actuator is described by equation (2.5). The function of the fuel actuator is making sure that the fuel enters the cylinder which most of the time is done under high pressure and thus assumed to be very fast. The output of the governor X_{set} determines the amount of fuel, the fuel actuator actuates X_f. The fuel actuator is assumed to work under ideal conditions, the dynamics are neglected and the fuel actuator will work infinitely fast. This assumption is made because it is expected that the time constant of the actuator is very small compared to the full shaft speed loop.

The diesel engine is described by a fuel rack map shown in equation (2.6). A fuel rack map shows the relation between the fuel rack, engine speed and engine torque. Therefore, the engine brake torque is dependent on the fuel rack and the engine speed. The engine brake torque is in relation with the shaft torque, gearbox ratio and gearbox efficiency which is shown in equation (2.7). The approach of modelling a diesel engine with a fuel rack map is a very simplified method.

The propeller is modelled and described by equation (2.9) to (2.12). A backward bollard push condition is taken into account, therefore the ship speed is zero. A ship speed equal to zero means that J is equal to zero, see equation (2.12). This causes the torque and thrust to become constant and only dependent of the shaft speed multiplied by a few constants. With the relative rotative efficiency, the propeller torque is calculated, see equation (2.11).

2.4. Linear Model

In this section the linearised model of the nonlinear model presented in section 2.3 is discussed. The linearisation is performed by Martinus [1] and is based on the linearisation of Vrijdag and Stapersma [7][8]. The linearisation of Vrijdag and Stapersma [7][8] is applicable for free sailing conditions. Martinus [1] linearised the model for bollard pull condition. This linearised model is used as model structure for system identification. The linear DAE of the model are shown in equation (2.13) to (2.23). The equations are normalised and this is mathematically noted as *.

$$\tau_n \frac{dn^*}{dt} = \delta M_s^* - \delta M_p^* \tag{2.13}$$

$$\frac{dE_n^*}{dt} = \delta n_{set}^* - \delta n^* \tag{2.14}$$

$$\delta E_n^* = \int_0^t \delta e_n^* dt \tag{2.15}$$

$$\delta X_{set}^* = K_p \delta e_n^* + K_i \delta E_n^* \tag{2.16}$$

$$\delta X_f^* = X_{set}^* \tag{2.17}$$

$$\delta M_b^* = g \delta n^* + v \delta X_f^* \tag{2.18}$$

$$\delta M_s^* = \delta M_b^* \tag{2.19}$$

$$\delta Q^* = 2 \delta n^* \tag{2.20}$$

$$\delta M_p^* = \delta Q^* \tag{2.21}$$

$$\delta T^* = 2 \delta n^* \tag{2.22}$$

The linearised and normalised shaft loop is described by equation (2.13). The integration constant τ_n is added to the model. This constant is dependent on the operating point and the mass moment of inertia. The constant τ_n can be determined with equation (2.23).

$$\tau_n = \frac{2\pi I_p n_0}{M_{s,0}} \tag{2.23}$$

The fuel actuator is still an ideal actuator, see equation (2.17). The linear and normalised governor is represented by equation (2.14) to (2.16). The governor is still described by a PI controller and dependent on the engine speed error.

The diesel engine is still described by a fuel rack map. Equation (2.18) shows the linearised and normalised description of the diesel engine. The parameter A_3 disappeared and the parameters A_1 and A_2 are replaced with respectively g and v. The definition of the parameters g and v is shown in equation (2.24) and (2.25). The parameter g represents the influence of an increase in engine speed on the engine torque multiplied by the linearisation point. Where v represents the influence of an increase in the fuel rack on the engine torque multiplied by the linearisation point. The transmission efficiency is constant, therefore the normalised shaft torque is equal to the normalised brake torque, see equation (2.19).

$$g \equiv \frac{n_{e,0}}{M_{b,0}} \frac{\delta M_b}{\delta n}\bigg|_X \tag{2.24}$$

$$v \equiv \frac{X_0}{M_{b,0}} \frac{\delta M_b}{\delta X}\bigg|_n \tag{2.25}$$

The propeller is linearised and normalised for the backward bollard push condition, see equation (2.20) to (2.22). Quadratic coefficients become a linear multiplier when they are linearised. This is visible in the equation 2.20 and 2.22 of the linearised torque and thrust. The relative rotative efficiency is assumed to be constant, therefore the propeller torque is equal to the linearised torque δQ^*.

2.4.1. Transfer Functions

A transfer function is a mathematical description of theoretical models representing the possible relations between input and output. The closed loop transfer functions are derived from the linear DAE by Martinus [1]. The input of each transfer functions is the engine speed set point, the outputs are respectively engine speed, integrated error and the shaft torque. The transfer functions of the linearised model are presented in equation (2.26) to (2.28).

$$\frac{\delta n^*}{\delta n^*_{set}} = \frac{\frac{vK_p}{\tau_n}s + \frac{vK_i}{\tau_n}}{s^2 + \frac{vK_p - g + 2}{\tau_n}s + \frac{vK_i}{\tau_n}} \tag{2.26}$$

$$\frac{\delta E_n^*}{\delta n^*_{set}} = \frac{s + \frac{2-g}{\tau_n}}{s^2 + \frac{vK_p - g + 2}{\tau_n}s + \frac{vK_i}{\tau_n}} \tag{2.27}$$

$$\frac{\delta M^*}{\delta n^*_{set}} = \frac{vK_p s^2 + \frac{vK_i\tau_n + 2vK_p}{\tau_n} + \frac{2vK_i}{\tau_n}}{s^2 + \frac{vK_p - g + 2}{\tau_n}s + \frac{vK_i}{\tau_n}} \tag{2.28}$$

All three the transfer functions are subjected to the lowest and highest frequencies to see if the response is logic. These tests are performed by Martinus [1]. The frequencies that are used for these tests are 0 and ∞. All three transfer functions showed a logic response. The results of subjecting the transfer functions to the extreme frequencies 0 and ∞ are presented in table 2.4. The results are presented as absolute value and in decibels.

Table 2.4: Overview of responses of the closed loop transfer functions subjected to extreme frequencies

Relation	$s \to 0$ [abs]	$s \to \infty$[abs]	$s \to 0$ [dB]	$s \to \infty$[dB]
$\frac{\delta n^*}{\delta n^*_{set}}$	1	0	0	$-\infty$
$\frac{\delta E_n^*}{\delta n^*_{set}}$	$\frac{2-g}{vK_i}$	0	$\log(\frac{2-g}{vK_i})$	$-\infty$
$\frac{\delta M^*}{\delta n^*_{set}}$	2	vK_p	0.3	$\log(vK_p)$

2.4.2. State Space Notation

A mathematical representation of a physical system as a set of input, output, and state variables related by first-order differential equations can be created with a state space notation [9]. State space notations can be written in different ways. The continuous time invariant state space notation is shown in equation (2.29) to (2.30).

$$\dot{\bar{x}} = A\bar{x} + B\bar{u} \tag{2.29}$$

$$\bar{y} = C\bar{y} + D\bar{u} \tag{2.30}$$

Vector $\bar{x}$ represents the state vector, $\bar{u}$ the input vector and $\bar{y}$ the output vector. Where matrix A is state matrix, B is the input-to-state matrix, C is the output-to-state matrix and D is the feedthrough matrix [9]. With a state space notation it is possible to represent different inputs and outputs, creating a model with multiple in- and/or outputs. With the linearised DAE the following state space is derived by Martinus [1]. The continuous time invariant closed loop state space of the linearised model is shown in equation (2.31) to (2.33). The closed loop state space notation has one input, two different outputs and two states. The closed loop state space notation is used by Martinus [1] as model structure for full-scale linear system identification.

$$\bar{x} = \begin{bmatrix} \delta n^* \\ \delta E_n^* \end{bmatrix}, \quad \bar{u} = \delta n_{set}^*, \quad \bar{y} = \begin{bmatrix} \delta n^* \\ \delta M_s^* \end{bmatrix} \tag{2.31}$$

$$A = \begin{bmatrix} \frac{-(2-g+vK_p)}{\tau_n} & \frac{vK_i}{\tau_n} \\ -1 & 0 \end{bmatrix}, \quad B = \begin{bmatrix} \frac{vK_p}{\tau_n} \\ 1 \end{bmatrix} \tag{2.32}$$

$$C = \begin{bmatrix} 1 & 0 \\ g - vK_p & vK_i \end{bmatrix}, \quad D = \begin{bmatrix} 0 \\ vK_p \end{bmatrix} \tag{2.33}$$

In the state space notation, five different parameters are visible. For an identification it will be needed to estimated these parameters. However, with the presented closed loop model structure it is not possible to identify all five parameters. Martinus [1] already investigated this matter and concluded that there are dependencies in the closed loop model structure. These dependencies cause that not all parameters can be identified individual. The four relations that will be identified during a system identification are shown in equation (2.34).

$$\begin{bmatrix} \tau_n & g & \frac{K_p}{K_i} & vK_p \end{bmatrix} \tag{2.34}$$

2.5. Searching Criterion

Three things are needed for system identification. One of them is the searching criterion. Different searching criterion are discussed within the performed literature research [6]. The basic principle of the searching criterion is as followed. The searching criterion is the method of minimizing a certain cost function based on a parameter set and a defined error. Minimizing the cost functions means that the output of the system and model structure will converge. Ideally, the end product is a dynamic model with a set of identified parameters that imitates the behaviour of a system.

The system identification is performed with the help of the Matlab System Identification Toolbox. The searching criterion is chosen by the software itself. This means that the System Identification Toolbox chooses the searching criterion method to determine a minimum. The methods that can be selected and used are the subspace Gauss Newton Least Squares (GNLS), Levenberg Marquard Least Squares (LMLS) and the Matlab function 'fmincon' [10]. Different options can be turned on within the System Identification Toolbox to increase the quality of the identification. The benchmark system identification is performed with the state space notation presented in section 2.4.2, which has two outputs. To prevent that the cost function only optimises for on single output, an output weight is added. This addition translates the cost function into a weighted cost function [10]. To prevent overestimation or over fitting of the parameters during the system identification, the cost function is extended with a regularization term [10].

To preclude that the searching criterion runs for a very long time in search for the ideal zero optimum, stopping criteria are used to constraint the benchmark identification. An easy way of constraining an identification is the addition of a maximum amount of iteration steps. For the benchmark identification of Martinus [1] a maximum of 100 iterations per identification is added as stopping criteria. To avoid that the minimum is already found during these 100 iterations or that the improvement steps become extremely small, a tolerance is used as stopping criteria. The tolerance is set to 0.01 percentage difference between the current value of the cost function and the expected improvement of the next iteration.

Boundaries of parameters are also introduced to prevent that the searching criterion searches for an optimum for a very long time. The boundary conditions of the parameters that will be identified are presented in the equations (2.36) to (2.40). The initial values of the parameters that are required for the searching criterion are presented in (2.35). The boundaries conditions and the initial values are determined by Martinus [1].

$$\begin{bmatrix} \tau_n & K_p & K_i & g & v \end{bmatrix} = \begin{bmatrix} 1.2 & 10 & 3 & -0.5 & 1 \end{bmatrix} \tag{2.35}$$

$$0 < \tau_n \leq 5 \tag{2.36}$$

$$0 < K_p \leq 15 \tag{2.37}$$

$$0 < K_i \leq 10 \tag{2.38}$$

$$-3 \leq g < 0 \tag{2.39}$$

$$0 < v \leq 5 \tag{2.40}$$

2.6. Benchmark Identification

The benchmark system identification performed by Martinus [1] is used for comparison. The three necessities to perform a system identification are discussed: model structure, data and a searching criterion. As model structure the state space notation in section 2.4.2 is used. As searching criterion and optimisation principles the methods presented in section 2.5 are used. The benchmark system identification with the best fit is performed with frequency domain data of the multiple sine waves experiment, discussed in section 2.2. The best fit is selected based on the fitting percentage. In equation (2.41) is shown how the fitting percentage is obtained in frequency domain. The calculations can also be done for identification in time domain. The fitting percentage is an automatic generated value by the System Identification Toolbox of Matlab. The 2-norm (root mean square) of the differences between measurement points and simulated points are used to calculated the fitting percentage.

$$FitPercentage = 100(1 - \frac{||\hat{y}(\omega)_{measured} - \hat{y}(\omega)_{simulated}||_2}{||\hat{y}(\omega)_{measured} - \hat{y}(\omega)_{MeanMeasured}||_2}) \tag{2.41}$$

The estimated relations of the benchmark identification are shown in table 2.5. Martinus [1] concluded that the estimated parameters of the propulsion system are not trustworthy. The values differed from the expected results and different parameter estimations showed large differences. However, the behaviour of the identified model showed promising agreement with the system [1]. The comparison of the processed frequency domain data of [1] and identified benchmark model is shown in figure 2.4. Up to a frequency of 10 [rad/s] they compare well.

Table 2.5: Results of benchmark identification with frequency domain data

	Parameters				Fitting	
	τ_n [s]	g [-]	$\frac{K_p}{K_i}$ [-]	vK_p [-]	δn^* [%]	δM_s^* [%]
Benchmark	0.275	-0.314	0.0010	0.010	55.2	20.81

(a) $\frac{\delta n^*}{\delta n^*_{set}}$ (b) $\frac{\delta M_S^*}{\delta n^*_{set}}$
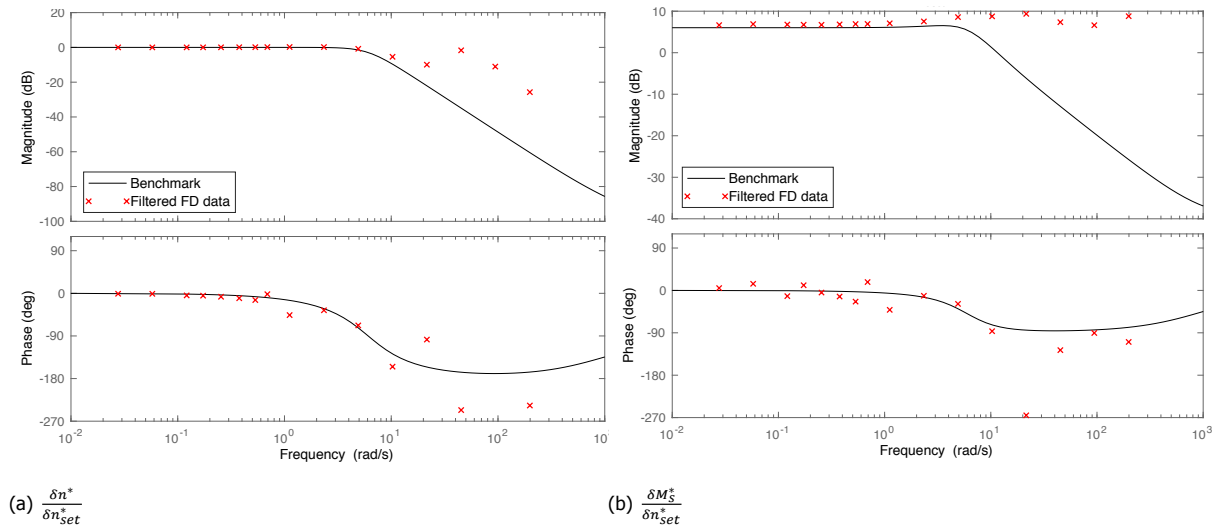
Figure 2.4: Bode plots of the relations $\frac{\delta M_S^*}{\delta n^*_{set}}$ and $\frac{\delta n^*}{\delta n^*_{set}}$ with the benchmark and the frequency domain data obtained by Martinus [1].

3

Data Processing & Improvements

In this chapter data processing and possible data improvements will be discussed. This chapter contains five main sections. In the first main section the revised pre-processing of the raw JVS measurements are discussed. Thereafter, in the second main section, certain analysis of the data are performed. In the third main section, frequency domain data of the multiple sine waves experiment is discussed. A new filtering approach is introduced and the noise variance is evaluated. In the fourth main section, the revised pre-processed and normalised data sets that will be used for system identification, comparisons and validation are presented. This chapter ends with an overview of the most important conclusions and findings.

The raw JVS measurements used for the data processing and improvements are the shaft torque M_s, the three pulse time modulation measurements and the engine speed set point voltage $U_{setpoint}$.

3.1. Pre-processing

In this first main section the revised pre-processing of Martinus [1] is of the measured raw data from the backward bollard push experiment is explained. Pre-processing the raw measured data is performed to create usable data sets for the system identification. The measured JVS data is in raw form, which is not convenient for system identification.

First, the three different PTM measurements are translated from pulse measurement to rpm. The raw data of JVS contains the PTM measurements of the measured one pulse engine speed, one pulse shaft speed and the four pulse shaft speed. The PTM measurements are converted to pulse periods with the Matlab function 'pulseperiod'[11]. A pulse period is the time between two increasing edges of pulses [11]. With the Matlab function, the pulse periods for the one pulse measurement T_{p1}, four pulse measurement T_{p4} and the engine speed T_{pe} are determined. One pulse period of T_{p1} and T_{pe} and four pulse periods of T_{p4} equal one rotation of the shaft. The equations in (3.1) show the conversion of the measurements to engine speed in rpm, with the help of calculated pulse periods.

$$n_e = \frac{60}{T_{pe}}, \quad n_{e,4} = \frac{i_{gb} \cdot 60}{T_{p4} \cdot 4}, \quad n_{e,1} = \frac{i_{gb} \cdot 60}{T_{p1}} \tag{3.1}$$

The engine speed set point is measured in voltage and needs to be converted to rpm. To make a conversion the relationship between voltage and engine speed is necessary. When the engine speed set point and the engine speed are constant, located in the step response experiment, this relationship can be determined. The average is taken of the constant measurements to cancel out oscillations. Table 3.1 shows the averaged relationships and in figure 3.1 the points are plotted with a trendline.

Table 3.1: Relationship between input signal and engine speed.

$U_{setpoint}$ [V]	n_{set} [rpm]
-3.031	676.57
-4.031	927.94
-5.035	1182.60
-6.024	1428.50
-7.022	1676.61
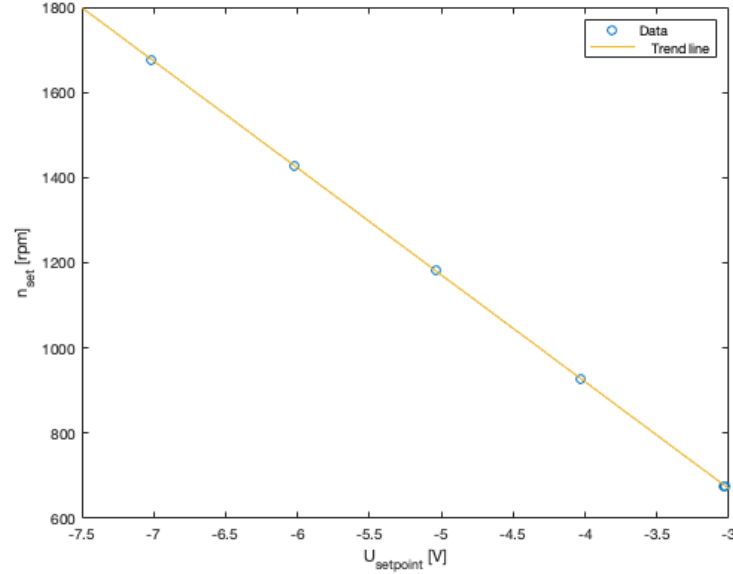
Figure 3.1: Engine speed as function of input voltage with trend line.

In figure 3.1 shows a linear relationship, therefore a linear function $n_{set} = a * U_{setpoint} + b$ can be derived. Using the trendline drawn in figure 3.1, the characteristics of this linear function are determined. Equation (3.2) shows the linear function used for the conversion of the engine speed set point from voltage to rpm.

$$n_{set} = -250.97 \cdot U_{setpoint} - 83.467 \qquad (3.2)$$

Furthermore, using the interpolation function "interp1" of Matlab all in- and output data sets are down sampled [12]. The down sampling is performed for different reasons. First, to reduce the amount of computer memory needed. Second, to speed up the parameter estimation. The JVS raw data is down sampled from 2000 Hz to 200 Hz. Interpolation of data can be performed with different methods [12]. For the interpolation of the JVS data, a previous neighbour interpolation is used. "The interpolated value at a query point is the value of the previous sample grid point" [12].

Multiple outliers are visible in the data sets of the shaft torque and engine speed set point measurements. The outliers are eliminated manually and a new point is inserted by taking the average of neighboring points. In figure 3.2, the pre-processed torque and engine speed set point measurements are shown with the removed outliers.
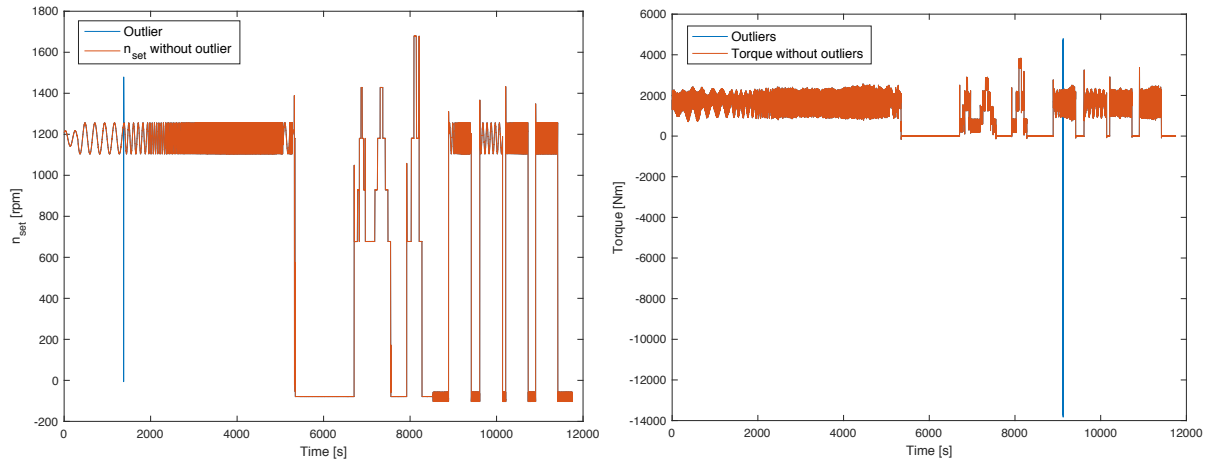
(a) Overview of the removed outliers in engine speed set point.

(b) Overview of the removed outliers in the torque response.

Figure 3.2: Overview of removed outliers in the revised pre-processed data before normalisation.

The system identification will be performed in a linear environment. The model structure is linearised, therefore a normalisation of the data sets is required. The normalisation points from a stable time period while running at constant is $U_{setpoint}$ = -5 [V]. The corresponding normalisation values are shown in table 3.2. The data sets of the different experiments after the revised pre-processing and normalisation are presented in section 3.4.

Table 3.2: Normalisation points of logging device of JVS [1].

Unit	Value
n_0 [rpm]	1183.8
$M_{s,0}$ [Nm]	1725

3.2. Data Analysis

In the second main section the analyses of the measured data sets are discussed. Martinus [1] stated that the measured data contains a time delay and that the PTM_4 measurement contains a rpm error. First, the time delay will be evaluated. Thereafter, the rpm error is investigated.

3.2.1. Time Delay

A time delay is visible between the input and output data, see figure 3.3. However, the magnitude of this time delay is unknown. It is possible to approximate the time delay with the help of the step response experiment. The step response is used to compare the engine speed set point n_{set} and the engine speed n_e. The step responses of the engine speed set point n_{set} and the engine speed n_e are shown in figure 3.3. Figure 3.3b zooms in on one single step to see the time delay that is present. The time difference of each step of the step response is determined, shown in table 3.3. The average of Δn is taken to approximate the time delay between the in- and output of the measured data sets. The time delay from the measured data is approximated at 0.4018 [s].

Table 3.3: Time differences per step of step response.

Step	n_{set} [s]	n_e [s]	Δn [s]
1	58.9100	59.2500	0.34
2	119.5050	119.8450	0.34
3	178.5950	179.0400	0.445
4	239.0450	239.5300	0.485
5	298.6950	299.0600	0.365
6	358.5850	359.0200	0.435
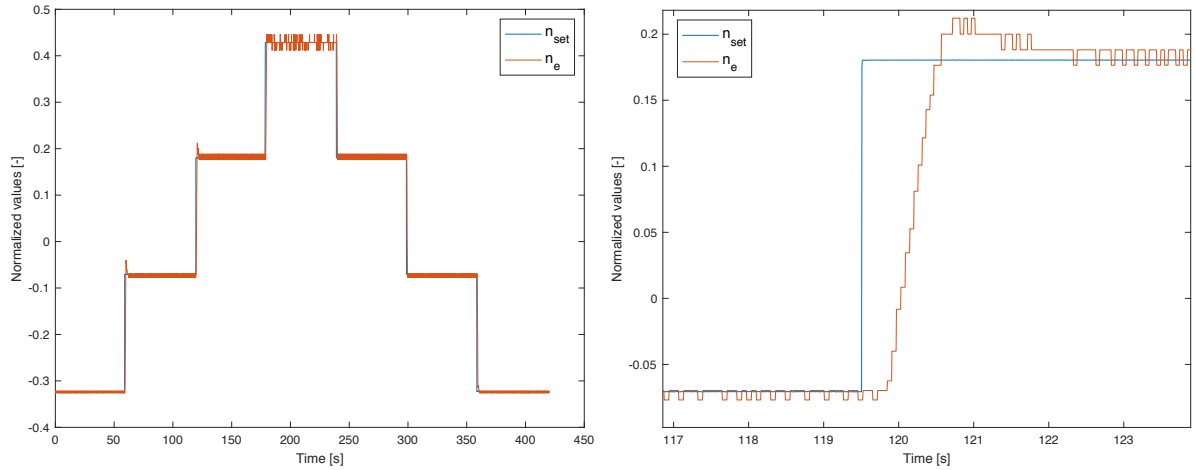
(a) Overview of step responses   (b) Step responses zoomed in.

Figure 3.3: Overview of normalised step responses of the input engine speed set point n_{set} and the output engine speed n_e.

3.2.2. Rpm Error

A possible error is present in the four pulse measurement PTM_4, inducing a rpm error. For this measurement four reflecting strips are glued on the shaft. This set-up is visible in figure 3.4. Ideally, the angles a, b, c and d are 90 degrees. However, these strips are glued on the shaft manually, which could cause that the angles are not exactly 90 degrees. This could provoke an error in the four pulse measurement and therefore in the pre-processed rpm data of $n_{e,4}$.
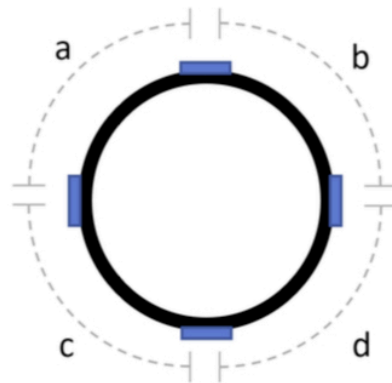
Figure 3.4: Set-up of the reflecting strips on a shaft with the four angles a, b, c and d [1].

From the papers of Resor *et al.* [13] and Braut *et al.* [14], a method is obtained to determine the rpm error. A location is selected where the measured rpm is constant, which is present in the step response. Ideally, when the rpm is constant the pulse periods of PTM_4 are constant too. However, the pulse periods of PTM_4 are not constant. With the help of the 'pulseperiod' function of Matlab, the pulse periods at a constant rpm are determined [11]. Equation (3.3) shows how the pulse periods for each reflection strip are obtained, with x indicating angle a, b, c or d. Furthermore, equation (3.4) shows the time needed for one rotation per reflection strip. The mean is taken to determine the average time needed for the shaft to rotate one time. With the average time needed for one rotation and the different pulse periods per reflection strip, each angle of the different reflection strips can be calculated. When a large amount of pulses is used, the angle calculated converges to the actual angle of the reflecting strips. Besides, the influence of noise in the measurement is then minimised. The actual angle of the reflecting strips is obtained with equation (3.5).

$$T_{\overline{Pulse},x}[s] = Pulse(x+1) - Pulse(x) \tag{3.3}$$

$$t_{\overline{onerotation},x}[s] = Pulse(x+4) - Pulse(x) \tag{3.4}$$

$$Angle_x[°] = mean\left(\frac{T_{\overline{Pulse},x}}{mean(t_{\overline{onerotation},x})}\right) \cdot 360° \tag{3.5}$$

The results always converged to the same angles for different constant measurements. The determined angles of the different reflection strips are shown in table 3.4. The differences between the angles are relatively small. Due to relatively small differences, the error is appointed as acceptable and therefore not removed from the four pulse four pulse measurement PTM_4.

Table 3.4: Overview of different angles of the reflection strips glued to the shaft.

Angle a	90.40°
Angle b	87.24°
Angle c	90.74°
Angle d	91.64°

3.3. Frequency Domain Data

In the third main section the conversion of the multiple sine waves data from time domain to frequency domain are discussed. First, the advantages of converting data from time domain to frequency domain are presented. Thereafter, the transformation of time domain data into frequency domain is discussed and what approach Martinus [1] used. Moreover, a new approach that selects the correct frequencies out of data sets is presented. This section ends with a noise variance evaluation of the multiple sine waves data in frequency domain.

In previous figures of the experimental data, the multiple sine waves were presented in time domain. Converting time domain data of the multiple sine waves into frequency domain provides different advantages. The response data, the engine speed and shaft torque, contain noise. In frequency domain it is possible to cancel out the noise at the frequencies where the sines have no power, influencing the system identification in a positive manner. Moreover, by cancelling out the noise, the data becomes more clean but also less computer memory is required. Another advantage is, the frequency domain data speeds up the system identification, mainly because the measured time domain data sets have a high sample rate.

As already stated in section 2.2, Martinus [1] used an algorithm that selects the highest amplitude peak of the data in frequency domain. For this filtering approach, the Matlab function 'SineFit' is used. This function is obtained from the Matlab file exchange [15]. The selected data is fitted into a single sine wave without noise with the help of the obtained offset, amplitude, frequency and phase shift [15]. Due too determination of the offset, which serves as the normalisation point of each frequency, it is not necessary to normalise the multiple sine waves data before it is put into frequency domain.

The 'SineFit' function first converts the measured time domain data to frequency domain and thereafter cancels out the noise by selecting the data point with the highest amplitude peak. The offset, amplitude, frequency and phase shift are obtained from the highest amplitude peak. The obtained points with the highest amplitude are used for system identification in frequency domain. However, wrong data points are selected when the noise at any frequency exceeds the amplitude of the linear response to the input signal at the frequency of interest. For most of the sine waves experiments this 'SineFit' filtering approach is accurate, but unfortunately for some experiments the wrong data in frequency domain are selected. The following section presents a new selecting procedure used to select the correct data points in frequency domain.

3.3.1. Selection Procedure

The new procedure calculates the correct frequencies to be selected. The method is a Gaussian approach that makes it possible to select the frequency of interest out of the measured sine waves data sets. The new selection procedure is incorporated in the 'SineFit' function instead of the maximum amplitude procedure. The input frequencies, starting time and stopping time of the different sine waves are known. From each sine waves experiment the location of the frequency of interest can be calculated when the length of the experiment is known. The frequencies of interest are the input frequencies of the measured data.

Equations (3.6) to (3.8) are used to determine the location of the frequency of interest in a frequency domain vector. ω_s in [rad/s] is the frequency of interest (fundamental frequency). Variable i is the location of the fundamental frequency in the frequency domain vector of a certain sine waves experiment. T is the length of the experiment in seconds and ω_0 [rad/s] is the smallest frequency that fits in the total length of a certain sine wave experiment. It is important that i integer is, meaning that the length of each sine waves experiment fits a round amount of periods of the fundamental frequency. First, equations (3.6) and (3.7) are used with the initial length of the sine waves experiments to calculate i. Thereafter, the calculated values of i are rounded to the nearest lower value (floor value). With equation (3.8) the new decreased value of T is calculated.

$$\omega_s = i \cdot \omega_0 \tag{3.6}$$

$$\omega_0 = \frac{2 \cdot \pi}{T} \tag{3.7}$$

$$T = i_{floor} \cdot \frac{2\pi}{\omega_s} \tag{3.8}$$

When knowing i, the points to be selected in the frequency domain vector of each sine waves experiment are known. The adjusted 'SineFit' function cancels out the noise at the frequencies where the sines have no power and returns the correct obtained offsets, amplitudes, frequencies and phase shifts. The calculated values of i, the new stopping times of each sine waves experiment and the eventually selected frequencies can be seen in table 3.5. The calculated values in table 3.5 are applicable for the engine speed, shaft torque and engine speed set point measurements.

Table 3.5: Overview of calculated values with the new selection procedure.

Sine	i [-]	Selected Freq [Hz]	Start [s]	Stop [s]
S1	4	0.0044	476.9	1385.99
S2	4	0.0092	1433	1867.78
S3	6	0.0193	1962	2272.88
S4	8	0.0275	2365	2655.91
S5	11	0.0405	2735	3006.61
S6	13	0.06	3048	3264.67
S7	18	0.0848	3282	3494.26
S8	21	0.11	3540	3730.91
S9	41	0.1778	3755	3985.60
S10	65	0.3728	4009	4183.36
S11	139	0.7814	4219	4396.89
S12	211	1.637	4481	4609.89
S13	240	3.433	4630	4699.91
S14	431	7.19	4840	4899.94
S15	450	15.01	5020	5049.98
S16	632	31.644	5234	5253.97

The correct selected frequencies can be represented in a Frequency Response Function (FRF) estimation. A FRF estimation represents the system dynamics per frequency of the output data set divided by the input data set. In figure 3.5, the FRF estimation with the new frequency selection procedure is

compared to the baseline FRF estimates from Martinus [1], for both the engine speed and shaft torque as output and the engine speed set point as input. The figure suggests that the new frequency selection procedure is the better selecting approach because it has logical gradients and no strange outliers. The methods are approximately the same for lower frequencies. However, at higher frequencies the new frequency selection procedure becomes more accurate.

(a) $\frac{\delta n^*}{\delta n^*_{set}}$

(b) $\frac{\delta M^*_S}{\delta n^*_{set}}$
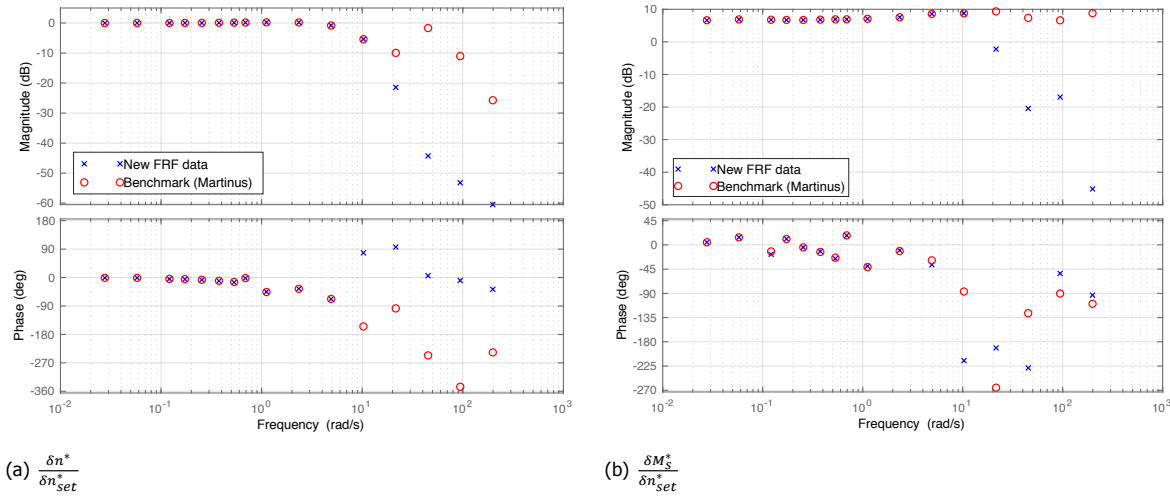
Figure 3.5: Comparison in Bode plot of the FRF estimation with the new frequency selection procedure and the baseline FRF estimates from Martinus [1].

3.3.2. Noise Variance

The data analysis of the torque performed by Martinus [1] showed that the noise present in the torque measurement is correlated to engine and propeller frequencies. The other data sets also contain noise in their measurements. Large amounts of noise cause a decrease of the reliability of a measurement, therefore increasing the uncertainty. It is possible to express the reliability of a measurement with the help of the signal to noise ratio (SNR). The SNR is calculated with the help of the variance. The power spectral density is used to calculate the different variances.

Overall Noise Variance

The overall SNR of each measured data set is calculated with the help of the frequency domain data of the multiple sine waves experiment. An overall SNR is calculated between the variance of the selected data points (X_{Signal}) and the variance of the unfiltered frequency domain data ($X_{overall}$). Ideally, when no noise is present, the calculated overall SNR is equal to 1. The closer the overall SNR gets to 0, the higher the amount of noise is. It is expected that the noise in the measured data influences the obtained fitting percentage during system identification. The overall SNR is rooted to make it comparable with the fit percentage that is calculated by Matlab after each system identification. The fit percentage is calculated with a root mean square and the variance is quadratic. When the overall SNR is lower than 1, the fitting percentage cannot become 100%. Table 3.6 shows the overall signal to noise ratio of each data set, calculated with equation (3.9).

$$SNR_{Overall} = \sqrt{\frac{\sum Var(X_{Signal})}{Var(X_{Overall})}} \tag{3.9}$$

Table 3.6: Overall signal to noise ratios of each data set.

Data Set	$SNR_{Overall}$
n_{set}	0.9986
n_e	0.9451
n_{e1}	0.9475
n_{e4}	0.8610
M_s	0.5751

Noise Variance per Input Frequency

The SNR per input frequency is calculated to obtain the quality of each sine waves experiment per data set. Only local points in the frequency domain vector around the selected frequencies are taken into account as noise. Local frequencies around the selected frequency, mostly influence the quality of the selected frequency signals. Before and after the selected frequency signal, 20 points in the frequency domain vector are taken into account as local noise. Variance of a selected signal (X_{Signal}) is divided by the variance of the local noise (X_{Local}), creating a local SNR per experiment and data set. Ideally, when no local noise is present, the local SNR in decibel converges to infinity. A local SNR of 0 [dB] means that the variance of the local noise is equal to the variance of the selected frequency. The boundary value of the local SNR is 3 [dB] [16]. Table 3.7 shows the local SNR in decibel of each data set and sine waves experiment, calculated with equation (3.10). The values that are higher than the boundary value are indicated green and the values lower than the boundary value are indicated red.

$$SNR_{Local}[dB] = 10 \cdot \log_{10} \left(\frac{Var(X_{signal})}{Var(X_{Local})} \right) \tag{3.10}$$

Table 3.7: Local signal to noise ratio per data set and sine waves experiment.

Sine	SNR [dB]				
	n_{set}	n_e	n_{e1}	n_{e4}	M_s
S1	57.8	40.6	40.6	40.6	18.4
S2	59.2	40.4	40.5	40.1	25.3
S3	59.7	44.9	45.2	44.9	20.7
S4	63.8	45.3	45.4	44.6	22.7
S5	68.6	45.7	45.8	44.9	23.5
S6	26.5	25.6	25.5	25.6	24.2
S7	73.6	38.0	37.8	37.9	23.6
S8	73.8	41.3	41.4	41.2	27.2
S9	59.5	38.5	38.5	38.0	34.9
S10	52.7	35.9	36.0	36.1	34.3
S11	45.7	31.9	31.7	31.8	31.9
S12	59.1	17.0	16.7	17.1	17.2
S13	49.4	7.8	-4.1	7.4	9.0
S14	43.9	-11.6	-27.3	-11.6	4.6
S15	17.5	-18.3	-13.5	-31.1	-23.9
S16	16.1	-22.4	-2.8	-30.3	-23.0

The local SNR shows when the frequency of the sine waves becomes higher, the uncertainty of the measurements becomes larger. As the boundary level is 3 [dB], it is clear the output of the sine waves experiments 14, 15 and 16 are beneath that. Still, these sine waves experiments are used for comparisons and system identification. Due to the new selection procedure in frequency domain, the correct data points are selected and these points still contain some information on response of the system. However, the high uncertainties will be included during considerations.

During the performed experiments, three times the engine speed is measured. When combining the results of the overall and local SNR, n_e (PTM_e measurement of the engine speed at the diesel engine) shows the highest overall certainty of the three engine speed measurements. Therefore, the measured data sets n_{set}, n_e and M_s are used for system identification, validation and comparison.

3.4. Data Sets

To conclude the data processing part of this research, the revised pre-processed and normalised data sets used for system identification, comparisons and validation are presented. First, the frequency domain data sets of the multiple sine waves experiment are shown. The frequency domain data sets can be obtained in closed and open loop. Thereafter, the time domain data sets are shown. The long chirp, short chirp and step response will be presented. Mainly, the frequency domain data sets will be used for system identification because the noise is cancelled out and the system identification speeds up in frequency domain.

3.4.1. Frequency Domain Data Sets

The frequency domain data sets represent the multiple sine waves experiment. The time domain measurements that are pre-processed are put into frequency domain. With the new selection procedure, the correct data point are selected and noise is mostly cancelled out of the data sets. The frequency domain data will be used in closed and open loop form. "The main difference between open loop and closed loop is, the required output within the open loop does not depend on the controlled act whereas, in closed loop, the required output mainly depends on the controlled act" [17]. The difference between open loop and closed loop models and data is shown in figure 4.1. Figure 4.1 also shows the open loop sub-models that are present.
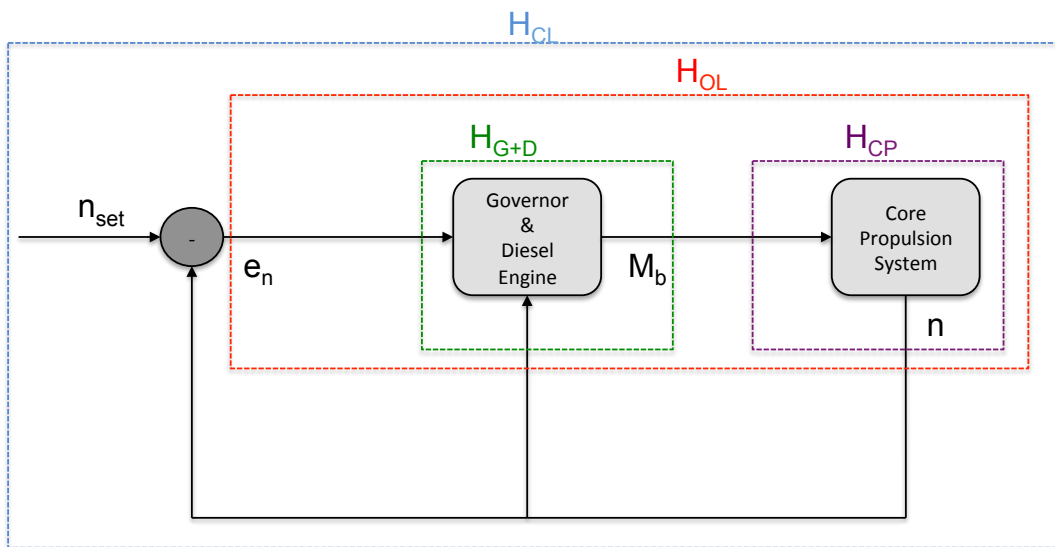
Figure 3.6: Model structure with open and closed loop sections.

Closed Loop

The closed loop frequency domain data sets are shown in figure 3.7. The input of the data sets is the engine speed set point δn_{set}^* and the outputs are the engine speed δn^* and the shaft torque δM_s^*. Clearly, the magnitude starts to decrease at approximately 10 [rad/s], for both the engine speed and shaft torque. Furthermore, the amount of measurements after 1 [rad/s] is small compared to the amount before 1 [rad/s]. The phase in figure 3.7a shows two points at approximately 90 degrees. These points can be translated -360 degrees to be located at -270 degrees. Taking this translation into account, both the phases of the engine speed and shaft torque show a decrease. The closed loop frequency domain data sets are used for linear closed loop system identification and comparisons.

(a) $\frac{\delta n^*}{\delta n^*_{set}}$ (b) $\frac{\delta M^*_s}{\delta n^*_{set}}$
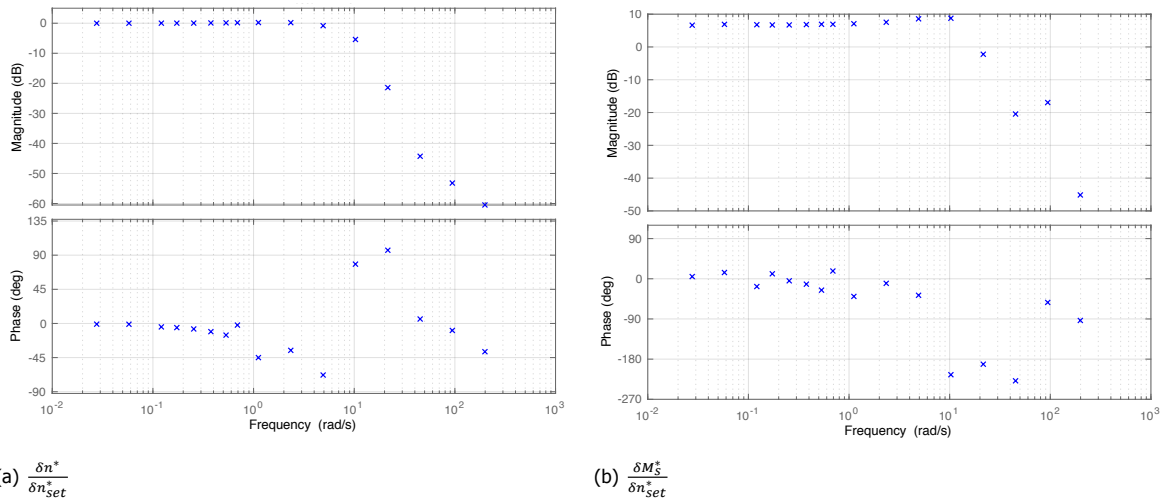
Figure 3.7: Closed loop frequency domain data for both the shaft torque and engine speed as output.

Open Loop

The open loop frequency domain data sets are shown in figure 3.8 and correspond with the open loop sub-models shown in figure 3.6. The open loop data set in figure 3.8a uses the error between the engine speed and engine speed set point δe^*_n as input and the shaft torque δM^*_s as output. This data set represents the relation between the input of the governor and the output of the diesel engine. Unfortunately, no measurements are performed between the governor and diesel engine, therefore it is impossible to obtain the response of the governor and diesel engine individually. The data set in figure 3.8b uses the shaft torque δM^*_s as input and the engine speed δn^* as output. This data set represents the response of the core propulsion system that describes the shaft loop and torque balance. The open loop frequency domain data sets are used for linear open loop system identification and comparisons.

(a) $\frac{\delta M^*_s}{\delta e^*_n}$ (b) $\frac{\delta n^*}{\delta M^*_s}$
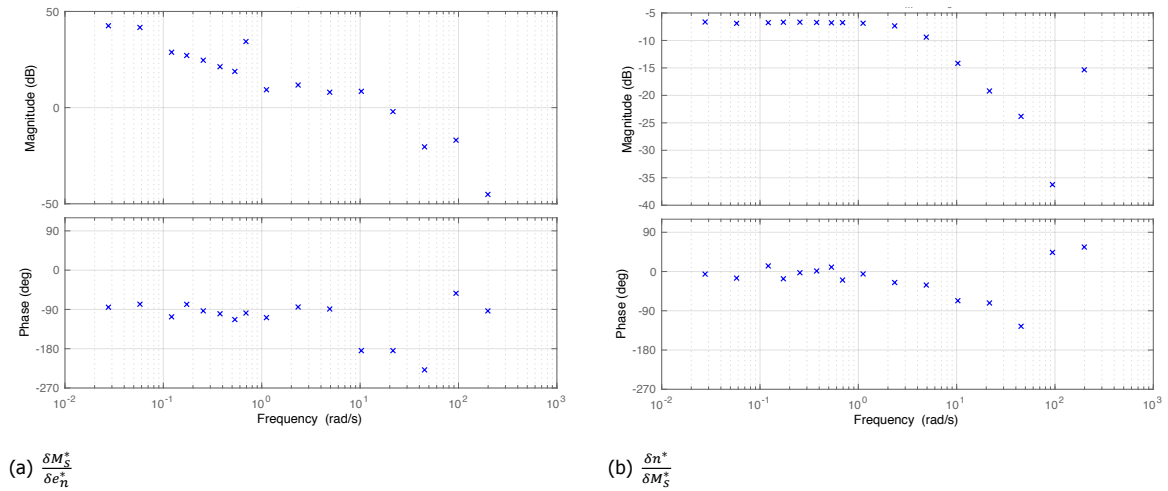
Figure 3.8: Open loop frequency domain data for both the shaft torque and engine speed as output.

3.4.2. Time domain Data Sets

The time domain data used are the long chirp, short chirp and step response. The revised pre-processing, transformed and normalised the raw time domain data into usable time domain data. However, the time domain data still contains noise which is mostly cancelled for the frequency domain data sets.

Long Chirp

The normalised and pre-processed long chirp in time domain is shown in figure 3.9, for both the engine speed and shaft torque response. The engine speed set point is also shown in the figures. Clearly a large amount of noise is present in the shaft torque response. At higher frequencies of the long chirp, the engine speed and shaft torque response are no longer able to follow the input frequencies. The normalised and pre-processed long chirp in time domain is used for linear closed loop system identification.
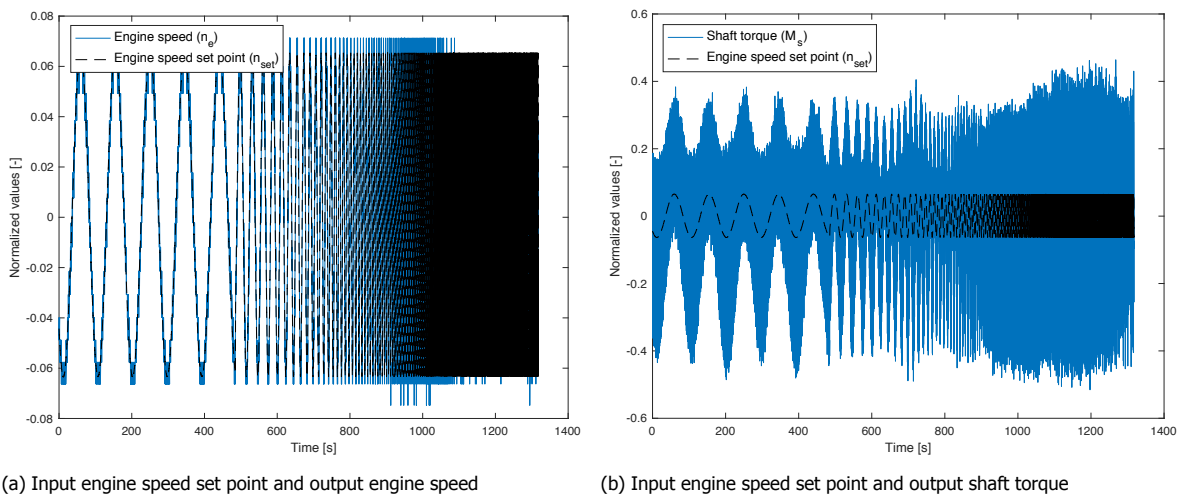
(a) Input engine speed set point and output engine speed   (b) Input engine speed set point and output shaft torque

Figure 3.9: Long chirp time domain data for both the shaft torque and engine speed as output.

Short Chirp

The normalised and pre-processed short chirp in time domain is shown in figure 3.10, for both the engine speed and shaft torque response. The engine speed set point is also shown in the figures. The short chirp is the same as the long chirp, only difference is the amount of time used to increase the frequency. The normalised and pre-processed short chirp in time domain is used for time domain validation and comparisons.
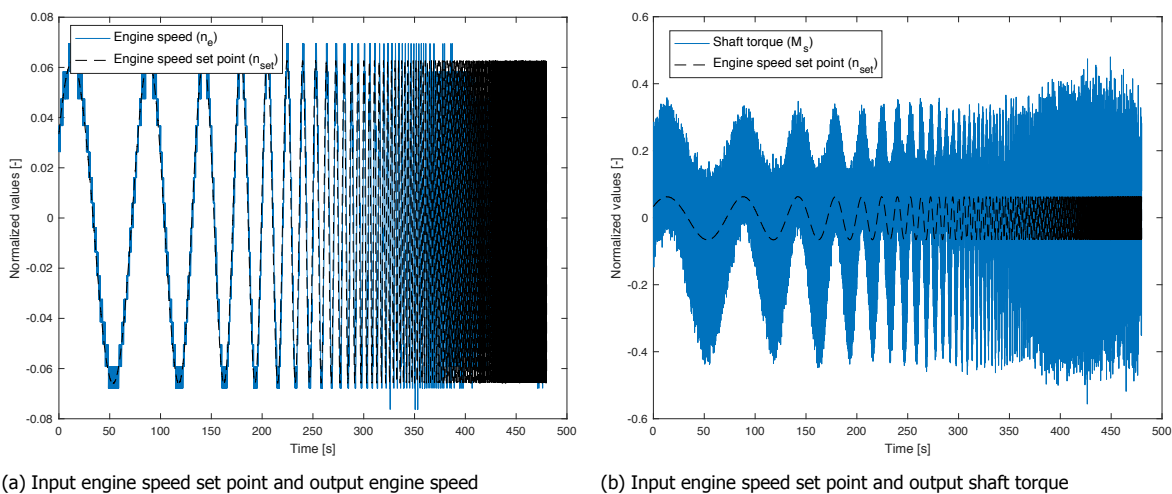
(a) Input engine speed set point and output engine speed   (b) Input engine speed set point and output shaft torque

Figure 3.10: Short chirp chirp time domain data for both the shaft torque and engine speed as output.

Step Response

The normalised and pre-processed step response in time domain is shown in figure 3.11. The measured input δn^*_{set} and the outputs, engine speed δn^* and shaft torque δM^*_s are shown. The step response presented, is indicated in table 2.3 as St2. As this step response has the least amount of disturbances it is selected. There is a difference between the increasing steps and the decreasing steps of the measured step response. This could indicate that possible nonlinear phenomena in the step response are present. The step response is used for time domain validation and comparisons.
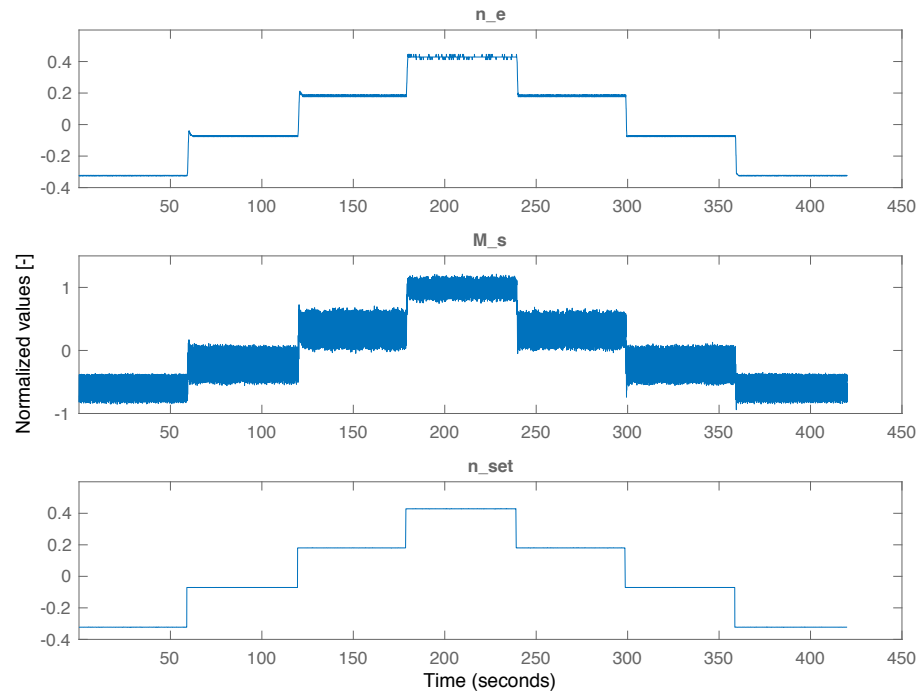
Figure 3.11: Step response time domain data of engine speed(output), shaft torque(output) and engine speed set point(input).

3.5. Overview of Conclusions

In this chapter multiple conclusions are stated. The following enumeration gives a summary of the most important conclusions and findings of the the data analysis and improvements stated in this chapter.

- The measured data contains a time delay between the input and output data, which is approximated at 0.4018 [s]. The four pulse measurement contains a rpm error. Due relatively small differences, the error is appointed as acceptable and therefore not removed from the four pulse four pulse measurement.

- The multiple sine waves data is converted from time domain to frequency domain. The new frequency selection procedure is a better selecting approach compared to the approach used by Martinus [1] because it has logical gradients and no strange outliers. The correct frequencies with corresponding information are selected and the noise is cancelled out at the frequencies where the sines have no power.

- The local SNR shows that when the frequency of the sine waves becomes higher, the uncertainty of the measurements becomes larger. The sine waves experiments 14, 15 and 16 are beneath the boundary condition but are still used for comparisons and system identification. Due to the new selection procedure, the correct data points are selected and these points still contain some information about the response of the system.

- When combining the results of the overall and local SNR, n_e (PTM_e measurement of the engine speed at the diesel engine) shows the highest overall certainty of the three engine speed measurements. Therefore, the measured data sets n_{set}, n_e and M_s are used for system identification, validation and comparison.

- The data sets used are the open and closed loop frequency domain data sets of the multiple sine waves experiment, the time domain long and short chirp data sets and the time domain step response data set. Mainly, the frequency domain data sets are used for system identification because the noise is cancelled out and the system identification speeds up in frequency domain.

- The frequency domain data of the sine waves showed that the amount of measurements after 1 [rad/s] is small compared to the amount before 1 [rad/s]. In open loop frequency domain, it is not possible to obtain the responses of the governor and diesel engine individually. No measurements are performed between the governor and diesel engine. Therefore, only the relation between the input of the governor and the output of the diesel engine can be taken into account.

4

Linear Model Analysis & Improvements

In this chapter possible improvements of the linear model structure are determined. This chapter exists out of five main sections. In the first main section, a sensitivity analysis is performed of each system parameter on the initial closed loop model. Besides, also an open loop sensitivity analysis is performed that is compared with the initial closed loop model structure response. In the second main section, a simplification of the diesel engine model is performed on the linear model structure. This simplification is applied in both closed and open loop environment. In the third main section, zooming in on the existing open loop sub-models with the simplified diesel engine model is discussed. The fourth main section, discusses the implementation of possible new terms to the model structure to improve the linear model. The chapter ends with an overview of the most important conclusions and findings.

The linear model presented in section 2.4 is used for analysis and improvement. To distinguish the different models form each other, the linear model presented in section 2.4 is referred to as *initial linear model*.

4.1. Sensitivity Analysis

The first main section discusses the sensitivity analysis of the initial linear model. A sensitivity analysis is performed to get insight in the influence of parameter variations on the model. The sensitivity analysis is executed with transfer functions and presented in frequency domain with Bode plots. Two different sensitivity analyses are carried out, closed loop and open loop. The difference between open loop and closed loop models is shown in figure 4.1. Figure 4.1 also shows the open loop sub-models of the simulation model.
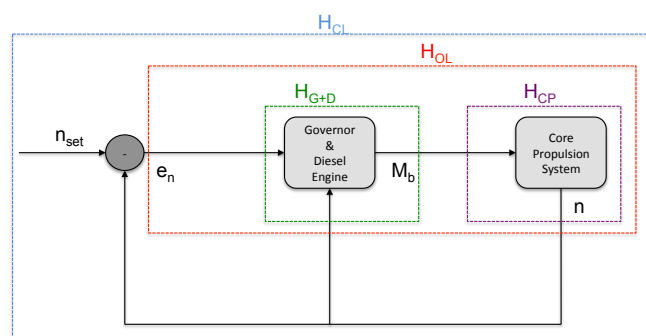
Figure 4.1: Model structure with open and closed loop sections.

The values of the parameters of the closed and open loop sensitivity analysis are varied between the upper and lower limits that are defined for the parameters[1]. The parameters that can be varied are

τ_n, K_p, K_i, g and v. The initial values used for the sensitivity analyses are presented in equation (2.35). The upper and lower limits of each parameter are shown in equation (2.36) to (2.40). These equations can be found in section 2.5.

4.1.1. Closed Loop

The response of the initial linear model is also verified by Martinus [1]. However, the influence of each parameter on the response is not yet investigated. The initial closed loop transfer functions that are used for the sensitivity analysis can be seen in equation (2.26) to (2.28). The initial closed loop model contains five parameters, τ_n, K_p, K_i, g and v. In this section only the relation $\frac{\delta n^*}{\delta n_{set}^*}$ is presented because it represents the whole closed loop system. The sensitivity analyses of the other closed loop relations of the initial linear model can be found in appendix B. In figure 4.2, the five different Bode plots for the variation of each parameter are shown.

(a) $\frac{\delta n^*}{\delta n_{set}^*}$ with K_p varying

(b) $\frac{\delta n^*}{\delta n_{set}^*}$ with K_i varying

(c) $\frac{\delta n^*}{\delta n_{set}^*}$ with τ_n varying

(d) $\frac{\delta n^*}{\delta n_{set}^*}$ with v varying

(e) $\frac{\delta n^*}{\delta n_{set}^*}$ with g varying
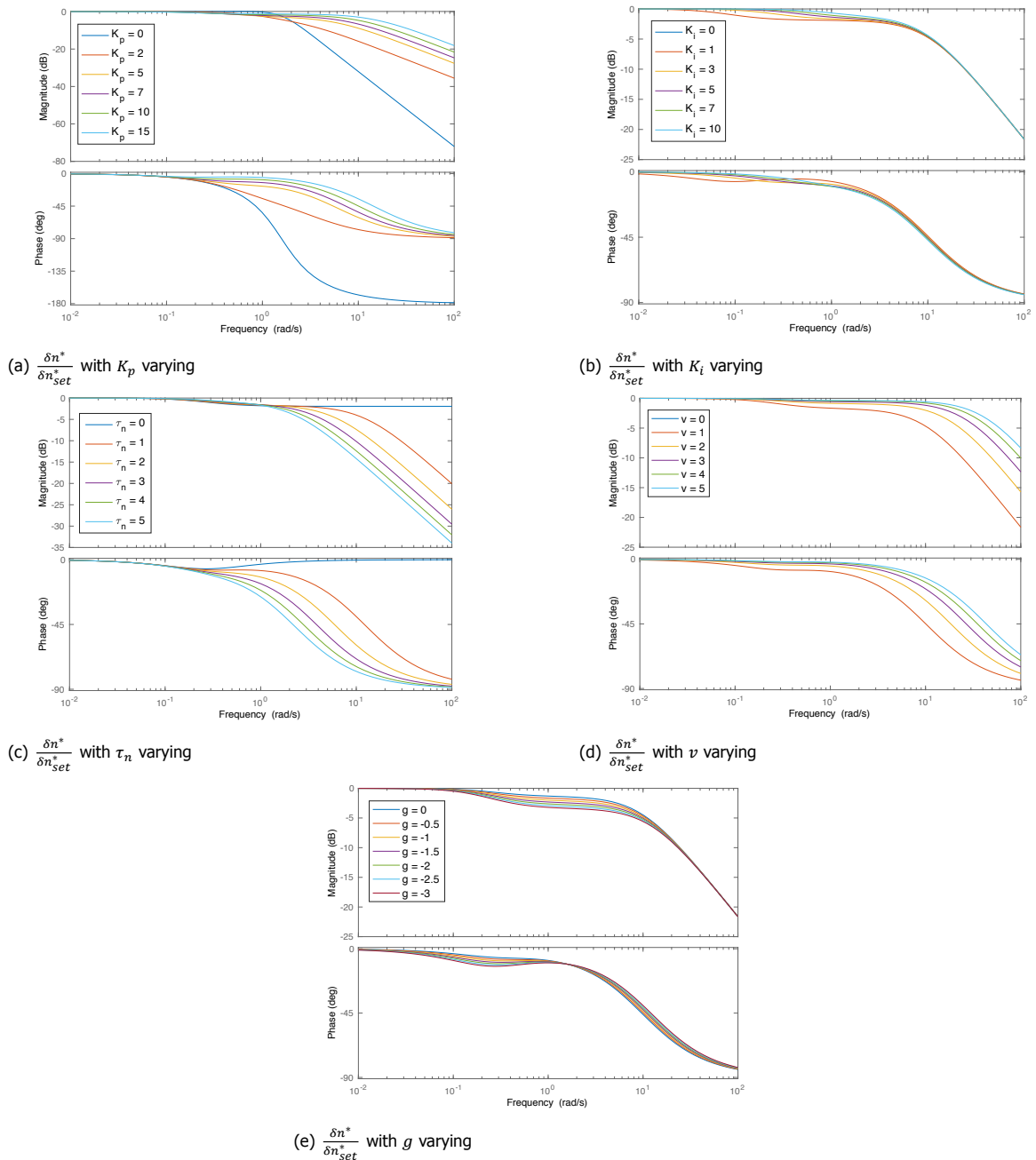
Figure 4.2: Sensitivity analysis of initial closed loop model with five different parameters.

The response to lowest and highest frequencies of the magnitude of the model compare with the expected values shown in table 2.4. In figure 4.2b the behaviour of K_i is visible. Sensitivity is visible in the low-frequency region up to 1 [rad/s]. Between 0.1 and 10 [rad/s], parameter g is slightly influencing the behaviour of the model. Outside this area different values of g have the same path and behaviour. From the five Bode plots of the sensitivity analysis, the parameters K_p, τ_n and v show their sensitivity in the high frequent region. Due to the sensitivity of most parameters in the high-frequency region and almost no sensitivity in the low-frequency region, it is difficult to extract the influence of a parameter on the response. This will make it more difficult to compare with measured data and see the individual influence of parameters.

4.1.2. Open Loop

Before an open loop sensitivity can be performed, the corresponding transfer functions have to be determined. For the open loop sensitivity analysis, the initial linear model is simplified by removing all the feedback loops. This is performed by setting parameter g to zero and therefore removing it from the model, meaning that the engine torque dependency on actual engine speed is removed. It is assumed that the influence of g on the model is minimal and the removal simplifies the open loop derivation. Further, the closed loop sensitivity analysis of parameter g presented in figure 4.2e, shows a low sensitivity. Moreover, the removal of g decreases the amount of identifiable parameters. Setting g to zero causes that equation (2.18) is transformed into equation (4.1).

$$\delta M_b^* = v\delta X_f^* \tag{4.1}$$

The open loop model exist out of two sub-models, which are shown in figure 4.1. These sub-models are described by the transfer functions shown in equation (4.2) and (4.3). Combining these two sub-models creates the open loop transfer function with the error between engine speed set point and engine speed as input and the engine speed as output. The open loop transfer function is shown in equation (4.4), which is the generic form of a second order transfer function [18]. The derivations of the open loop transfer functions is shown in appendix C.

$$H_{CP} = \frac{\delta n^*}{\delta M_s^*} = \frac{1}{\tau_n s + 2} \tag{4.2}$$

$$H_{G+D} = \frac{\delta M_s^*}{\delta e_n^*} = v(K_p + \frac{K_i}{s}) \tag{4.3}$$

$$H_{OL} = H_{G+D} \cdot H_{CP} = \frac{\delta n^*}{\delta e_n^*} = \frac{\frac{vK_p}{\tau_n}s + \frac{vK_i}{\tau_n}}{s^2 + \frac{2}{\tau_n}s} \tag{4.4}$$

With the open loop transfer function (4.4) a sensitivity analysis is performed. The four different parameters, τ_n, K_p, K_i and v are varied to investigate the sensitivity. In figure 4.3 the four Bode plots of the open loop sensitivity analysis are shown. The initial values and variation of the parameters are shown in section 2.5.

(a) $\frac{\delta n^*}{\delta e_n^*}$ with K_p varying

(b) $\frac{\delta n^*}{\delta e_n^*}$ with K_i varying

(c) $\frac{\delta n^*}{\delta e_n^*}$ with τ_n varying

(d) $\frac{\delta n^*}{\delta e_n^*}$ with v varying
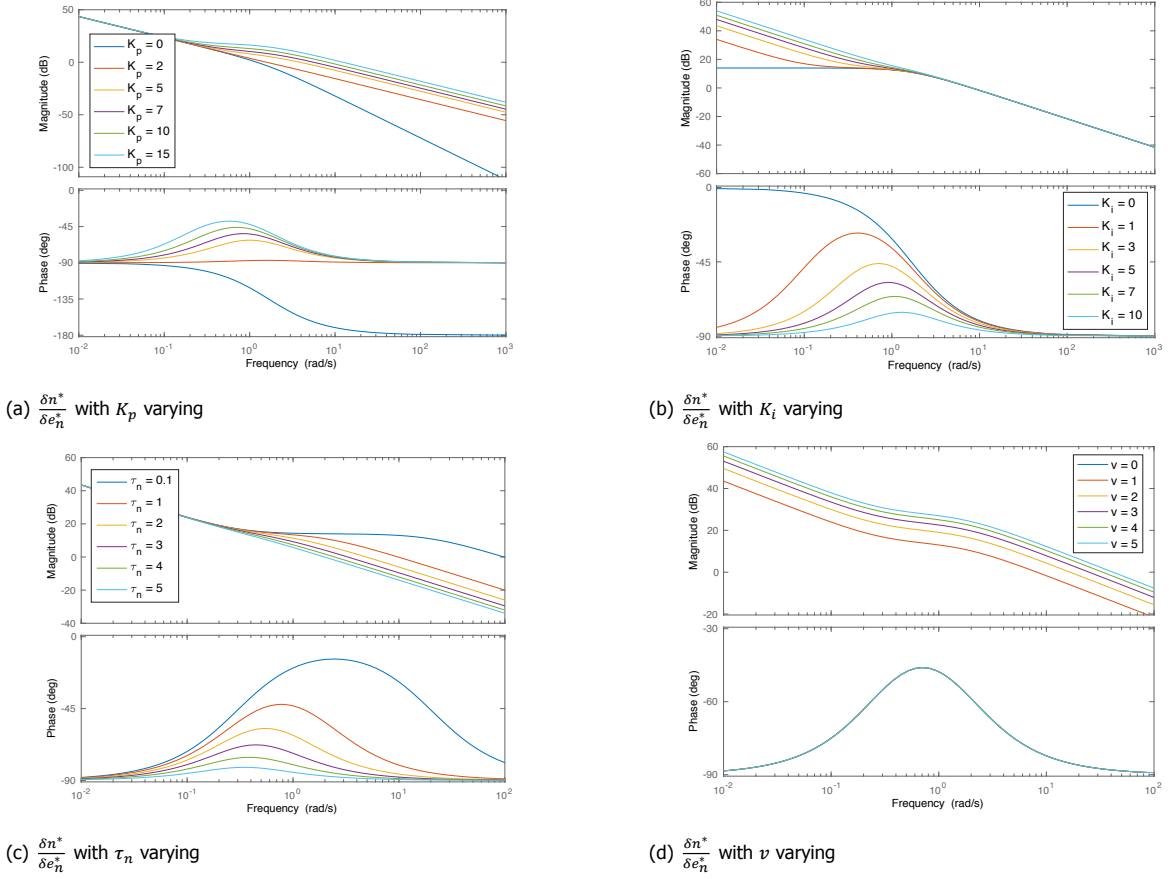
Figure 4.3: Sensitivity analysis of open loop system with four different parameters.

Clearly, the sensitivity of K_i is visible in the low frequent region. At a frequency of 1 [rad/s] when the influence of a varying K_i becomes zero, the influence of K_p starts to take effect on the model. The sensitivity of τ_n starts to have effect in the same region as K_p. Parameter v, shown in figure 4.3d, behaves like a gain. An increase of v causes an overall increase of the open loop model in terms of the magnitude. The value of v does not effect the phase.

Concluding, in open loop the influence of each individual parameter is visible. All four parameters show a good sensitivity and have a different influence on the response of the model. Compared to the closed loop sensitivity analysis, the influence of an individual parameter can be determined much better in an open loop environment.

4.2. Simplification

In the second main section a simplification to improve the linear model structure is discussed. The initial linear model is already simplified in the previous section by the removal of parameter g. The initial linear model presented in section 2.4 is further simplified by fixing parameter v to one. First, setting v to one decreases the amount of identifiable parameters. Secondly, Damen Shipyards does not work with fuel rack maps in their simulation models and expect that these parameters are not needed to obtain the correct system behaviour. Further, the open loop sensitivity analysis of parameter v presented in figure 4.3d, shows that it behaves like a gain. Moreover, dependencies of the parameters indicate that parameter v is always coupled with K_p or K_i, making it impossible to identify the parameters individually. By setting v to one and g to zero, the diesel engine changes into a constant torque machine. Equation (2.18) describing the brake torque, changes into equation (4.5). The remaining identifiable parameters are K_p, K_i and τ_n.

$$\delta M_b^* = 1 \cdot \delta X_f^* \tag{4.5}$$

The simplification of the initial linear model causes changes in transfer functions and state space notation of the initial model structure. The closed loop simplified transfer functions, state space notation and sensitivity analysis are shown in appendix D. The sensitivity analysis with the simplified closed loop model structure compare, as expected, very well to figure 4.2a, 4.2b and 4.2c of the sensitivity analysis of the initial linear model. Simplifying the initial linear model by omitting g and fixing parameter v to one, does not affect the response of relation $\frac{\delta n^*}{\delta n^*_{set}}$.

4.3. Open Loop Sub-models

In the third main section, zooming in on the existing open loop sub-models with the applied simplification is discussed. The open loop sensitivity analysis in section 4.1.2 is performed with transfer function H_{OL} that combines the sub-models. Zooming in on single sub-models creates more simple model structures with a lower amount of identifiable parameters. Figure 4.1 shows the sub-models that are present in the linear model of the propulsion system: governor described by a PI controller, diesel engine and the core propulsion system. The governor and diesel engine is considered as one sub-model, the governor+diesel engine sub-model, because between the governor and diesel engine no measurements are performed.

4.3.1. Core Propulsion Sub-model

The core propulsion sub-model describes the ship dynamics, comprising the shaft loop and torque balance. The simplification of the initial linear model does not affect the core propulsion sub-model. Zooming in on the core propulsion in the open loop linear model shows a very simple sub-model. The transfer function of the core propulsion sub-model is already derived for the open loop sensitivity analysis. The input is the shaft torque δM_s^* and the output is the engine speed δn^*. Equation (4.6) shows the transfer function of the core propulsion sub-model. The core propulsion system, only dependent on parameter τ_n, is shown in equation (2.23).

$$H_{CP} = \frac{\delta n^*}{\delta M_s^*} = \frac{1}{\tau_n s + 2} \tag{4.6}$$

The core propulsion sub-model is a single input, single output system with one state. With transfer function (4.6) known, a state space notation is derived. For the conversion from transfer function to state space notation, the controllable canonical method is used [19]. The state space notation is used as model structure for the system identification of the core propulsion system. The continuous time invariant state space notation of the core propulsion sub-model is shown in equation (4.7) to (4.11). Corresponding with transfer function (4.6), the state space notation is only dependent on τ_n.

$$\bar{x} = A\bar{x} + B\bar{u} \tag{4.7}$$

$$\bar{y} = C\bar{y} + D\bar{u} \tag{4.8}$$

$$\bar{x} = \bar{y} = \delta n^*, \quad \bar{u} = \delta M_s^* \tag{4.9}$$

$$A = -\frac{2}{\tau_n}, \quad B = \frac{1}{\tau_n} \tag{4.10}$$

$$C = 1, \quad D = 0 \tag{4.11}$$

With transfer function $\frac{\delta n^*}{\delta M_s^*}$, a sensitivity analysis of the sub-model is performed. The sensitivity analysis shows the response of parameter τ_n of the core propulsion sub-model. The sensitivity analyses of the core propulsion sub-model is compared with the corresponding open loop frequency domain data $\frac{\delta n^*}{\delta M_s^*}$. Parameter τ_n is varied between 0 and 3 [s]. Figure 4.4 shows the sensitivity analysis of the core propulsion system together with the open loop frequency domain data.
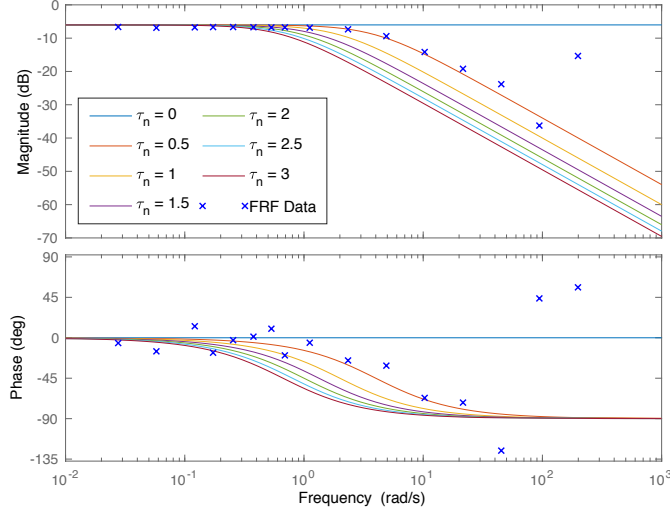
Figure 4.4: Bode diagram of sensitivity analysis of open loop core propulsion system $\frac{\delta n^*}{\delta M_s^*}$ with τ_n varying and corresponding open loop frequency domain data $\frac{\delta n^*}{\delta M_s^*}$.

The core propulsion sub-model $\frac{\delta n^*}{\delta M_s^*}$ compares very well with the corresponding frequency domain data. The behaviour of the model structure seems to be the same as the multiple sine wave data. It must be noted that the last three points of the frequency domain data have a high uncertainty. In figure 4.4, the magnitude and phase show that the value of τ_n is bigger than 0 [s] but smaller than 0.5 [s].

4.3.2. Governor and Diesel Engine Sub-model

The simplification is taken into account for the governor+diesel engine sub-model. Therefore, the governor+diesel engine sub-model contains only two identifiable parameters. These parameters are the proportional and integral gain K_p and K_i of the PI controller. Zooming in on the sub-model shows the response of the governor and diesel engine with the engine speed error δe_n^* as input and the shaft torque δM_s^* as output. In section 4.1.2, the transfer function of the governor+diesel engine sub-model is derived. Parameter v from equation (C.4) is set to one and is not an identifiable parameter anymore, which is shown in equation (4.12).

$$H_{G+D} = \frac{\delta M_s^*}{\delta e_n^*} = 1 \cdot \left(\frac{K_p s + K_i}{s} \right) \tag{4.12}$$

The governor+diesel engine sub-model is also a single input, single output system with one state. With transfer function (4.12) known, a state space notation is created using the controllable canonical method [19]. The state space notation is used as model structure for the system identification of the governor+diesel engine system. The continuous time invariant state space notation of the governor+diesel engine sub-model is shown in equation (4.13) to (4.17). Corresponding with transfer function (4.12), the state space notation is dependent of the parameters K_p and K_i. The input is the error δe_n^* and the output is the shaft torque δM_s^*.

$$\bar{\dot{x}} = A\bar{x} + B\bar{u} \tag{4.13}$$

$$\bar{y} = C\bar{y} + D\bar{u} \tag{4.14}$$

$$\bar{x} = \bar{y} = \delta M_s^*, \quad \bar{u} = \delta e_n^* \tag{4.15}$$

$$A = 0, \quad B = 1 \tag{4.16}$$

$$C = K_i, \quad D = K_p \tag{4.17}$$

A sensitivity analysis is performed with transfer function $\frac{\delta M_S^*}{\delta e_n^*}$ to investigated the response of the governor+diesel engine sub-model dependent on parameters K_p and K_i. The sensitivity analyses is compared with the corresponding open loop frequency domain data. The variation of the values of K_p and K_i are bounded by upper and lower limits presented in section 2.5. The initial values for K_p and K_i are respectively 5 and 3. Figure 4.5 shows the sensitivity analysis of the governor+diesel sub-model dependent on two parameters, together with the open loop frequency domain data.

(a) $\frac{\delta M_S^*}{\delta e_n^*}$ with K_p varying

(b) $\frac{\delta M_S^*}{\delta e_n^*}$ with K_i varying
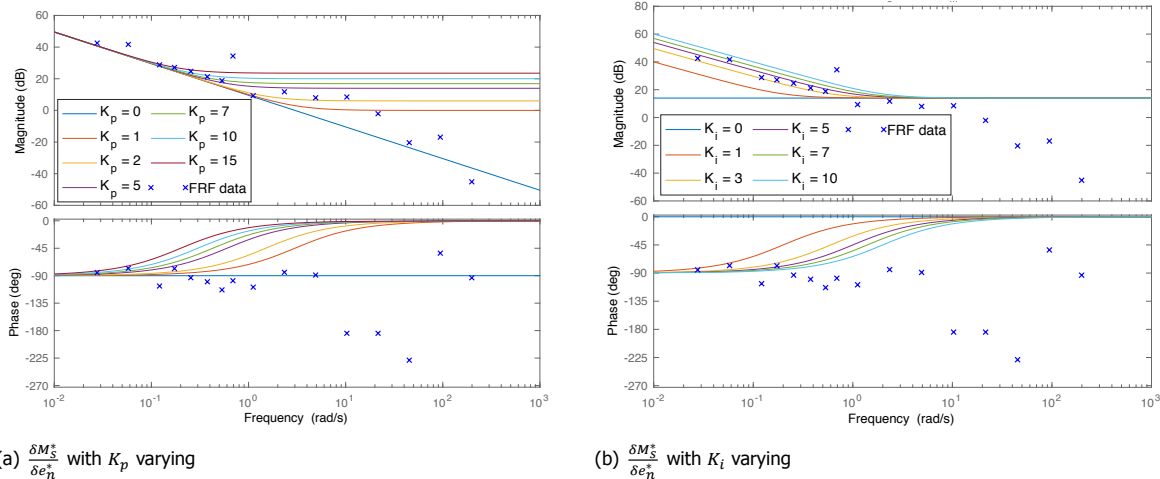
Figure 4.5: Bode diagrams of sensitivity analysis of open loop governor+diesel sub-model with two different parameters and corresponding open loop frequency domain data $\frac{\delta M_S^*}{\delta e_n^*}$.

The magnitude of the governor+diesel sub-model seems to compare fine with the corresponding frequency domain data. The conclusion can be drawn that the system contains at least a gain and an integral term for the controller. At low frequencies up to 1 [rad/s], the influence of K_i is visible and compares with the data. The magnitude shows that the value of K_i probably lies between 3 and 5. Between 1 and 10 [rad/s], the influence of K_p is visible and compares with the data. The magnitude shows that the value of K_p probably lies between 1 and 5. At high frequencies, the magnitude of the data becomes smaller than that of the model. The phase shows an even bigger difference, the data becomes more negative and the model converges to zero. It must be noted that the last three points of the frequency domain data have a high uncertainty. These differences between governor+diesel engine sub-model and the corresponding frequency domain data can be explained by the absence of actuators, sensors, inertia in the diesel engine and certain software of the governor in the model structure. Such components can induce delays and lag which change the behaviour of the system.

4.4. Implementations

In the fourth main section, the implementation of possible new terms to improve the linear model structure is discussed. Martinus [1] recommended the implementation of multiple terms to the model structure. Together with the findings during the comparison of the governor+diesel engine sub-model with the corresponding data, three implementation are investigated. The addition of a derivative term to the governor, adding a time delay and the addition of a second order system are determined. The following points give some additional explanation why these terms might improve the model structure.

- A derivative term changes the governor and could be an improving addition. Besides, it is unknown if the Stan Tug 1205 is equipped with a PI or PID controller. The derivative term will influence the magnitude and phase response of the governor+diesel engine sub-model.

- The phases of the measured data and model shown in figure 4.5 behave differently. The phase of the measured data shows a path downwards, which can be caused by a time delay. Time delays can be induced by actuators, sensors present in the system [20] and by the diesel engine and software in the governor. Time delays are very common in computer controlled systems [21]. Besides, a time delay of 0.4 [s] is estimated in section 3.2.1.

- The magnitude in figure 4.5 of the governor+diesel engine sub-model and the corresponding frequency domain data behave differently in the high frequent region. The addition of a second order system could improve the model structure. A second order system induces lag and causes that the frequency response of the magnitude and phase becomes smaller in the middle to high frequent region. The presence of lag could be explained by different things. Lag could be induced by actuators, sensors, inertia in the diesel engine and software in the governor.

4.4.1. PID Controller

Adding a derivative term changes the PI controller into a PID controller. A continuous-time PID controller with proportional, integral, and derivative gains K_p, K_i, and K_d with a first-order derivative filter time constant T_f is implemented in the model[22]. The first order derivative filter time constant T_f is added to prevent the PID controller from overloading to infinity. Equation (4.18) shows the transfer function of the governor and diesel engine sub-model with a PID controller. Equation (4.19) shows the standard form of the transfer function of the governor+diesel engine sub-model.

$$H_{G+D,PID} = \frac{\delta M_s^*}{\delta e_n^*} = \left(K_p + \frac{K_i}{s} + \frac{K_d s}{T_f s + 1} \right) \tag{4.18}$$

$$H_{G+D,PID} = \frac{(K_p T_f + K_d)s^2 + (K_i T_f + K_p)s + K_i}{T_f s^2 + s} \tag{4.19}$$

To investigate if the governor of a Stan Tug 1205 can be described with a PID controller, a sensitivity analysis is performed. The sensitivity analyses is compared with the corresponding open loop frequency domain data. The sensitivity analysis is performed with the transfer function shown in equation (4.19). The initial values of K_p and K_i are respectively 10 and 3. The parameters K_d and T_f are varied for the sensitivity analysis. The value of K_d is varied between 0 and 5 with an initial value of 1 and T_f is varied between 0 and 0.05[s] with an initial value of 0.01[s]. Figure 4.6 shows the sensitivity analysis of the governor+diesel engine sub-model with a PID controller and the corresponding frequency domain data.

(a) $\frac{\delta M_s^*}{\delta e_n^*}$ with K_d varying   (b) $\frac{\delta M_s^*}{\delta e_n^*}$ with T_f varying
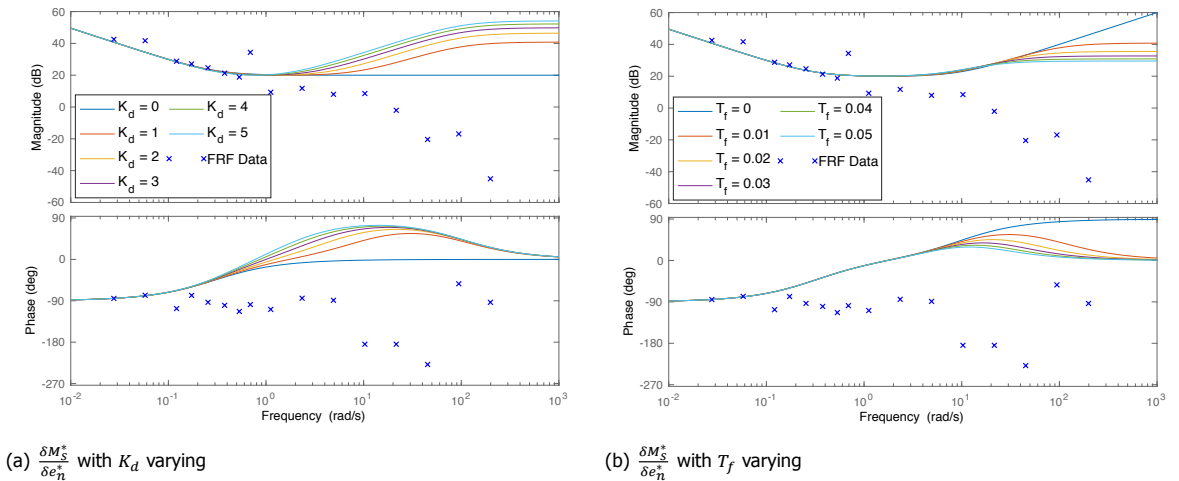
Figure 4.6: Bode diagrams of sensitivity analysis of open loop governor+diesel engine sub-model with a PID controller and corresponding open loop frequency domain data $\frac{\delta M_s^*}{\delta e_n^*}$.

The governor+diesel engine sub-model with a PID controller does not compare well with the corresponding frequency domain data. The differences which were indicated do not resolve but become bigger by the addition of a derivative term K_d with a first-order derivative filter time constant T_f. The magnitude of the frequency domain data becomes smaller. However, the magnitude of the model becomes more positive. Comparing the phase of the data and model shows the same difference that was observed with a PI controller, the data becomes more negative and the model converges to zero. It must be noted that the last three points of the frequency domain data have a high uncertainty. Concluding, the system does not contain a derivative term. Therefore, a PID controller will not be taken into account during the system identification.

4.4.2. Time Delay

To create a possible better response of the phase, a time delay is implemented. A time delay described by an exponential function does not affect the magnitude but only the phase of a system [21]. Martinus [1] also showed that the data contains a time delay. This is verified in section 3.2.1 by comparing the step response time domain data of the engine speed set point with the engine speed. The time delay is implemented in the governor+diesel engine sub-model as exponential function $e^{-t_d \cdot s}$ [21]. This results in a model structure with three identifiable parameters. Parameter t_d is indicates the time delay is seconds. The transfer function with time delay is shown in equation (4.21).

$$H_{td} = e^{-t_d \cdot s} \tag{4.20}$$

$$H_{G+D+td} = \frac{\delta M_s^*}{\delta e_n^*} = e^{-t_d \cdot s} \cdot \left(\frac{K_p s + K_i}{s} \right) \tag{4.21}$$

To investigate if a time delay has a positive influence on the response of the governor+diesel engine sub-model, a sensitivity analysis is performed. The sensitivity analyses is compared with the corresponding open loop frequency domain data. With transfer function (4.21) a sensitivity analysis is executed. The initial values of K_p and K_i are respectively 3 and 4. The parameter t_d is varied between 0 and 0.5 seconds. Figure (4.7) shows the sensitivity analysis of the governor+diesel engine sub-model with a time delay and the corresponding frequency domain data.
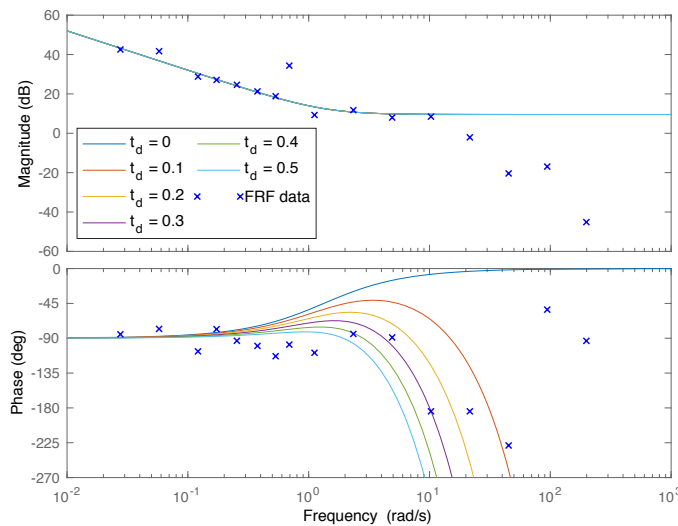

Figure 4.7: Bode diagram of sensitivity analysis of open loop governor+diesel engine sub-model with varying time delay and corresponding open loop frequency domain data $\frac{\delta M_s^*}{\delta e_n^*}$.

Clearly. the addition of a time delay function to the governor+diesel engine sub-model influences the phase in a positive manner. The time delay causes that the phase becomes more negative at higher frequencies. This response compares well with the corresponding frequency domain data, noted that the last three point have a high uncertainty. The magnitude of the sub-model stays unchanged although a time delay is added. The sensitivity analysis shows that the value of t_d probably lies between 0.1 and 0.5 [s]. The time domain data shows a time delay and that the phase of the frequency domain data compares well with the governor+diesel engine sub-model with time delay. Therefore, an exponential function as time delay will be taken into account with the linear system identification.

Rewriting transfer function (4.21) to a state space notation is very difficult with an exponential function. Besides, the System Identification Toolbox of Matlab is not very fond of time delays in state space notation. Therefore, the system identification of the governor+diesel engine sub-model with time delay will be performed with a transfer function as model structure.

4.4.3. Second Order System

To create a possible better response of the magnitude, a second order system is implemented to induce lag. In transfer function (4.22) a second order system is shown, which is indicated as H_{lag}. This second order system is based on a mass-spring-damper system and contains the parameters ω_n and ζ [23]. Parameter ω_n determines the break frequency in [rad/s] and parameter ζ determines the amount of damping of the peak at the break frequency [23]. Adding the second order system transfer function to the governor+diesel engine sub-model generates transfer function (4.23).

$$H_{lag} = \frac{\omega_n^2}{s^2 + \zeta \omega_n s + \omega_n^2} \tag{4.22}$$

$$H_{G+D+lag} = \frac{\delta M_s^*}{\delta e_n^*} = \left(\frac{K_p s + K_i}{s} \right) \cdot \frac{\omega_n^2}{s^2 + \zeta \omega_n s + \omega_n^2} \tag{4.23}$$

To investigate if a second order system has a positive influence on the response of the governor+diesel engine sub-model, a sensitivity analysis is performed. The sensitivity analyses is compared with the corresponding open loop frequency domain data. With transfer function (4.23) a sensitivity analysis is executed. The initial values of K_p and K_i are respectively 3 and 4. Parameter ω_n is varied between 6 and 18 [rad/s] and has an initial value of 10 [rad/s]. Parameter ζ is varied between 0 and 1 [-] and has an initial value of 0.5 [-]. Figure 4.8 shows the sensitivity analysis of the governor+diesel engine sub-model with a second order system and the corresponding frequency domain data.


(a) $\frac{\delta M_s^*}{\delta e_n^*}$ with ω_n varying   (b) $\frac{\delta M_s^*}{\delta e_n^*}$ with ζ varying
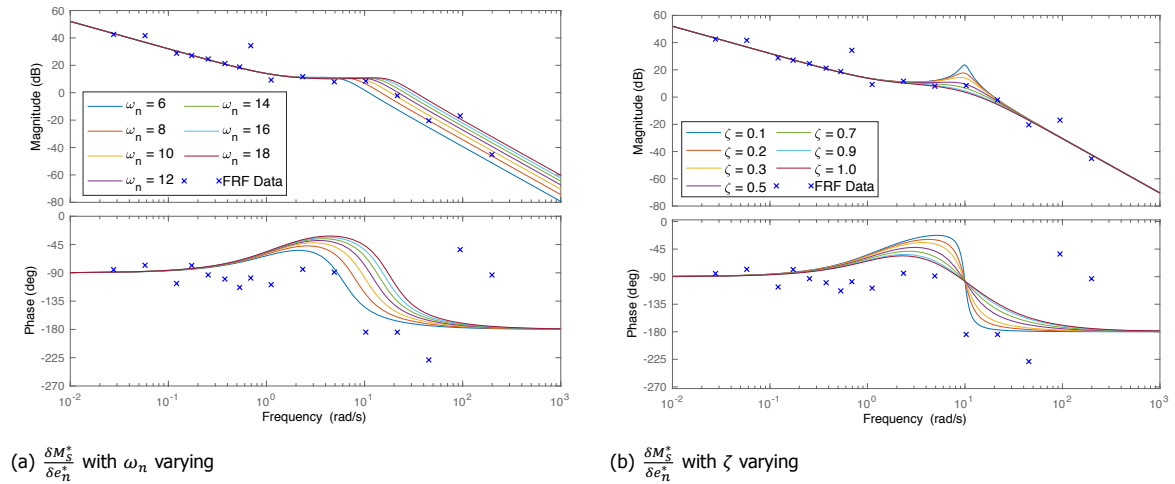
Figure 4.8: Bode diagram of sensitivity analysis of open loop governor+diesel engine sub-model with varying second order system parameters ω_n and ζ s and corresponding open loop frequency domain data $\frac{\delta M_s^*}{\delta e_n^*}$.

The second order system has a clear effect on the FRF magnitude. In the high frequent region, the response of the governor+diesel engine sub-model with second order system becomes smaller. This behaviour compares with the corresponding frequency domain data, noted that the last three points have a high uncertainty. However, the phase still needs improvement despite the fact that the second order system influences the phase in a positive way. This could be improved by adding the time delay. The expectation is that the best estimation with parameters ω_n and ζ is between the values respectively 7 and 13 [rad/s] and 0.4 or higher. The addition of the second order system improves the response of the model but can be seen as a black box addition. The ope loop system identifications with second order system will be performed with transfer functions, therefore the state space notation is not given.

4.4.4. Closed Loop Implementation

The second order system and the time delay showed to be improvements for the model structure. These improvements are implemented in the open loop governor+diesel engine sub-model. To perform a system identification and comparisons in closed loop, these implementations are integrated in a closed loop model structure. However, implementing a time delay in closed loop as $e^{-t_d \cdot s}$ creates an internal delay. Internal delays are not supported by the System Identification Toolbox and therefore it is chosen to use a Padé approximation. A Padé approximation can be used as an approximation of a time delay $e^{-t_d \cdot s}$ and with different orders. How higher the order, the better the approximation of $e^{-t_d \cdot s}$. However, high-order Padé approximations tend to be very sensitive for perturbations in the system [24]. Therefore, it is chosen to use a fifth order Padé approximation for the closed loop model structure. A fifth order Padé approximation of a time delay with parameter t_d is shown in equation (4.24).

$$H_{td,Pad} = \frac{30240 - 15120t_d + 3360t_d^2 - 420t_d^3 + 30t_d^4 - t_d^5}{30240 + 15120t_d + 3360t_d^2 + 420t_d^3 + 30t_d^4 + t_d^5} \tag{4.24}$$

The closed loop transfer functions with Padé approximation and second order system of the relations $\frac{\delta n^*}{\delta n^*_{set}}$ and $\frac{\delta M_s^*}{\delta n^*_{set}}$ are shown in (4.25) and (4.26). Due to the fifth order Padé approximation the whole function is not shown because it becomes extremely large and unclear. Equation (4.27) shows the transfer function of the combined relations, creating a model structure with one input and two outputs.

$$\frac{\delta n^*}{\delta n^*_{set}} = \frac{H_{cp} \cdot H_{G+D} \cdot H_{lag} \cdot H_{td,Pad}}{H_{cp} \cdot H_{G+D} \cdot H_{lag} \cdot H_{td,Pad} + 1} \tag{4.25}$$

$$\frac{\delta M_s^*}{\delta n^*_{set}} = \frac{H_{G+D} \cdot H_{lag} \cdot H_{td,Pad}}{H_{cp} \cdot H_{G+D} \cdot H_{lag} \cdot H_{td,Pad} + 1} \tag{4.26}$$

$$\begin{bmatrix} \dfrac{\delta n^*}{\delta n^*_{set}} \\[2em] \dfrac{\delta M_s^*}{\delta n^*_{set}} \end{bmatrix} = \begin{bmatrix} \dfrac{H_{cp} \cdot H_{G+D} \cdot H_{lag} \cdot H_{td,Pad}}{H_{cp} \cdot H_{G+D} \cdot H_{lag} \cdot H_{td,Pad} + 1} \\[2em] \dfrac{H_{G+D} \cdot H_{lag} \cdot H_{td,Pad}}{H_{cp} \cdot H_{G+D} \cdot H_{lag} \cdot H_{td,Pad} + 1} \end{bmatrix} \tag{4.27}$$

Equation (4.27) is rewritten to state-space notation with Matlab function 'ss'[25]. Other combinations of sub-models can also be used for the closed loop model structure. For instance, the fifth order Padé approximation of a time delay can be left out of (4.27) to create a closed loop model structure with only the addition of a second order system. The closed loop model structures with second order system and fifth order Padé approximation will be used for linear closed loop system identification and comparisons in time and frequency domain.

4.5. Overview of Conclusions

In this chapter multiple conclusions are stated. The following enumeration gives a summary of the most important conclusions and findings of the linear model structure improvements stated in this chapter.

- In open loop the influence of each individual parameter is visible. All four parameters show a good sensitivity and have a different influence on the response of the model. Compared to the closed loop sensitivity analysis, the influence of an individual parameter can be determined much better in an open loop environment.

- The initial model is simplified by setting v to one and g is set to zero. The diesel engine changes into a constant torque machine and the parameters K_p or K_i are not dependent on parameter v anymore. The remaining identifiable parameters of the simplified model structure are K_p, K_i and τ_n.

- Zooming in on the core propulsion system, reveals a very simple system that is dependent on one parameter, τ_n. The core propulsion sub-model compares very well with the corresponding frequency domain data.

- The governor+diesel engine sub-model shows differences with the corresponding frequency domain data. Therefore, new terms are implemented in the open model structure to investigate possible improvements. The addition of a derivative term, changing the governor in a PID controller, does not have the desired improving effect on the response. However, the addition of a time delay and second order system have the desired effect on respectively the phase and magnitude. The time delay is implemented in open loop as an exponential function.

- The second order system and time delay are also implemented in the closed loop model structure. However, internal delays are not supported by the System Identification Toolbox. Therefore, it is chosen to use a fifth order Padé approximation of a time delay for the closed loop model structure.

With the conclusions and findings from this chapter, the linear model/sub-model structures that will be used for the linear system identification are selected. The model structures that will be determined during the linear system identification are divided in closed loop and open loop model structures. In open loop, the core propulsion sub-model and the governor+diesel engine sub-model will be used. The second order system and exponential time delay will be implemented in the governor+diesel engine sub-model. In closed loop, the simplified model structure will be used and the second order system and fifth order Padé approximation of the time delay will be implemented.

5

Linear System Identification

In this chapter the results of different performed identifications are presented. This chapter exist out of eight main sections. In the first main section, the searching criterion used for these system identifications is discussed. In the second main section, the assembly of the measured data sets and the model structures to perform a system identification is presented. In the third and fourth main sections, the results of open and closed loop identifications are shown. In the fifth and sixth main sections, the best results of the open and closed loop system identification are compared and validated in frequency and time domain. In the seventh main section, the obtained parameter values are discussed. This chapter ends with an overview of the conclusions and findings from the linear open and closed system identification results, comparisons and validation.

5.1. Searching Criterion

In this main section, the searching criterion needed to perform a system identification is discussed. The optimisation approach and boundary conditions of the system identification are also discussed in this section. In section 2.5 the searching criterion used during the benchmark identification is introduced. For the linear system identifications that will be performed in this chapter, the same searching criterion is used. Important is that the cost function contains a weighted cost function term. This term is added to optimize the minimisation for multiple outputs. The open loop sub-models presented in section 4.3 are single input, single output systems. For the identification of the open loop sub-models the weighted cost function term is removed from the cost function. Besides, the regularization extension used by Martinus [1] is also removed because it did not improve the system identification.

For the optimisation of the linear system identification, different constraints and approaches are used. The problem might arise that a local minimum is found instead of the preferable global minimum. An approach to optimise the identification by using a large amount of different initial parameters sets is selected. There will be 50 random but feasible starting sets of initial parameters per system identification to find the global minimum. From these 50 different identifications, the lowest cost function minimum is selected. However, the chance exist that the identified parameter set with the lowest cost function minimum is an unstable system. When this occurs, the parameter set with the lowest cost function minimum that is stable is selected. Important to note, the lowest cost function compares with the highest fitting percentage. Therefore, the fitting percentage of each selected identification will be presented.

To prevent that the searching criterion runs for a very long time in search for the ideal zero optimum, stopping criteria are used to constraint each identification. An easy way of constraining an identification is the addition of a maximum amount of iteration steps. For the linear system identifications a maximum of 100 iterations per identification is added. To avoid that the minimum is already found during these 100 iterations or that the improvement steps become extremely small, also a tolerance is used as stopping criteria. The tolerance is set to 0.001 percentage difference between the current value of the cost function and the expected improvement of the next iteration.

Boundaries of the parameters are also introduced to prevent that the searching criterion searches for an optimum for a very long time. These boundary conditions are also the range within the 50 random but feasible starting sets of initial parameters are varied. The boundary conditions of the identifiable parameters are presented in table 5.1.

Table 5.1: Overview of boundary conditions of the identifiable parameters.

	τ_n [s]	K_p [-]	K_i [-]	t_d [s]	ζ [-]	ω_n [rad/s]
Lower bound	0	0	0	0	0.3	7
Upper bound	5	10	10	0.5	4	13

5.2. Data & Model Structure

This main section presents the assembly of the improved measured data sets and the model structures to perform a system identification. For system identification, a data set, model structure and searching criterion are needed. In the previous section the searching criterion for the linear system identification is introduced. In section 3.4 the data sets available for system identification are shown. The step response and short chirp data set are used for the time domain validation, see section 5.6. The frequency domain data sets of the multiple sine waves and the time domain data set of the long chirp are used for the system identifications.

In chapter 4 different open and closed loop model structures are presented. The closed loop simplified model is identified with and without the implementations that are discussed. The open loop sub-models are the core propulsion sub-model and the governor+diesel engine sub-model with different additions. These different model structures can be combined with different data sets to perform a system identification. However, the measured data is of closed loop origin. Due to the characteristics of the multiple sine waves in frequency domain, it will work as an instrumental variable and make an open loop system identification possible. Therefore, an identification with open loop sub-models is only possible with the frequency domain data of the multiple sine waves. The following two summations show the combinations of model structures and data sets that are used to perform a system identification. CL indicates the closed loop identifications that are performed. OL represents the open loop identification with sub-models that are executed.

- **OL1**: Core propulsion sub-model with multiple sine waves open loop frequency domain data $\frac{\delta n^*}{\delta M_s^*}$. Identifiable parameter is τ_n.

- **OL2**: Governor+diesel engine sub-model with multiple sine waves open loop frequency domain data $\frac{\delta M_s^*}{\delta e_n^*}$. Identifiable parameters are K_p and K_i.

- **OL3**: Governor+diesel engine sub-model with a time delay, combined with multiple sine waves open loop frequency domain data $\frac{\delta M_s^*}{\delta e_n^*}$. Identifiable parameters are t_d, K_p and K_i.

- **OL4**: Governor+diesel engine sub-model with a second order system, combined with multiple sine waves open loop frequency domain data set $\frac{\delta M_s^*}{\delta e_n^*}$. Identifiable parameters are K_p, K_i, ζ and ω .

- **OL5**: Governor+diesel engine sub-model with a second order system and time delay, combined with multiple sine waves open loop frequency domain data $\frac{\delta M_s^*}{\delta e_n^*}$. Identifiable parameters are K_p, K_i, ζ, ω and t_d.

- **CL1**: Closed loop simplified model structure with multiple sine waves closed loop frequency domain data. Identifiable parameters are τ_n, K_p and K_i.

- **CL2**: Closed loop simplified model structure with long chirp closed loop time domain data. Identifiable parameters are τ_n, K_p and K_i.

- **CL3**: Closed loop simplified model structure with a second order system, combined with multiple sine waves closed loop frequency domain data. Identifiable parameters are τ_n, K_p, K_i, ζ and ω.

- **CL4**: Closed loop simplified model structure with time delay (Padé) and second order system, combined with multiple sine waves closed loop frequency domain data. Identifiable parameters are τ_n, K_p, K_i, ζ, ω and t_d.

5.3. Results Open Loop System Identification

In this section the results and figures of the open loop system identifications are discussed. Five different open loop system identifications are performed which are indicated with OL1 to OL5. The results of the best sub-models are combined to create a parameter set that can be compared with the closed loop system identifications. The estimated results of the open loop system identifications are shown in table 5.2. The open loop estimated parameters show resemblances concerning the parameter K_i. However, differences are visible in the estimation of parameter K_p.

Table 5.2: Results of different full-scale open loop linear system identifications.

	Parameters						Fitting	
	τ_n [s]	K_p [-]	K_i [-]	t_d[s]	ω_n [rad/s]	ζ [-]	δn^* [%]	δM_s^* [%]
OL1	0.3897	-	-	-	-	-	56.01^x	-
OL2	-	1.003	4.2725	-	-	-	-	54.99^{xx}
OL3	-	3.4363	4.2639	0.4022	-	-	-	55.17^{xx}
OL4	-	2.902	4.2699	-	8.2912	0.5616	-	55.17^{xx}
OL5	-	4.36	4.2664	0.1023	8.202	0.88	-	54.88^{xx}

^{x}: This is the fitting of $\frac{\delta n^*}{\delta M_s^*}$.

^{xx}: These are the fittings of $\frac{\delta M_s^*}{\delta e_n^*}$.

5.3.1. Core Propulsion Sub-model

The core propulsion sub-model is only dependent on the parameter τ_n. The estimated value is 0.3897, which is between the predicted area 0 and 0.5 from the sensitivity analysis in section 4.3.1. However, τ_n is lower than the expected value based on the system inertia. Section 5.7.1 elaborates on this difference. The response of the core propulsion sub-model with the identified parameter τ_n is compared with the corresponding open loop frequency domain data $\frac{\delta n^*}{\delta M_s^*}$ and the benchmark. This comparison is presented in figure 5.1.

System identification OL1 has almost a perfect fit when compared to the corresponding frequency domain data. The response compares very well for low and high frequencies, for both the magnitude and phase. Besides, all 50 identification with a different initial parameter set resulted in the same estimated value of τ_n. Due to the measurement noise, the last three points of the measured data slightly deviate from the sub-system response. The benchmark shows a less good comparison. The break frequency at 2 [rad/s] does not compare, τ_n is to low.
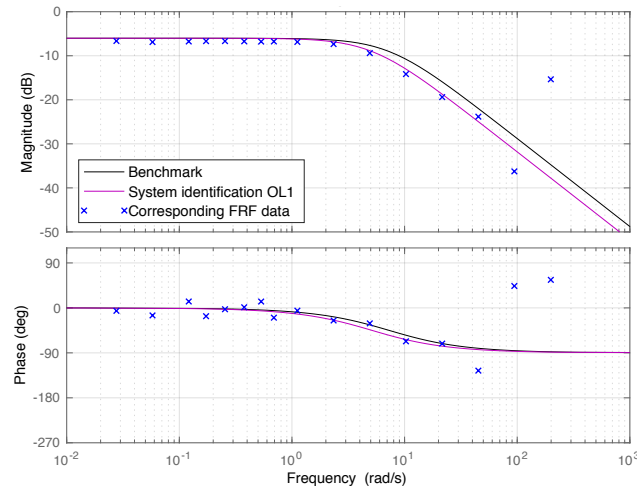
Figure 5.1: Bode diagram of system identification of open loop core propulsion sub-model OL1, benchmark and corresponding open loop frequency domain data $\frac{\delta n^*}{\delta M_s^*}$.

5.3.2. Governor and Diesel Engine Sub-model

The governor+diesel engine sub-model identifications correspond with OL2, OL3, OL4 and OL5. The estimations of the governor+diesel engine sub-models can be seen in table 5.2. All the identified values fall within the expected range that is determined with the sensitivity analysis in section 4.3.2. When zooming in on the identification of parameter K_i, four times the same value is identified. Compared to the calculated value, the identified value for the time delay is estimated approximately the same with system identification OL3. System identification OL5 identifies a lower time delay due to the addition of the second order system. The second order system also influences the phase, therefore a lower estimated value than the calculated time delay was expected.

The values of K_p that are identified differ from each other. This could be caused by the low amount of measurement points in the sensitivity region of K_p between 1 and 10 [rad/s]. The value of ω_n is estimated two times approximately the same and the two estimated values of ζ are somewhat different. The response of the governor+diesel engine sub-model is compared to the corresponding open loop frequency domain data $\frac{\delta M_s^*}{\delta e_n^*}$. The comparison is presented in figure 5.2a.
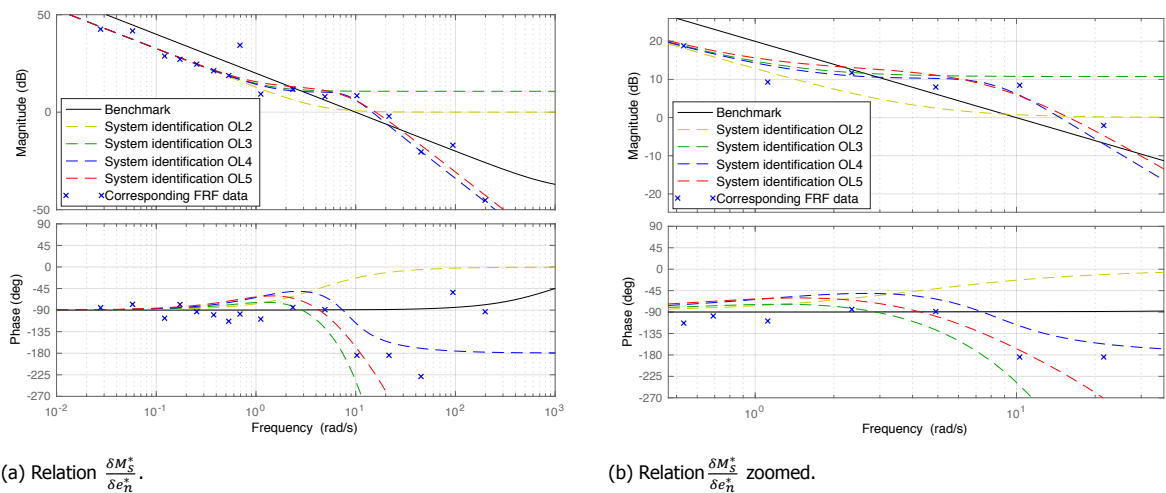
(a) Relation $\frac{\delta M_s^*}{\delta e_n^*}$.

(b) Relation $\frac{\delta M_s^*}{\delta e_n^*}$ zoomed.

Figure 5.2: Bode diagram of system identification of open loop governor+diesel engine sub-models, benchmark and corresponding open loop frequency domain data $\frac{\delta M_s^*}{\delta e_n^*}$.

The benchmark does not compare with the open loop frequency domain data, the values of K_p and K_i are not correct. The four identifications with the governor+diesel engine sub-model compare well up to 1 [rad/s], which is the sensitivity region of K_i. Identification OL2 without time delay does not compare well with the corresponding frequency domain data. The phase does not show the correct behaviour and the magnitude does not compare after a frequency of 1 [rad/s]. System identification OL3 with time delay compares well with the corresponding frequency domain data up to a frequency of 10 [rad/s], for both the magnitude and phase. System identification OL4 with a second order system shows a good response overall concerning the magnitude. However, the behaviour of the phase does not converge enough to the negative region. The identification OL5 of the governor+diesel engine sub-model with second order system and time delay compares very well with the frequency domain data, concerning the phase and magnitude response.

In figure 5.2b, the response of all different open loop identifications of the governor+diesel engine sub-model in the region between 1 and 10 [rad/s] is presented. In this region, the parameters K_p, ζ, ω and t_d influence the behaviour of the model. All four the open loop models have difficulties with the identification between 1 and 10 [rad/s]. As already mentioned, there is a low amount of measurement points between 1 and 10 [rad/s].

Concluding, the implementation of a second order system and time delay increases the quality of the open loop system identification of the governor+diesel engine sub-model. The second order system and time delay seem to cover the absence of certain actuators, sensors, inertia in the diesel engine and certain software of the governor in the model structure. The result of the core propulsion sub-model and the best results of the governor+diesel engine sub-model are combined. An identified parameter set that is implementable in the closed loop model structure and comparable with the closed loop system identifications is created. The core propulsion sub-model has only one result which compares very well with the measured data. The identifications of the governor+diesel engine sub-model with second order system and with/without a time delay show the best behaviour. Besides, the estimated parameters fall within the expected range and are reliable. Therefore, the identifications OL4 an OL5 are combined with identification OL1 and are referred to as OL1+OL4 and OL1+OL5.

5.4. Results Closed Loop System Identification

In this main section, closed loop models are directly fitted to the measurement data to estimate the model parameters. Four different closed loop models are fitted which are indicated with CL1 to CL4. The best closed loop models are selected, to be compared with the open loop model fits. The estimated results of the four different closed loop fitted models are presented in table 5.3.

Table 5.3: Results of different full-scale closed loop linear system identifications.

	Parameters						Fitting	
	τ_n [s]	K_p [-]	K_i [-]	t_d [s]	ω_n [rad]	ζ [-]	δn^* [%]	δM_s^* [%]
CL1	0.278	0.01	5.99	-	-	-	54.77	32.37
CL2	0.6027	0.01	5.0534	-	-	-	51.84	18.86
CL3	0.3537	1.1833	5.3967	-	7.2133	0.4	67.93	40.07
CL4	0.3290	1.6004	4.4388	0.1161	9.7705	0.4	74.50	62.10

The results of the closed loop system identifications without any implementations CL1 and CL2 show unreliable results concerning the value of K_p. Parameter K_p is estimated at the minimum of the boundary condition. The obtained values of K_p are small, this means that an error will be cancelled out very slow. This phenomena is not visible in the measured input and output signals shown in section 3.4. System identification CL3 and CL4 show far more reliable results. The values of τ_n and K_i converge to the open loop fitted values, which compared very well with the data. However, the values estimated by CL3 and CL4 of K_p and ω differ somewhat from each other and the open loop estimated values. Important to note is that the estimated values of ζ are identified at the lowest bound of the boundary condition. The results of the closed loop system identification are plotted with the corresponding closed loop frequency domain data. In figure 5.3, the relation $\frac{\delta n^*}{\delta n_{set}^*}$ and $\frac{\delta M_s^*}{\delta n_{set}^*}$ presented.

(a) Relation $\frac{\delta n^*}{\delta n_{set}^*}$.

(b) Relation $\frac{\delta M_S^*}{\delta n_{set}^*}$.
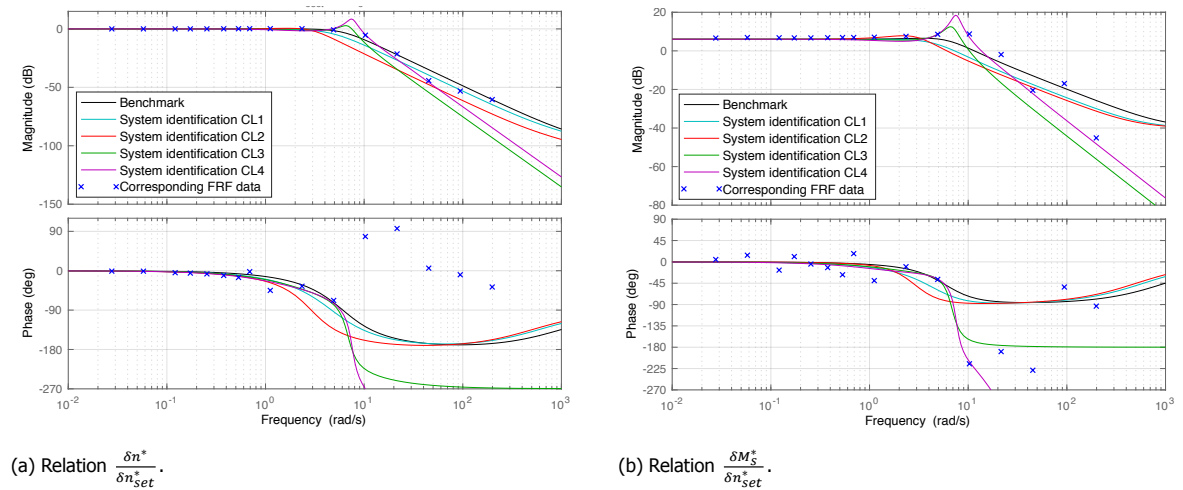
Figure 5.3: Comparison of closed system identifications with corresponding closed loop frequency domain data and benchmark.

At frequencies up to 2 [rad/s] the magnitude of the benchmark and the closed loop identifications respond the same, concerning the magnitude. This response is in line with what is expected. However, the break frequency of the magnitude of the benchmark, system identification CL1 and CL2 is to early, for both engine speed and shaft torque response. The addition of a second order system for identification CL3, pushes the break frequency forward to almost 10 [rad/s]. Still, the break frequency of identification CL3 is to early. Therefore, the response of identification CL3 has an offset in the high frequent region. System identification CL4 with a second order system and time delay compares very well with the measured data up to a frequency of 30 [rad/s], concerning the magnitude of the engine speed and shaft torque. However, a peak is visible between 5 and 10 [rad/s], which is to a lesser extend visible in identification CL3.

When zooming in on the phase responses of the closed loop system identifications, different behaviour can be seen. Important to note is that the two points at 90 degrees in figure 5.3b can be translated -360 degrees to a phase of approximately -270 degrees. The benchmark, system identification CL1 and CL2 do not compare well, for both the phase of the engine speed and shaft torque. The quality of the response of the phase of system identification CL3 increases due to the addition of the second order system. The addition of a time delay and second order system for identification CL4 improves the phase response even more, for both the engine speed and shaft torque.

Concluding, system identification CL3 and CL4 show the best behaviour concerning magnitude and phase, for both engine speed and shaft torque. Besides, the parameters fall within the expected range and converge to the values of the best identified open loop parameters. The addition of a second order system and time delay increases the quality of the behaviour of the closed loop identified models in frequency domain. Therefore, system identification CL3 and CL4 are used for comparison with the open loop identifications. Important to note is that system identification CL3 and CL4 show a peak between 5 and 10 [rad/s].

5.5. Frequency Domain Comparison

In this main section, the selected closed and open loop identified parameter sets are compared with each other, the open/closed loop frequency domain data and the benchmark from section 2.6. First, the identified models are compared in closed loop. Thereafter, the identified models are compared in the open loop relation $\frac{\delta M_S^*}{\delta e_n^*}$. These comparisons are performed to see if there are any resemblances and/or differences. The best identified parameter sets that are selected are: CL3, CL4, the combination OL1+OL4 and OL1+OL5.

For the closed loop comparison, the identified parameter sets are implemented in the closed loop model structure to simulate a closed loop response in frequency domain. Important to note is that the time delays in closed loop are all implemented with the Padé approximation. In figure 5.4 the comparisons for relations $\frac{\delta n^*}{\delta n_{set}^*}$ and $\frac{\delta M_S^*}{\delta n_{set}^*}$ are shown. The open loop identified parameter sets are indicated with a dashed line and the closed loop identified parameters sets including the benchmark with a solid line. This denotation is used in all the following graphs with closed loop and open loop parameter sets.

(a) Relation $\frac{\delta n^*}{\delta n_{set}^*}$.

(b) Relation $\frac{\delta M_S^*}{\delta n_{set}^*}$.
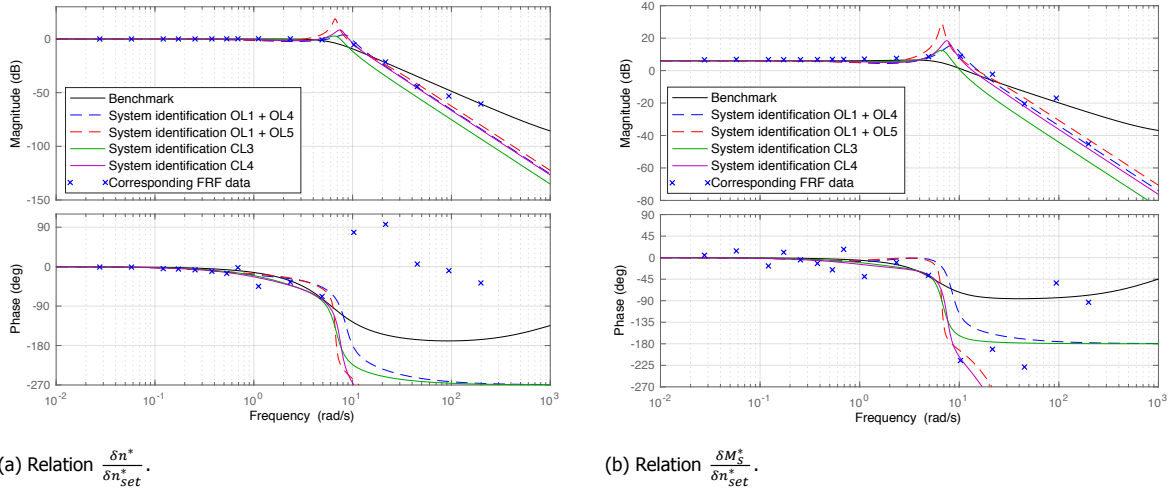
Figure 5.4: Comparison of selected identified parameter sets with corresponding closed loop frequency domain data and benchmark.

Clearly visible is that the benchmark shows a less good response compared to the other identification. The benchmark compares well up to a frequency of 5 [rad/s]. Thereafter the response is not correct. System identifications CL4, OL1+OL4, OL1+OL5 and CL3 to some lesser extend, compare well with the closed loop data, concerning the magnitude. Besides, the magnitudes show about the same response for both the engine speed and shaft torque. Up to a frequency of 1 [rad/s] and after 10 [rad/s], the open and closed loop identifications compare well with the data. Differences arise between 1 and 10 [rad/s].

Between 1 and 5 [rad/s], a small difference between the data and system identifications CL3, CL4, OL1+OL4 and OL1+OL5 is present. The closed and open loop identifications show a small dip. The dip is mainly present at the open loop identifications OL1+OL4 and OL1+OL5. However, the benchmark does not show this dip. Between 5 and 10 [rad/s], a more clear difference in the magnitude is present. A small peak is present in the measured data of the shaft torque response and no peak is present in the measured data of the engine speed response. The open and closed loop identifications have much larger peaks which all differ in size. These peaks possibly arise because the damping in the identified models is not high enough.

Focusing on the phase, differences arise also between 1 and 10 [rad/s]. The benchmark does not compare well with the phase of the measured data, for both the engine speed and shaft torque. The identification with second order system CL3 and OL1+OL4, show already a better phase response but still not sufficient. The addition of a time delay generates a better phase response which compares with the measured data up to a frequency of approximately 10 [rad/s].

In open loop it is easier to determine which parameters have influence on for instance the region between 1 and 10 [rad/s]. For the open loop comparison the identified parameter sets are implemented in open loop model structure of the governor+diesel engine sub-model to simulate an open loop response in frequency domain. Important to note is that the time delays in open loop are all implemented with an $e^{-td \cdot s}$. In figure 5.5 the comparison for relation $\frac{\delta M_S^*}{\delta e_n^*}$ is shown.

(a) Relation $\frac{\delta M_S^*}{\delta e_n^*}$.

(b) Relation $\frac{\delta M_S^*}{\delta e_n^*}$.
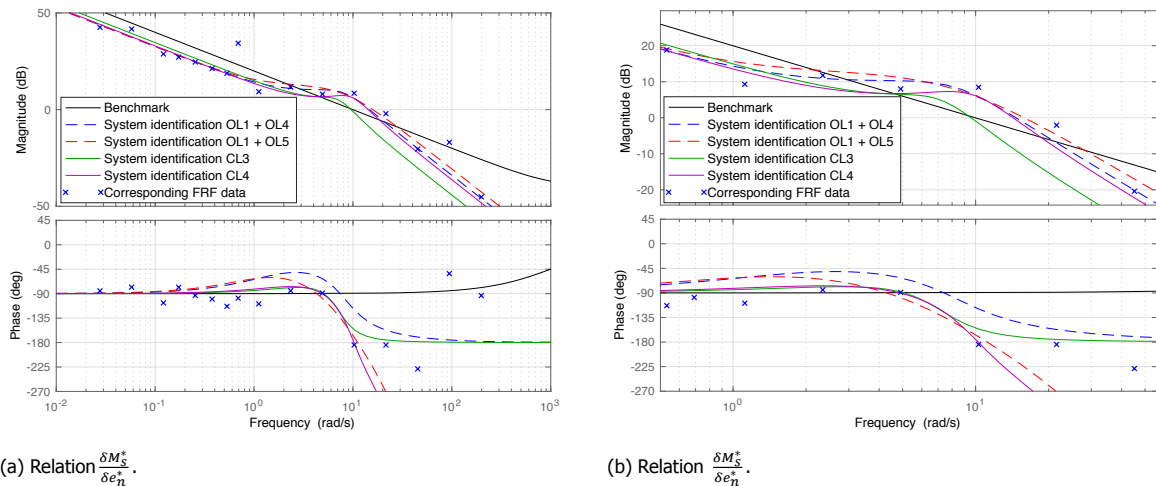
Figure 5.5: Comparison of selected identified parameter sets with corresponding open loop frequency domain data and benchmark.

Clearly, the benchmark does not compare with the open loop frequency domain data of the multiple sine waves experiment. The open and closed loop identifications show a good comparison with the open loop frequency domain data up to a frequency of 1 [rad/s] and in the higher frequent region after 10 [rad/s]. However, system identification CL3 has an offset in both these regions. When zooming in on the frequencies of the multiple sine waves between 1 and 10 [rad/s], again clear differences are present for the open and closed loop identifications, which can be seen figure 5.5b. In this region, the parameters K_p, ζ, ω and t_d influence the behaviour of the model. The closed loop identifications CL3 and CL4 show a lower response compared to the magnitude of the measured data. The open loop identifications OL1+OL4 and OL1+OL5 show a higher response compared to the magnitude of the measured data.

The difficulties for system identifications CL3, CL4, OL1+OL4 and OL1+OL5 between 1 and 10 [rad/s] can be explained by the fact that parameters K_p, ζ, ω and t_d are fluctuating around the correct value but are still not correct. Besides, there is also a low amount of measurement points in this region. Another explanation is that there is not enough damping in the model structure. A response with too little damping could be flattened by limiters. Limiters are nonlinear and not incorporated in the nonlinear model structure. Such limits are induced by the fuel actuator, which is assumed ideal and the limits of the diesel engine concerning maximum brake power and engine speed output. Other limits are ramp and response limiters, which could be present in the governor of the Stan Tug 1205.

A solution to enhance the quality of the identification is increasing the amount of experiments of the sine waves between 1 and 10 [rad/s]. Another solution is tightening up the boundary conditions of the parameters during the identifications. Creating a smaller area of movement of the parameters during system identification, forces the searching criterion to vary the parameters in a smaller but expected region. Moreover, adding limits to the nonlinear model structure could flatten the areas where too little damping is present and increase the quality of the identification between 1 and 10 [rad/s]. However, limiters are nonlinear and therefore nonlinear system identification should be performed. Damping is also induced by torsional vibration dampers which are not incorporated in the model structure. The TVC report in appendix E shows that the propulsion system of the Stan Tug 1205 contains such dampers.

Concluding, system identifications CL3, CL4, OL1+OL4 and OL1+OL5 compare very well with the data up to a frequency of 1 [rad/s] and in the higher frequent region after 10 [rad/s]. Problems arise between 1 and 10 [rad/s] in open and closed loop and it is easier to see which parameters have influence in open loop. In open loop the benchmark does not compare well with the measured data and in closed loop only up to a frequency of 5 [rad/s].

5.6. Time Domain Validation

In this main section the selected parameter sets and benchmark that are compared in frequency domain in section 5.5 are validated with obtained time domain data. For the time domain validation, a step response and short chirp are used, both measured during the backward bollard push experiment. A step response is a high frequent event, in a very short time a fast response is asked. The short chirp contains different frequencies varying from 0.001 [rad/s] to 25 [rad/s]. Important to note is that the short chirp and the step response are closed loop time domain data sets.

The short chirp is cut up in three parts, from low to high frequencies. The response of the open and closed loop identified models with a second order system and time delay, CL4 and OL1+OL5, are plotted in one figure. The response of the open and closed loop identified models with only a second order system, CL3 and OL1+OL4, will also be plotted in one figure. The benchmark is shown in both figures. In figure 5.6 the short chirp up to a frequency of approximately 1 [rad/s] is shown.
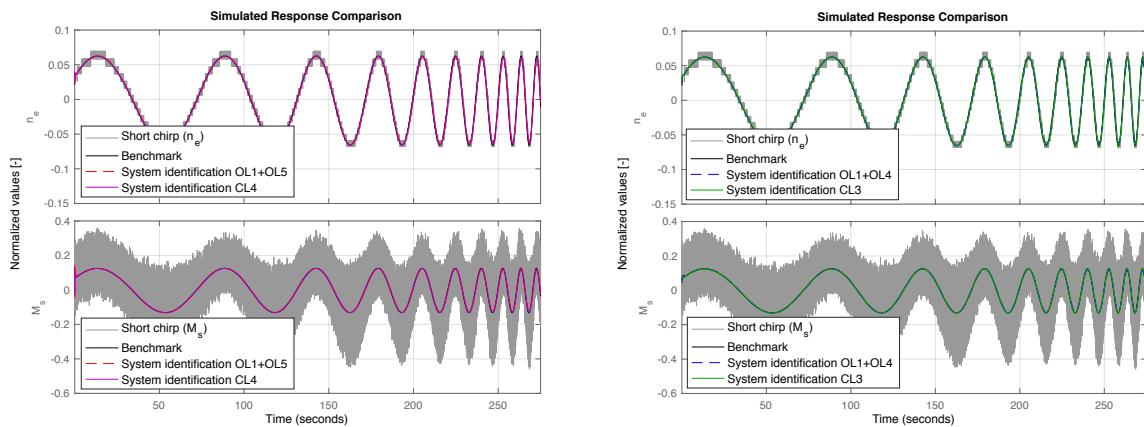
(a) CL4, OL1+OL5 and benchmark.   (b) CL3, OL1+OL4 and benchmark.

Figure 5.6: Comparison of selected identified parameter sets with short chirp data and benchmark up to approximately 1 [rad/s].

The frequency domain comparison showed that system identifications CL3, CL4, OL1+OL4, OL1+OL5 and the benchmark compare well with the measured data up to a frequency of 1 [rad/s]. This can also be seen in time domain in figure 5.6. All the simulated responses compare good with the short chirp data, for both the engine speed and shaft torque. Figure 5.7 shows the simulated responses between the frequencies of 1 and 5 [rad/s] of the short chirp data in time domain.
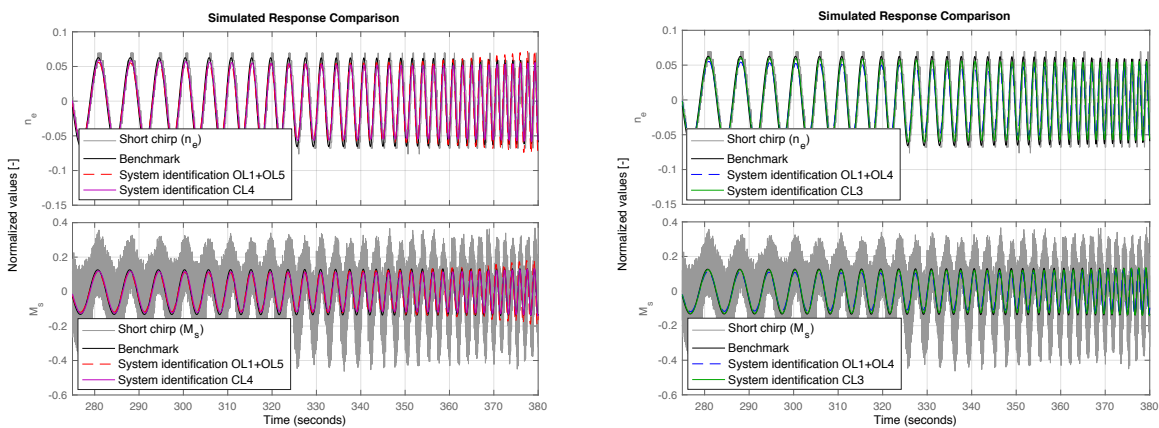
(a) CL4, OL1+OL5 and benchmark.   (b) CL3, OL1+OL4 and benchmark.

Figure 5.7: Comparison of selected identified parameter sets with short chirp data and benchmark from approximately 1 to 5 [rad/s].

The frequency domain comparisons showed that system identifications CL3, CL4, OL1+OL4 and OL1+OL5 have difficulties concerning their response between 1 and 5 [rad/s]. A small dip in the magnitude was present for system identification CL3, CL4, OL1+OL4 and OL1+OL5, which is not present in the benchmark. System identifications CL3, CL4, OL1+OL4 and OL1+OL5 also show a small dip in the amplitudes in figure 5.7, which is not present at the benchmark. Figure 5.8 shows the simulated responses between the frequencies of 5 and 10 [rad/s] of the short chirp data in time domain.
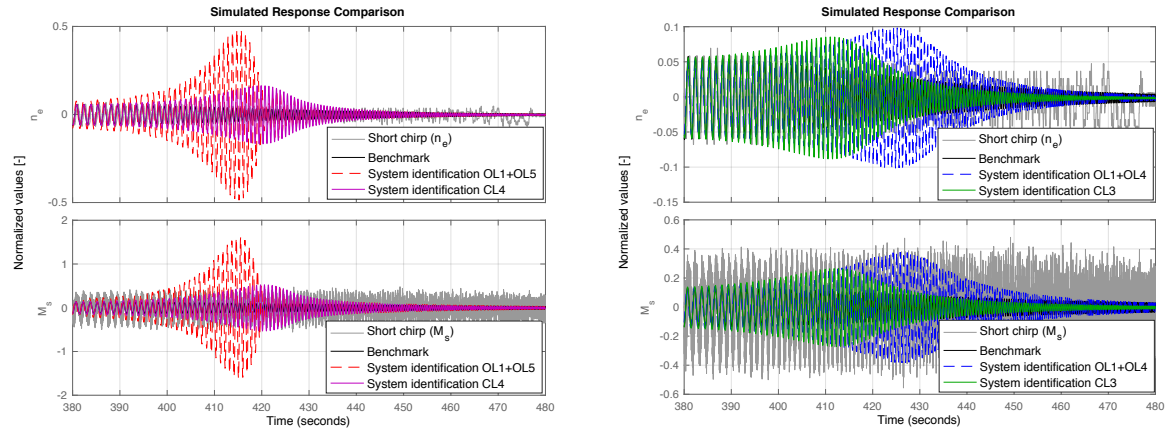

(a) CL4, OL1+OL5 and benchmark.

(b) CL3, OL1+OL4 and benchmark.

Figure 5.8: Comparison of selected identified parameter sets with short chirp data and benchmark higher than approximately 5 [rad/s].

The open and closed loop frequency domain comparisons showed that system identifications CL3, CL4, OL1+OL4 and OL1+OL5 have difficulties concerning their response between 5 and 10 [rad/s]. The closed and open loop frequency domain identifications showed peaks and offsets. Moreover, the benchmark compared well with closed loop frequency domain data up to 5 [rad/s]. In figure 5.8 these phenomena are also present. The peaks of the simulated responses of system identifications CL3, CL4, OL1+OL4 and OL1+OL5 correspond with the peaks in closed loop frequency comparison and the offsets in open loop frequency comparison. Difficult to see is that the benchmark starts too lag to early at 5 [rad/s], corresponding with the too early break frequency. At higher frequencies than 10 [rad/s] all the simulated responses and the time domain data start to lag concerning the amplitude. In figure 5.9 a better response of the phase at a frequency of 10 [rad/s] of the short chirp data is shown.
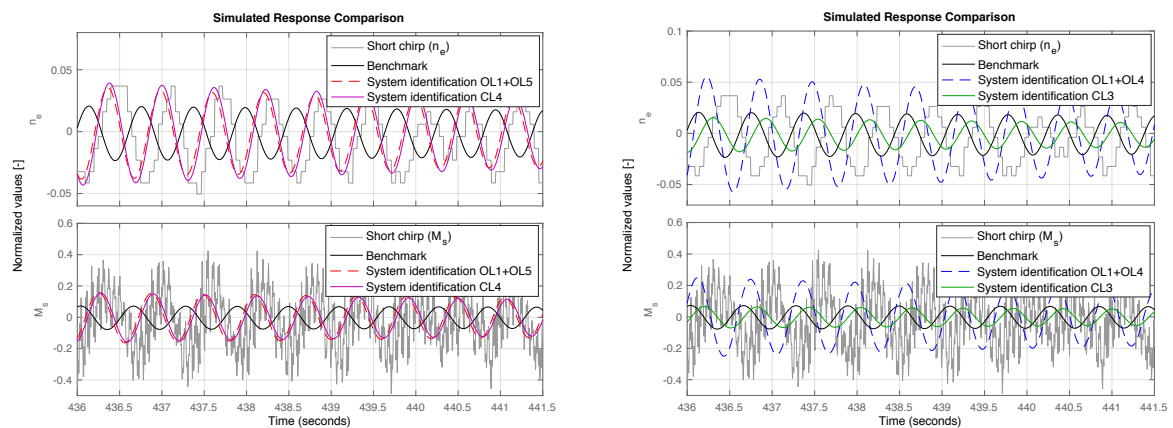
(a) CL4, OL1+OL5 and benchmark.

(b) CL3, OL1+OL4 and benchmark.

Figure 5.9: Comparison of selected identified parameter sets with short chirp data and benchmark at approximately 10 [rad/s].

System identifications CL3, CL4, OL1+OL4, OL1+OL5 and the benchmark all show a time delay in figure 5.9. The addition of a second order system for system identification CL3 and OL1+OL4 decreases this time delay. The addition of a time delay and second order system for CL4 and OL1+OL5 decreases this delay even more. The benchmark shows the largest delay compared to the measured short chirp data. However, the identified time delays are not sufficient and therefore an offset is present at approximately 10 [rad/s]. That the identified systems still have a delay is also visible in simulated step responses. Figure 5.10 shows the overall step responses of the measured data, identifications and benchmark.
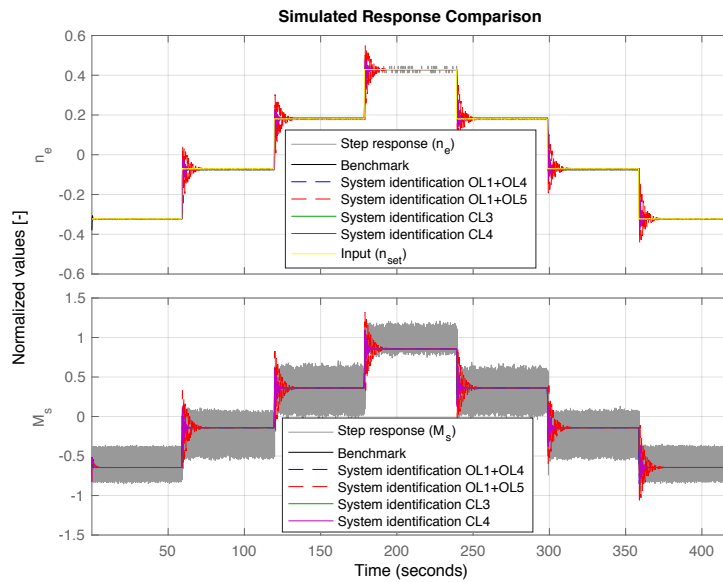
Figure 5.10: Comparison of selected identified parameter sets with step response data and benchmark.

System identifications CL3, CL4, OL1+OL4, OL1+OL5 and the benchmark follow the overall behaviour of the step response. Differences are present at the response and stabilisation during a single step. Zooming in on the simulated responses of one step shows more details. Important to note is that the engine speed set point is only present in the comparison of the engine speed response. Figure 5.11 zooms in on one response.
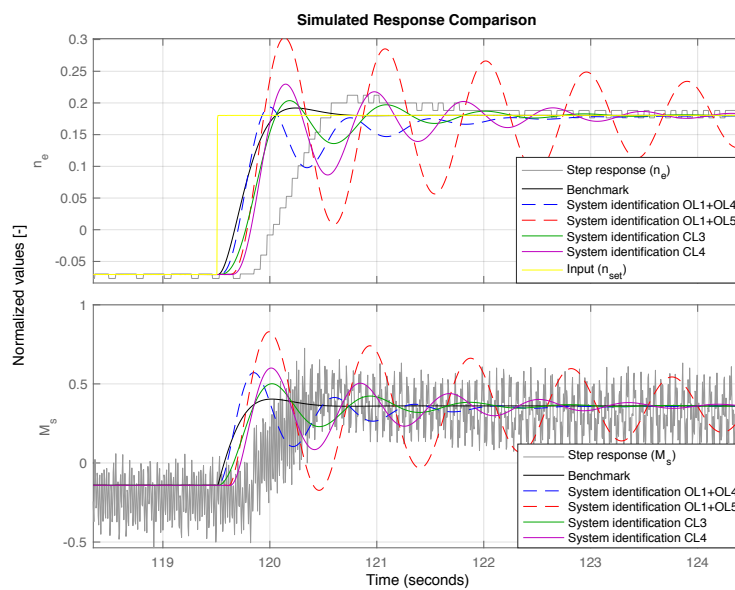

Figure 5.11: Zoomed comparison of selected identified parameter sets with step response data and benchmark.

The engine speed and shaft torque measured data of the step response shown in figure 5.11, have a frequency of approximately 9 [rad/s]. The benchmark compares with the data, for both the engine speed and shaft torque. However, the measured data shows an overshoot, this is to a very less extend visible in the benchmark. Besides, the benchmark does not contain any time delay and therefore starts the step response at the same time as the engine speed set point. The behaviour of the benchmark corresponds with the bad phase response and too early break frequency of the magnitude in frequency domain.

System identifications CL3, CL4, OL1+OL4 and OL1+OL5 all show different behaviour during the step response. In closed loop frequency domain the system identification showed large peaks between approximately 5 and 10 [rad/s]. The larger the peak, the larger the overshoot and stabilisation time becomes during the simulated step response. Besides, the slopes of the simulated responses are steeper than the measured data. This could indicate that nonlinear limiters are present in the system and are exceeded by the simulated responses of system identifications CL3, CL4, OL1+OL4 and OL1+OL5. The identified time delays are not sufficient and therefore a clear offset is present during the step response.

Concluding, the time domain validations confirm what is stated and concluded during the frequency domain comparison in section 5.5. Behaviour that can be seen in frequency domain, is also present in time domain simulations of the short chirp and step response. The validation with the short chirp and step response confirm that the identifications between 1 and 10 [rad/s] have difficulties. However, in frequency domain it was difficult to evaluate how good the phase response was and if the identified time delay was sufficient. The simulations of the short chirp and step response showed that a time delay was still present despite the addition of a time delay and second order system to the model structure.

Remarkable is that the benchmark shows good behaviour in time domain, but in frequency domain the behaviour was not very good. Mainly in open loop, the benchmark did not show a good response. Besides, the parameters estimated do not have a realistic value. An explanation for the good response in time domain, is that the searching criterion combines the parameters such way that the behaviour of the system gets imitated and dynamics, not explicitly included in the model structure, are still covered. This is done without taking into account whether the parameters have realistic values.

5.7. Parameter Validation

In this main section, the identified parameters for both the open and closed loop identification are discussed and compared. It is difficult to validate the parameters K_p, K_i, ζ and ω. These values are not known and therefore the estimated values cannot be compared with the expected values. However, it is possible to evaluate the estimations and determine if these are realistic. In addition, the reliability can be determined with the different identifications that are performed.

In open loop, K_i is estimated four times the same and compares very well with the open loop data. In closed loop, the estimated values of K_i converges to the same value when a second order system and a time delay are present in the model structure. The obtained value of K_i during the open loop identifications can be labelled as reliable and correct.

The parameters K_p, ζ, ω and t_d are fluctuating around the correct value but are still not correct, both for closed loop and open loop identifications. This can be seen in open loop between 1 and 10 [rad/s]. The value of the time delay parameter is calculated in section 3.2.1. As expected, t_d decreases when a second order system is present. However, the time domain validations showed that the total delay identified by the combination of a second order system and time delay is not sufficient. The following section evaluates the estimated value of τ_n.

5.7.1. Inertia

The estimated value of τ_n can be compared with the calculated value. The value of τ_n is calculated with the help of the mass moment of inertia and the normalisation points defined in section 3.1. The total mass moment of inertia is obtained with the help of a torsional vibration calculation (TVC). For the propulsion line of the Stan Tug 1205 a TVC report is available. The mass moment of inertia overview from a TVC report of the Stan Tug 1205 can be seen in appendix E. The open loop system identification of the core propulsion sub-model OL1 compared very well with the data. Therefore, the estimated value 0.3897 for τ_n will be used for the comparison.
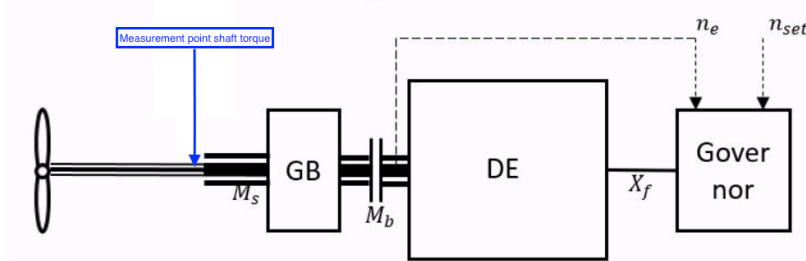

Figure 5.12: The propulsion system with the indicated measurement point of the shaft torque.

The total reflected mass moment of inertia of the propulsion system seen from the propeller is equal to $66.2960[kg \cdot m^2]$. The total reflected mass moment of inertia is a summation of the mass moments of inertia up to the measurement point. The gearbox has a quadratic influence on the magnitude of the total reflected mass moment of inertia [26]. However, the measurement point of the shaft torque is not located at the propeller, see figure 5.12. Therefore, the total reflected mass moment of inertia is deducted with the mass moment of inertia of the propeller and equals $54.0060[kg \cdot m^2]$. The expected value of τ_n is calculated, shown in equation (5.1).

$$\tau_n = \frac{2\pi I_p n_0}{M_{s,0}} = \frac{2\pi \cdot 54.0060 \cdot \frac{1184}{3.82 \cdot 60}}{1725} = 1.016 \tag{5.1}$$

The estimated value of τ_n is almost a factor 3 smaller than the expected value. However, all 50 identification of the open loop system identification of the core propulsion sub-model OL1 with different initial parameter resulted in the same estimated value of τ_n. Besides, the sensitivity analysis in figure 4.4 shows that a value of 1.016 does not compare very well with the corresponding data. The difference is possibly explainable by deficiencies in the model structure.

The parameter τ_n is a product from the linearisation of the nonlinear model structure. Multiple assumptions are done for the nonlinear model and the linearisation of the model structure. These assumptions are taken into account during the system identifications and the calculations of the inertia with equation 5.1. The assumptions of the shaft speed dynamics are presented by Stapersma and Vrijdag [8], which are shown in the following enumeration.

- The shaft speed dynamics are described by equation 2.1. The shaft inertia is assumed constant, therefore the change of mass of water, entrained by the propeller and the inflow angle are neglected [8].

- The linearised equation for τ_n is only valid for a nominal point that is in equilibrium [8].

- For steady nominal conditions the shaft and propeller torque are equal. Therefore, only small changes are of importance [8].

During the experiments with the Stan Tug 1205, multiple sine waves and different chirps are performed. Although, these experiments fluctuate around one working point, still accelerations take place. These accelerations cause that the propeller and shaft torque are not equal anymore. Besides, the accelerations provoke the change of mass of water entrained by the propeller, which is neglected for the linearisation and the nonlinear model.

The propeller torque in the model structure is described by the open water propeller diagram, which is a static description. The dynamics, that take into account the change of mass of water entrained by the propeller and the inflow angle, are neglected. Equation 5.2 shows the formula that describes the shaft loop of the model structure with the assumptions stated by Stapersma and Vrijdag [8]. In reality the shaft loop is described by equation 5.3, with the inertia changing over time when accelerations take place. The accelerations cause change of mass of water entrained by the propeller and different inflow angles, which have influence on the magnitude of the propeller torque. The differences between the model structure and the reality have influence on the calculation of τ_n and therefore the inertia.

$$2\pi \cdot I_p \frac{d(n_s)}{dt} = M_s - M_p \tag{5.2}$$

$$2\pi \frac{d(I_p \cdot n_s)}{dt} = M_s - M_p \tag{5.3}$$

The system identification of the core propulsion sub-model matches with the measured data but the model structure does not match the system. The incorrectness of the model structure of the shaft loop dynamics explains some of the factor 3 difference between the expected and the estimated value of τ_n. Adding the dynamics could solve a part of this factor 3 difference. However, a factor 3 is very large. Therefore, there is also a suspicion that the test set-up of the backward bollard push with the Stan Tug 1205 has influence on the difference between the expected and the estimated value of τ_n. The test was performed in restricted water, which could affect the water flow of the propeller. A possible solution concerning the test set-up is to perform the experiment in free sailing conditions.

Another explanation is the linearisation of the propeller torque. Equation 5.4 shows the nonlinear and linearised propeller torque. When the fluctuations around the working point increase, the error between the nonlinear model and linear model will increase as well. It is possible that the fluctuations of the experiments are to large and cause a large error which has influence on the difference between the expected and the estimated value of τ_n. Performing nonlinear system identification with the actual measured data and nonlinear model structure could reduce the difference between the expected and the estimated value of τ_n.

$$Q = \rho n^2 D^5 K_Q \rightarrow \delta Q^* = 2\delta n^* \tag{5.4}$$

It is important to note that the change of mass of water entrained by the propeller is neglected in most of the simulation models that are build. However, influence of the change of mass entrained the propeller is scarcely investigated in the literature. Therefore, research is needed to learn how to implement these propeller dynamics. One of the few investigations concerning the influence of the change of mass of water is performed for simulations models of ROVs [27][28]. The total mass of these ROVs is very small and therefore the influence of the change of mass entrained by the thrusters is large.

5.8. Overview of Conclusions

In this chapter multiple conclusions are stated. The following enumeration gives a summary of the most important conclusions and findings from the linear open and closed system identification results, comparisons and validation stated in this chapter.

- To increase the chance to find the global minimum, 50 random but feasible starting sets of initial parameters are used per identification. The lowest cost function minimum is selected combined with the fact that the identified model is stable. Stopping criteria and boundary conditions of the parameters are used to constraint each identification.

- The open loop identification of the core propulsion sub-model, identified 50 times the same result ($\tau_n = 0.3890$) for parameter τ_n. The response compares very well for low and high frequencies, for both the magnitude and phase. The estimated value falls within the identified range but is lower than expected.

- The addition of a time delay and second order system improve the open and closed loop identifications and compare very well up to a frequency of 1 [rad/s] and after 10 [rad/s]. Difficulties arise between between 1 and 10 [rad/s]. The parameters of these open and closed loop identifications fall within the expected range and show trustworthy results. The second order system and time delay seem to cover the absence of certain actuators, sensors, the diesel engine and certain software of the governor in the model structure.

- Difficulties arise between 1 and 10 [rad/s]. An explanation for these problems is that parameters K_p, ζ, ω and t_d are fluctuating around the correct value but are still not correct. Besides, there is also a low amount of measurement points in this region. Another explanation is that there is not enough damping in the model structure.

- A solution to enhance the quality of the identifications is increasing the amount of experiments of the sine waves between 1 and 10 [rad/s]. Another solution is tightening up the boundary conditions of the parameters during the identifications, forcing the searching criterion to vary the parameters in a smaller but expected region. Moreover, adding limits to the nonlinear model structure could flatten the areas where too little damping is present and increase the quality of the identification. However, limiters are nonlinear and therefore nonlinear system identification should be performed. Damping is also induced by torsional vibration dampers which are present in the system and not in the model structure.

- The time domain validations confirm what is stated and concluded during the frequency domain comparison. Behaviour that can be seen in frequency domain, is also present in time domain simulations of the short chirp and step response.

- The benchmark shows good behaviour in time domain, but in frequency domain the behaviour was not very good. Besides, the parameters estimated do not have a realistic value. An explanation for the good response in time domain, is that the searching criterion combines the parameters such way that the behaviour of the system gets imitated and dynamics, not explicitly included in the model structure, are still covered. This is done without taking into account whether the parameters have realistic values.

- The obtained value of K_i during the open loop identifications is labelled as reliable and correct. Four times the same value of K_i is estimated and the response compares very well with the open loop measured data. The parameters K_p, ζ, ω and t_d are fluctuating around the correct value but are still not correct, both for closed loop and open loop identifications. The total delay identified by the combination of a second order system and time delay is not sufficient.

- There is factor 3 difference between the expected and the estimated value of τ_n. First, the absence of the dynamics that take into account the change of mass of water entrained by the propeller and the inflow angle explains some of the factor 3 difference. Secondly, there is a suspicion that the test set-up of the backward bollard push with the Stan Tug 1205 has influence on this difference. Moreover, it is possible that the fluctuations of the experiments are to large and cause an error due to the linearisation of the propeller torque.

6

Conclusions & Recommendations

In this final chapter, conclusions are drawn based on the findings in this thesis. Furthermore, recommendations are given concerning future research and use of full-scale system identification of ship propulsion systems.

6.1. Conclusions

In section 1.4, the main question and sub-questions of this research were presented. First, all three sub-questions are answered. Thereafter, with the help of the sub-questions, the main question is answered.

6.1.1. First Sub-question

The first sub-question is: *"What are possible improvements concerning data, model structure and searching criterion for the linear system identification of a full-scale propulsion system?"*. This sub-question is answered with the help of the three pillars of system identification that can be improved, which is shown in figure 1.1. As stated in section 1.3, this research aims to improve the system identification results obtained by Martinus [1].

Data

Obtaining a good model depends on the quality of the measured data of the system. Different improvements concerning the measured data are performed in chapter 3. The multiple sine waves experiment is put into frequency domain because the noise can be cancelled out easily at the frequencies where the sines have no power. As a result, the system identification speeds up. A new procedure is used that calculates the correct frequencies to be selected in frequency domain. The Gaussian approach makes it possible to select the frequency of interest out of the measured sine waves data sets. Based on figure 3.5 and table 3.5, it is concluded that the new selection procedure of data points in frequency domain improves the measured data and is a better selecting approach compared to the method used by Martinus [1]. Due to the advantages and improved selecting procedure, mainly frequency domain data sets are used for the linear system identification

With the correct selected frequencies in frequency domain, the reliability of each data set with respect to the amount of noise is evaluated. The overall and local signal to noise ratios are determined in section 3.3.2. Based on the signal to noise ratios presented in table 3.6 and 3.7, it is concluded that n_e (PTM_e measurement of the engine speed at the diesel engine) has the highest overall certainty of the three different performed engine speed measurements. Therefore, the measured data sets n_{set}, n_e and M_s are used for system identification, validation and comparison.

However, during the linear system identification and the analysis of the data, several deficiencies are found. The frequency domain figures 3.7 and 3.8 showed that there is a low amount of measurements after 1 [rad/s]. Combined with the results presented in section 5.5, this concludes that the amount of measurements is to low between 1 and 10 [rad/s] specific for the measurements of the propulsion system of the Stan Tug 1205. Besides, with these performed measurements it is not possible to obtain the responses of the governor and diesel engine individually.

Model Structure
The initial linear closed loop model structure used by Martinus [1] is adjusted and different implementations are determined. The initial linear model structure is simplified by omitting parameter g and fixing v to one, changing the diesel engine in a constant torque machine. Therefore, the parameters K_p or K_i are not dependent on parameter v anymore. Based on the sensitivity analysis in section 4.1 and 4.3, it is concluded that in open loop the influence and a more clear response of the individual parameters is visible compared to closed loop. Besides, zooming in on the open loop core propulsion and the governor+diesel engine sub-model creates more simple model structures with a lower amount of identifiable parameters.

The open loop identification of the core propulsion sub-model, identified 50 times the same result ($\tau_n = 0.3890$). Although the estimated value falls within the identified range, the estimated value is lower than expected. However, based on the sensitivity analysis in figure 4.4 and the results of the system identification shown figure 5.1, it is concluded that the open loop core propulsion sub-model has almost a perfect fit with the corresponding FRF measured data.

Differences between the governor+diesel engine sub-model and the corresponding frequency domain data were visible in figure 4.5. Besides, section 3.2.1 showed that a time delay is present between the input and output of the measured data. New terms are added to the model structure for improvement. Based on figure 4.6, the conclusion is drawn that the addition of a derivative term to the governor does not improve the response of the model structure. However, with the sensitivity analysis in figure 4.7 and 4.8 and the system identification results presented in section 5.3 and 5.4, the conclusion is that the addition of a time delay and second order system improve the linear system identification.

The figures in section 5.5 and 5.6 show that the open and closed loop system identifications with a time delay and second order system, compare well in frequency and time domain up to a frequency of 1 [rad/s] and after 10 [rad/s]. However, difficulties arise between between 1 and 10 [rad/s]. Based on the simulated response in time and frequency domain of these model structures between 1 and 10 [rad/s] in figure 5.4, 5.8 and 5.11, it is concluded that there is not enough damping present in the model structure.

The identified parameters are evaluated and if possible compared with the expected value. Table 5.2 shows that parameter K_i is estimated four times the same. Based on this finding combined with figure 5.2 and 5.5, it is concluded that obtained value of K_i in open loop is reliable and correct. Furthermore, the conclusion is drawn that parameters K_p, ζ, ω and t_d are fluctuating around the correct value but are still not correct, both for closed loop and open loop identifications with a second order system and time delay. Figure 5.9 and 5.11 show that the identified models still have a time delay. Therefore, it is concluded that the total delay identified by the combination of a second order system and time delay is still not sufficient. The calculated expected value of τ_n in section 5.7.1 is a factor 3 larger than the estimated value. This and the evaluation in section 5.7.1, concludes that the system identification of the core propulsion sub-model matches with the measured data but the sub-model structure does not match the system.

Searching Criterion
The type of model structure influences the selection of a searching criterion. The System Identification Toolbox chooses the searching criterion method to determine a minimum. The methods that can be selected and used are the subspace Gauss Newton Least Squares (GNLS), Levenberg Marquard Least Squares (LMLS) and the Matlab function 'fmincon' [10]. Mainly the searching criterion is improved concerning optimisation strategies. In section 5.7.1 the approach to optimise the identification by using

a large amount of different initial parameters sets is presented. Based on this and the different performed identifications in chapter 5, it is concluded that the 50 random but feasible starting sets of initial parameters used per identification, increase the chance to find the global instead of a local minimum. To have a better optimisation of the searching criterion, stopping criteria are used to constraint each identification. Besides, boundary conditions are set up for parameters to decrease the searching range of the searching criterion.

Figure 5.5 showed that between 1 and 10 [rad/s] the parameters K_p, ζ, ω and t_d are fluctuating around the correct value but are still not correct. Although boundary conditions of the parameters are present, shown in figure 5.1, it is concluded that the freedom of movement between the lower and upper bound of the boundary conditions of the parameters is to large. Besides, the searching criterion is still able to identify unstable models.

Section 5.4 and 5.6 showed that the benchmark has good behaviour in time domain and closed loop frequency domain. However, figure 5.5 showed that the response of the benchmark in open loop is not very well and Martinus [1] concluded that the identified parameters are not trustworthy. From these findings, the conclusion is drawn that the searching criterion is able to combine the parameters such way that the behaviour of the system gets imitated and dynamics, not explicitly included in the model structure, can still be covered. This is behaviour is determined without taking into account if the parameters have realistic values.

6.1.2. Second Sub-question
The second sub-question is: *"How does the implementation of a nonlinear model structure affect the full-scale system identification?"*. Although a nonlinear system identification is not performed, based on the findings of the performed linear system identifications advantages and disadvantages of nonlinear system identification can be determined.

To perform a nonlinear system identification, a nonlinear model structure is needed. In section 5.5 is stated that the addition of nonlinear limiters to the model structure could flatten the areas where too little damping is present and increase the quality of the identification. In section 5.7.1 is stated that it is possible that the fluctuations of the performed experiments are too large and cause an error due to the linearisation of the propeller torque. Based on this, it is concluded that nonlinear system identification will have the advantages that nonlinear limits can be implemented and it is possible to use non normalised 'real' data. However, nonlinear system identification is only possible with time domain data. In section 3.3 the advantages of the use of frequency domain as data for system identification are stated. Concluding, nonlinear system identification loses the advantage of the usage of frequency domain data and therefore the identification becomes more complex.

Although some of the advantages and disadvantages of nonlinear system identification are known, the full affect is still unknown. To find out the full affect of the implementation of a nonlinear model structure on the system identification of a propulsion system, it is necessary to perform such system identification. Concluding, further research is needed to know the full affect of a nonlinear model structure on the system identification of a full-scale propulsion system.

6.1.3. Third Sub-question
The third sub-question is: *"What is required to implement the most suitable fingerprinting method on a Damen ship?"*. Although the linear system identification is very much improved, no in depth analysis is performed concerning implementation of a fingerprinting method on a ship. The initial plan was to determine what kind of sensors and measurement equipment were needed to implement a fingerprinting method on a ship. However, this sub-question will be answered with an helicopter view, using the findings and lessons learned of the different performed and improved linear system identifications.

With a fingerprinting method on board of a ship, predictive maintenance can be executed. Decay of parameters can be registered over time and can be used to predict possible upcoming problems of the propulsion system. Anther purpose of a fingerprinting method on board of a ship, is that it can be used to obtain up to date performance simulations models of the propulsion system.

In section 3.4 and 5.2 is stated that mainly the frequency domain data of the multiple sine waves experiment is used for linear system identification. During the revised pre-processing of the measured data in section 3.1, constant input and output measurements of the step response are used. Furthermore, data sets in section 3.4 are obtained with the engine speed set point, engine speed and shaft torque measurements. Concluding that the implementation of a fingerprinting method with linear system identification, at least a step response, frequency domain data of a multiple sine waves experiment and the three different performed measurements are needed. To enhance the quality of a fingerprint, it is recommended to increase the amount of experiments of the sine waves between 1 and 10 [rad/s] specifically for the propulsion system measurements of the Stan Tug 1205. Besides, measurements between the governor and the engine are recommended.

As already stated, open loop model structures, a second order system and time delay improve the linear system identification. Based on this, it is concluded that for the implementation a fingerprinting method with linear system identification, the usage of open loop model structures, a second order system and time delay are needed. Important is that the deficiencies concerning the data between 1 and 10 [rad/s], the shaft loop with parameter τ_n, the too little damping in the model structure and the fluctuation of the parameters K_p, ζ, ω and t_d are resolved before such a method is implemented on a Damen ship.

6.1.4. Main Question

With the three sub-questions answered, it is possible to answer the main question. The main question is: **"What is a suitable method to obtain dynamic model- behaviour and parameters of a full-scale propulsion system in short time, based on controlled tests?"**.

Based on the answers on the sub-questions, it is concluded that linear system identification is a suitable method to obtain dynamic model- behaviour and parameters of a full-scale propulsion system in short time. There are still some deficiencies concerning data, model structure and searching criterion. However, these deficiencies are solvable and possibly further increase the quality of the obtained dynamic model- behaviour and parameters of a full-scale propulsion. Therefore, it is recommended to continue developing linear open loop system identification with a second order system and time delay combined with open loop frequency domain data.

6.2. Recommendations

This final section contains recommendations concerning future research and use of full-scale system identification. Recommendations are stated to enhance the quality of the system identification of the propulsion system and for future researches.

- It is recommended to increase the amount of measurements of the sine waves experiment between 1 and 10 [rad/s]. The results showed that this is a critical region during the system identification of the propulsion system of the Stan Tug 1205. More measurement points between 1 and 10 [rad/s] make it easier to identify the parameters that have their sensitivity in that region. Besides, the certainty of all the measurements combined increases when more measurements are added. Important to note is that this critical region is possibly located somewhere else for different propulsion systems and ships.

- A very suitable method to obtain obtain dynamic model- behaviour and parameters of a full-scale propulsion system is with open loop model structures and measured data. With the current measurements it is not possible to evaluate the governor and diesel engine individually. It is recommended to perform measurements between the governor and diesel engine during the experiments. However, measuring the output of the governor is very difficult and appointed as almost impossible. Another possible solution is to start the conversation with the manufacturer of the governor and diesel engine to obtain more knowledge and information.

- During this research problems arose with the use of the System Identification Toolbox of Matlab. The System Identification Toolbox of Matlab has restrictions and does not support internal delays. In the future it is recommended to perform system identifications without the help of the System Identification Toolbox of Matlab. It is possible to write these algorithms without the help of the Matlab toolbox.

- The conclusion is drawn that not enough damping is present in the identified model structures. The addition of nonlinear limiters to the model structure could flatten the areas where too little damping is present and increase the quality of the identification. It is recommended to incorporate limiters in a nonlinear model structure. To investigate the effect of nonlinear limiters, nonlinear system identification is necessary to perform. Furthermore, the propulsion system of the Stan Tug 1205 contains torsional vibration dampers. These are not incorporated in the model structure. Such dampers can be implemented in the model structure as a mass-spring-damper system. Therefore, it is also recommended to investigate the affect of the implementation of torsional vibration dampers in the model structure.

- Although some of the advantages and disadvantages of nonlinear system identification are known, the full affect is still unknown. To find out the full affect of the implementation of a nonlinear model structure on the system identification of a full-scale propulsion system, it is necessary to perform such system identification. Further research on the affect of nonlinear system identification of a full-scale propulsion system is recommended.

- The identifications between 1 and 10 [rad/s] showed that the parameters K_p, ζ, ω and t_d are fluctuating around the correct value but are still not correct. Tightening up the boundary conditions of the parameters during the identification is recommended. This creates a smaller area of movement for the parameters during system identification and forces the searching criterion to vary the parameters in a smaller but expected region. It is also recommended to take into account the stability of identified models when tightening up the boundary conditions of the parameters.

- The validation of the parameter τ_n showed that the model structure does not match the reality concerning the shaft loop. To decrease the difference between the estimated value and calculated value of the inertia, it is recommended to add dynamics that take into account the change of mass of water entrained by the propeller and the inflow angle to the model structure. Incorporating propeller dynamics creates a more realistic and truthful model structure. Important to note is that the change of mass of water entrained by the propeller is neglected in most of the simulation models and is scarcely investigated in the literature. Therefore, research is needed to learn how to implement these propeller dynamics.

- It is recommended to perform system identification with measured data obtained during free sailing conditions. First of all because possible deficiencies during the backward bollard push measurements could be removed. Furthermore, with measured data obtained during free sailing it will also be possible to identify hydrodynamic coefficients (wake and thrust deduction) of a ship. However, the model structure of the propulsion system will become more complex because the speed loop has to be taken into account.

- Last but not least, this research shows that linear system identification is a suitable method to obtain dynamic model- behaviour and parameters of a full-scale propulsion system of a ship. Therefore, it is a recommendations to continue developing linear system identification for full-scale propulsion systems.

Bibliography

[1] T. Martinus, *Parameter identification on full scale propulsion systems*, Msc thesis, Delft University of Technology (2020).

[2] A. Vrijdag, D. Stapersma, and T. van Terwisga, *Systematic modelling, verification, calibration and validation of a ship propulsion simulation model,* Journal of Marine Engineering and Technology **8**, 3 (2009).

[3] A. Vrijdag and Y. Sang, *Fingerprinting the ship propulsion system: low hanging fruit or mission impossible?* Proceedings of the International Ship Control Systems Symposium (iSCSS) **1** (2018).

[4] R. D. Geertsma, R. R. Negenborn, K. Visser, M. A. Loonstijn, and J. J. Hopman, *Pitch control for ships with diesel mechanical and hybrid propulsion: Modelling, validation and performance quantification,* Applied Energy **206**, 1609 (2017).

[5] F. Cipollini, L. Oneto, A. Coraddu, A. Murphy, and D. Anguita, *Condition-based maintenance of naval propulsion systems with supervised data analysis,* Ocean Energy **149**, 268 (2018).

[6] K. Hageman, *MT54010 - Literature Research - System Identification of Full-scale Propulsion Systems*, Literature research, Delft University of Technology (2020).

[7] A. Vrijdag and D. Stapersma, *Extension and application of a linearised ship propulsion system model,* Ocean Engineering **143**, 50 (2017).

[8] D. Stapersma and A. Vrijdag, *Linearisation of a ship propulsion system model,* Ocean Engineering **142**, 441 (2017).

[9] *State space,* https://www.mathworks.com/help/control/ref/ss.html.

[10] *Greyestoptions,* https://www.mathworks.com/help/ident/ref/greyestoptions.html.

[11] *Pulseperiod,* https://www.mathworks.com/help/signal/ref/pulseperiod.html.

[12] *Interp1,* https://www.mathworks.com/help/matlab/ref/interp1.html?searchHighlight=interp1&s_tid=srchtitle.

[13] B. Resor, M. Trethaway, and K. Maynard, *Compensation for encoder geometry and shaft speed variation in time interval torsional vibration measurement,* Journal of Sound and Vibration **286**, 897 (2005).

[14] S. Braut, R. Zigulic, G. Stimac, and A. Skoblar, *Efficient approach for encoder geometry compensation in time interval measurement of torsional vibration,* 10th International Conference on Vibrations in Rotating Machinery , 809 (2012).

[15] *Sine fitting,* https://www.mathworks.com/matlabcentral/fileexchange/66793-sine-fitting.

[16] *Signal-to-noise-ratio,* http://www.scholarpedia.org/article/Signal-to-noise_ratio.

[17] *Difference between open loop closed loop control system,* https://www.elprocus.com/difference-between-open-loop-closed-loop-control-system/.

[18] *The unit response,* https://lpsa.swarthmore.edu/Transient/TransInputs/TransStep.html.

[19] *Transformation: Transfer function - state space,* `https://lpsa.swarthmore.edu/Representations/SysRepTransformations/TF2SS.html`.

[20] *Lead-lag (discrete or continuous),* `https://www.mathworks.com/help/physmod/sps/ref/leadlagdiscreteorcontinuous.html`.

[21] *Time-delay systems,* `http://www.cds.caltech.edu/~murray/courses/cds110/fa15/pdf/L7-3_delay+nyquist.pdf`.

[22] *Pid,* `https://www.mathworks.com/help/control/ref/pid.html`.

[23] G. Franklin, J. Powell, and A. Emami-Naeini, *Feedback Control of Dynamic Systems*, 6th ed. (Pearson, 2010).

[24] *Pade,* `https://www.mathworks.com/help/control/ref/pade.html`.

[25] *State-space model ss,* `https://www.mathworks.com/help/control/ref/ss.html`.

[26] *Gear drive motor mass moment of inertia equation,* `https://www.engineersedge.com/motors/gear_drive_system.htm`.

[27] A. Healey, S. Rock, and s. Cody, *Toward an improved understanding of thruster dynamics for underwater vehicles,* IEEE Journal of Oceanic Engineering **20**, 354 (1995).

[28] M. Blanke, K. Lindegaard, and T. Fossen, *Dynamic model for thrust generation of marine propellers,* IFAC Proceedings Volumes **33**, 353 (2000).

A
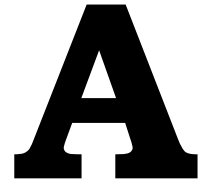
Stan Tug 1205

Product sheet of the Stan Tug 1205 - TOR

STAN TUG 1205
"TOR"

GENERAL

Yard number	502520
Delivery date	December 2017
Basic functions	Towing and mooring operations
Classification	Bureau Veritas
	I ⊕ HULL ● MACH Seagoing Launch
Flag	Sweden
Owner	Marin & Haverikonsult KA AB

DIMENSIONS

Length overall	13.08 m
Beam overall	5.28 m
Depth at sides	2.30 m
Draught aft	1.80 m
Displacement	54 t
(98% consumables)	

TANK CAPACITIES

Fuel oil	5.60 m³
Fresh water	0.35 m³
Sewage	0.33 m³
Bilge water	0.30 m³

PERFORMANCES

Bollard pull	9.1 t
Speed	9.9 kn

PROPULSION SYSTEM

Main engines	2x Volvo D9 MH
Total power	442 bkW (600 bhp) at 1800 rpm
Gearboxes	Twin Disc MG 5091 / 3.82:1
Propellers	2x Kaplan fixed pitch 1050 mm diameter
Nozzles	2x Van de Giessen 'Optima' with stainless steel innerrings
Engine control	Volvo EVC
Rudders	2x double plate high performance
Steering gear	Powered-hydraulic 2x 50º + rudder indicator

AUXILIARY EQUIPMENT

|	
Battery sets	2x 24 V 230 Ah, changeover facility
Generator	Onan MDKBR-eQD 230 V, 17.5 kVA, 50 Hz
Alarm system	Engines, gearboxes and bilge alarm
General service/ bilge pump	SIWI VWSI 5013, 15 m³/h at 2.3 bar
Fuel oil system	Water separator, filters and SOS valve
Cooling system	Closed cooling channels
Sanitary system	Speck 24 V pressure set, Rheinstrom 24 V sewage discharge pump
Engine room ventilation	Mechanical ventilation 8000 m³/h
Fire extinguishers	2x 5 kg CO₂ and 2x 6 kg dry powder

DECK LAY-OUT

|	
Anchor winch	Electrically driven 24 V
Towing hook	Mampaey Disc type, 15 ton SWL
Side/astern fender	Rubber D-fender 150 x 150 mm
Push bow	Cylindrical rubber fender 380 mm

ACCOMMODATION

The air-conditioned wheelhouse is resiliently mounted and has an extremely low noise level of approx. 55 dB(A). The wheelhouse and below deck accommodation are completely insulated and finished with durable modern linings and composite synthetic floor. Wheelhouse with a bench for two persons and a table. Windows are fitted in aluminium frames. Below deck a kitchen unit, shelves and 4 lockers are arranged.

**NAUTICAL AND COMMUNICATION EQUIPMENT**

|	
Searchlight	Den Haan 250 W, 24 V
Compass fluxgate	Cassens & Plath, type Kotter
GPS	Furuno GP-32
Echosounder	Furuno LS-6100
VHF radio telephone	Sailor Compact 6248, 25 W
Navigation lights	Navigation lights incl. towing and side lights
Floodlight	150 W on aft deck

Main deck

Top deck

Below Main deck

DAMEN
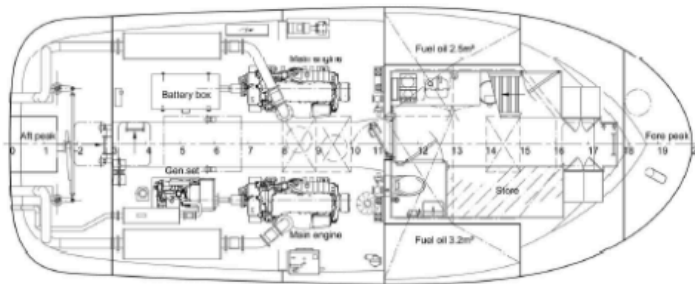
B

Closed Loop Sensitivity Analysis
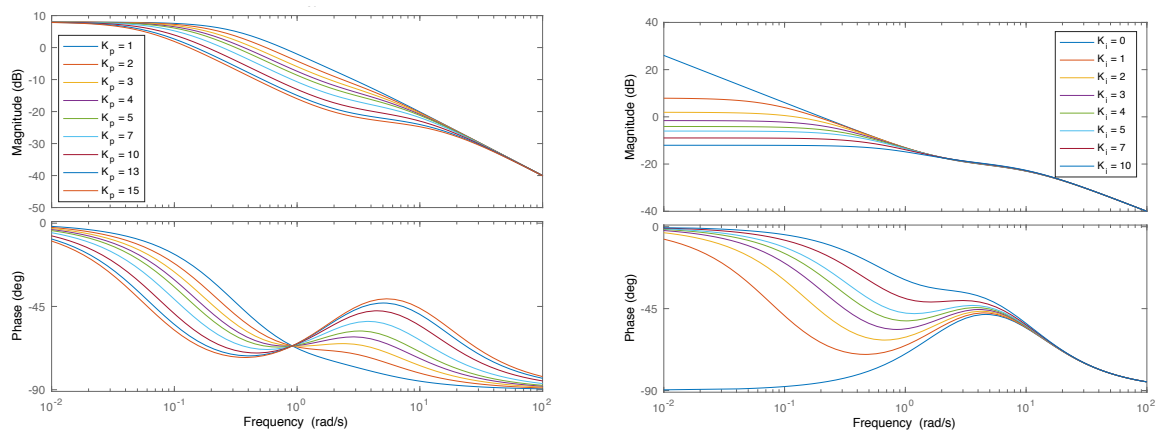
(a) $\frac{\delta E_n^*}{\delta n_{set}^*}$ with K_p varying

(b) $\frac{\delta E_n^*}{\delta n_{set}^*}$ with K_i varying
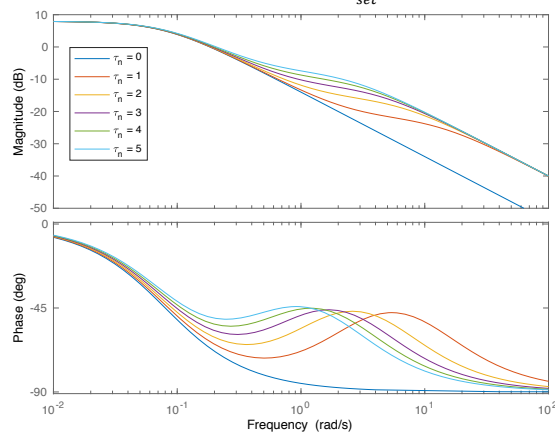
(c) $\frac{\delta E_n^*}{\delta n_{set}^*}$ with τ_n varying

Figure B.1: Sensitivity analysis of closed loop model $\frac{\delta E_n^*}{\delta n_{set}^*}$ with five different parameters.
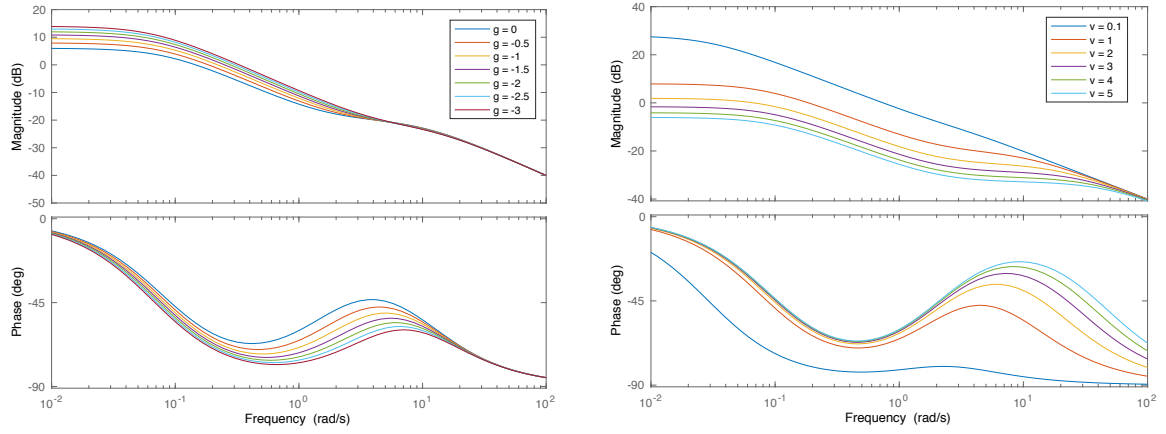
(a) $\frac{\delta E_n^*}{\delta n_{set}^*}$ with g varying

(b) $\frac{\delta E_n^*}{\delta n_{set}^*}$ with v varying

Figure B.2: Sensitivity analysis of closed loop model $\frac{\delta E_n^*}{\delta n_{set}^*}$ with five different parameters.
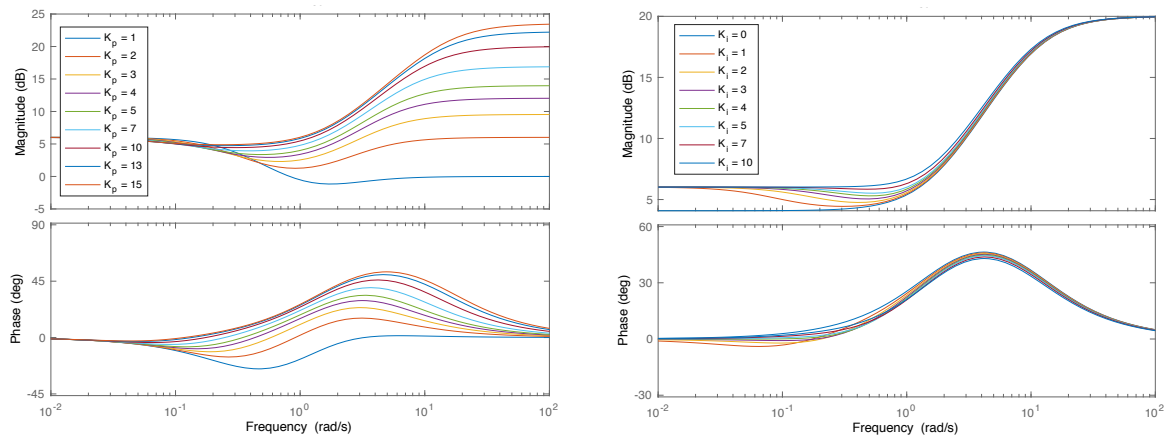
(a) $\frac{\delta M_s^*}{\delta n_{set}^*}$ with K_p varying

(b) $\frac{\delta M_s^*}{\delta n_{set}^*}$ with K_i varying
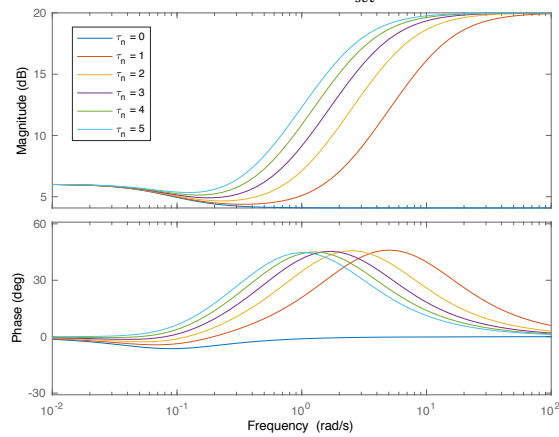
(c) $\frac{\delta M_s^*}{\delta n_{set}^*}$ with τ_n varying

Figure B.3: Sensitivity analysis of closed loop model $\frac{\delta M_s^*}{\delta n_{set}^*}$ with five different parameters.
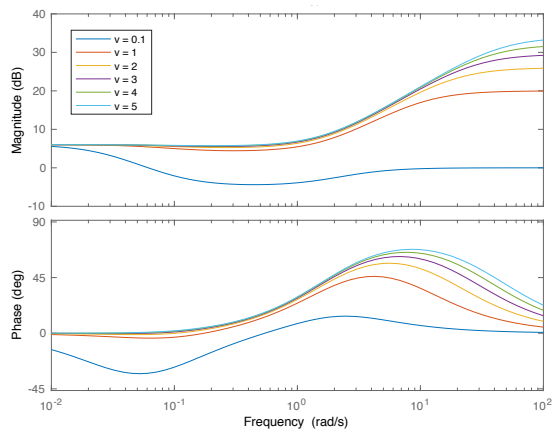
(a) $\frac{\delta M_S^*}{\delta n_{set}^*}$ with v varying
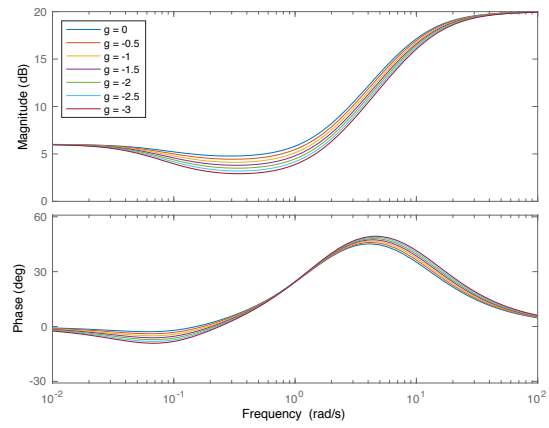
(b) $\frac{\delta M_S^*}{\delta n_{set}^*}$ with g varying

Figure B.4: Sensitivity analysis of closed loop model $\frac{\delta M_S^*}{\delta n_{set}^*}$ with five different parameters.

C

Derivation Open Loop Transfer Functions

For the derivation of the transfer function concerning the core propulsion, equation (2.13) is used. Equation (C.1) is a Laplace transform of the shaft loop equation 2.13. Rewriting equation (C.1) shows the relation between the engine speed δn^* and the shaft torque δM_s^*. The core propulsion of the ship is described by transfer function C.2.

$$\tau_n s \delta n^* = \delta M_s^* - 2\delta n^* \tag{C.1}$$

$$H_{CP} = \frac{\delta n^*}{\delta M_s^*} = \frac{1}{\tau_n s + 2} \tag{C.2}$$

The governor+diesel engine sub-model is described by the transfer function H_{G+D}. With equation (2.17) concerning the governor and with use of a Laplace transform, equation (C.3) is derived. Implementing equation (C.3) in equation (4.1), the simplified shaft torque characteristics, creates equation (C.4). Rewriting equation (C.4) to the relation with the error δe_n^* as input and the shaft torque δM_s^* as output, creates the transfer function of the governor+diesel engine sub-model in equation (C.5).

$$\delta X_{set}^* = (K_p + \frac{K_i}{s})\delta e_n^* \tag{C.3}$$

$$\delta M_s^* = v\delta X_{set}^* = v(K_p + \frac{K_i}{s})\delta e_n^* \tag{C.4}$$

$$H_{G+D} = \frac{\delta M_s^*}{\delta e_n^*} = v(K_p + \frac{K_i}{s}) \tag{C.5}$$

With the transfer functions of the core propulsion sub-model and the governor+diesel sub-model known, the open loop transfer function H_{OL} can be derived. The derivation is shown in equation (C.6) to (C.8).

$$H_{OL} = H_{G+D} * H_{CP} = \frac{\delta n^*}{\delta e_n^*} \tag{C.6}$$

$$H_{OL} = v(K_p + \frac{K_i}{s}) * \frac{1}{\tau_n s + 2} \tag{C.7}$$

$$H_{OL} = \frac{\delta n^*}{\delta e_n^*} = \frac{\frac{vK_p}{\tau_n}s + \frac{vK_i}{\tau_n}}{s^2 + \frac{2}{\tau_n}s} \tag{C.8}$$

D

Closed Loop Simplification

D.1. Transer Functions

$$\frac{\delta n^*}{\delta n^*_{set}} = \frac{\frac{K_p}{\tau_n}s + \frac{K_i}{\tau_n}}{s^2 + \frac{K_p+2}{\tau_n}s + \frac{K_i}{\tau_n}} \tag{D.1}$$

$$\frac{\delta E_n^*}{\delta n^*_{set}} = \frac{s + \frac{2}{\tau_n}}{s^2 + \frac{K_p+2}{\tau_n}s + \frac{K_i}{\tau_n}} \tag{D.2}$$

$$\frac{\delta M_s^*}{\delta n^*_{set}} = \frac{K_p s^2 + \frac{K_i \tau_n + 2K_p}{\tau_n} + \frac{2K_i}{\tau_n}}{s^2 + \frac{K_p+2}{\tau_n}s + \frac{K_i}{\tau_n}} \tag{D.3}$$

Table D.1: Overview of responses of the closed loop simplified transfer functions subjected to highest and lowest frequencies

Relation	$s \to 0$ [abs]	$s \to \infty$ [abs]	$s \to 0$ [dB]	$s \to \infty$ [dB]
$\frac{\delta n^*}{\delta n^*_{set}}$	1	0	0	$-\infty$
$\frac{\delta E_n^*}{\delta n^*_{set}}$	$\frac{2}{K_i}$	0	$\log(\frac{2}{K_i})$	$-\infty$
$\frac{\delta M^*}{\delta n^*_{set}}$	2	K_p	0.3	$\log(K_p)$

D.2. State Space Notation

$$\dot{\bar{x}} = A\bar{x} + B\bar{u} \tag{D.4}$$

$$\bar{y} = C\bar{y} + D\bar{u} \tag{D.5}$$

$$\bar{x} = \begin{bmatrix} \delta n^* \\ \delta E_n^* \end{bmatrix}, \quad \bar{u} = \delta n^*_{set}, \quad \bar{y} = \begin{bmatrix} \delta n^* \\ \delta M_s^* \end{bmatrix} \tag{D.6}$$

$$A = \begin{bmatrix} \frac{-(2+K_p)}{\tau_n} & \frac{K_i}{\tau_n} \\ -1 & 0 \end{bmatrix}, \quad B = \begin{bmatrix} \frac{K_p}{\tau_n} \\ 1 \end{bmatrix} \tag{D.7}$$

$$C = \begin{bmatrix} 1 & 0 \\ -K_p & K_i \end{bmatrix}, \quad D = \begin{bmatrix} 0 \\ K_p \end{bmatrix} \tag{D.8}$$

D.3. Sensitivity Analysis

(a) $\frac{\delta n^*}{\delta n^*_{set}}$ with K_p varying

(b) $\frac{\delta n^*}{\delta n^*_{set}}$ with K_i varying

(c) $\frac{\delta n^*}{\delta n^*_{set}}$ with τ_n varying
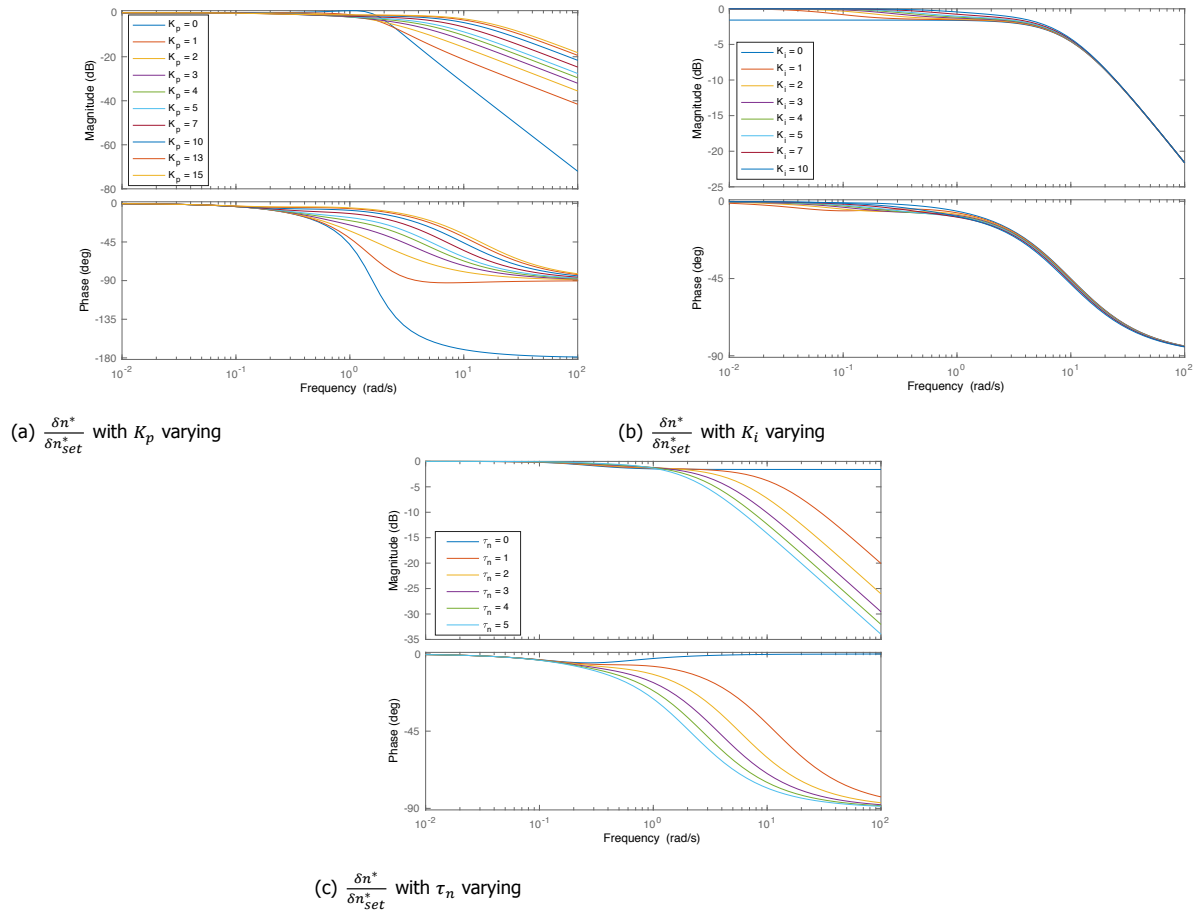
Figure D.1: Bode diagrams of sensitivity analysis of closed loop simplified system with three different parameters.

E

Inertia from TVC Report

```
Project: Stan Tug 1205

Input file: F100.IN        Run started: 12-01-2009/13:49:15

TORPACK-TORFREE version 4.60-P
Copyright (c) TNO 1989-2008  All rights reserved.


M A S S - E L A S T I C   S Y S T E M   (W I T H   G E A R S)

Engine speed for calculation of mean torques in springs and gears   1800.
r/min.
Actual total power at this engine speed  2.210E+05 W.

Mass mom. of inertia without equivalent mass(es) of mass damper(s).
------------------------------------------------------------------------
         Description              Mass mom.   Speed rel.         Firing
                                  of inertia  to mass 1          angle
                                  [kg.m2]     [r/min]            [deg]
------------------------------------------------------------------------
Mass  1  Damper housing               0.216   1.000E+00
Mass  2  Cyl.1                     9.395E-02   1.000E+00  Cyl. 1    +0.0
Mass  3  Cyl.2                     7.030E-02   1.000E+00  Cyl. 2  +480.0
Mass  4  Cyl.3                     9.395E-02   1.000E+00  Cyl. 3  +240.0
Mass  5  Cyl.4                     9.395E-02   1.000E+00  Cyl. 4  +600.0
Mass  6  Cyl.5                     7.030E-02   1.000E+00  Cyl. 5  +120.0
Mass  7  Cyl.6                     9.395E-02   1.000E+00  Cyl. 6  +360.0
Mass  8  Rear crank                8.838E-02   1.000E+00
Mass  9  Flywheel                     1.800   1.000E+00
Mass 10  CX45 prim                    0.590   1.000E+00
Mass 11  CX45 sec                  8.160E-02   1.000E+00
Mass 12  Clutch+transfer gear      5.400E-02   1.000E+00
Mass 13  Pinion                    1.000E-02   1.000E+00
Mass 14  output gear                  0.513   2.618E-01
Mass 15  Flanges                      0.281   2.618E-01
Mass 16  Propeller-3 bl              12.290   2.618E-01
Mass 17  Rev.clutch+transfer gear  5.400E-02   1.000E+00
Mass 18  Rev.pinion                1.000E-02   1.000E+00
Mass 19  Damper ring                  0.230   1.000E+00
------------------------------------------------------------------------
```

Figure E.1: Overview of different mass moment of inertia of the propulsion line of the Stan Tug 1205.
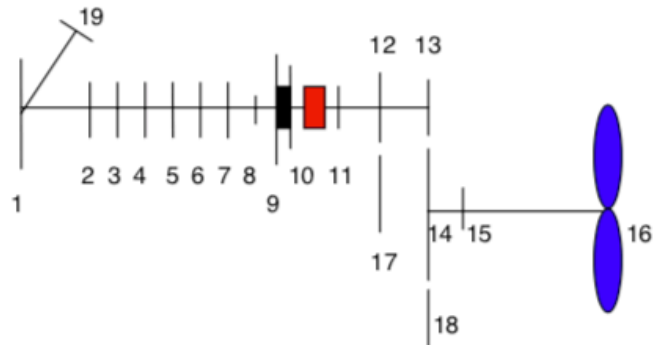
Figure E.2: The propulsion line with indicated masses taken into account for the total mass moment of inertia.